

AD-A227 933

2

REPORT DOCUMENTATION PAGE

1a. REPORT SECURITY CLASSIFICATION Unclassified		1b. RESTRICTIVE MARKINGS	
2a. SECURITY CLASSIFICATION AUTHORITY DTIC SELECTED OCT 26 1990 S B D		3. DISTRIBUTION / AVAILABILITY OF REPORT Approved for public release; distribution unlimited.	
2b. DECLASSIFICATION / DOWNGRADING SCHEDULE		4. PERFORMING ORGANIZATION REPORT NUMBER(S) TELAC Report 90-14	
4. PERFORMING ORGANIZATION REPORT NUMBER(S)		5. MONITORING ORGANIZATION REPORT NUMBER(S) ARL 24023.4-EG	
5a. NAME OF PERFORMING ORGANIZATION Technology Laboratory for Advanced Composites, M.I.T.	6b. OFFICE SYMBOL (if applicable)	7a. NAME OF MONITORING ORGANIZATION U. S. Army Research Office	
6c. ADDRESS (City, State, and ZIP Code) M.I.T. Rm 33-309 77 Massachusetts Ave. Cambridge, MA 02139		7b. ADDRESS (City, State, and ZIP Code) P. O. Box 12211 Research Triangle Park, NC 27709-2211	
8a. NAME OF FUNDING / SPONSORING ORGANIZATION U. S. Army Research Office	8b. OFFICE SYMBOL (if applicable)	9. PROCUREMENT INSTRUMENT IDENTIFICATION NUMBER DAAL03-87-K-0024	
8c. ADDRESS (City, State, and ZIP Code) P. O. Box 12211 Research Triangle Park, NC 27709-2211		10. SOURCE OF FUNDING NUMBERS	
		PROGRAM ELEMENT NO	PROJECT NO.
		TASK NO.	WORK UNIT ACCESSION NO
11. TITLE (Include Security Classification) Nonlinear Large Amplitude Vibration of Composite Helicopter Rotor Blade at Large Static Deflection			
12. PERSONAL AUTHOR(S) Taehyoun Kim and John Dugundji			
13a. TYPE OF REPORT Interim Technical	13b. TIME COVERED FROM TO	14. DATE OF REPORT (Year, Month, Day) 1990 July 25	15. PAGE COUNT 88
16. SUPPLEMENTARY NOTATION The view, opinions and/or findings contained in this report are those of the author(s) and should not be construed as an official Department of the Army position, policy, or decision, unless so designated by other documentation.			
17. COSATI CODES FIELD GROUP SUB-GROUP		18. SUBJECT TERMS (Continue on reverse if necessary and identify by block number) Helicopter blade, Nonlinear vibration, Composites	
19. ABSTRACT (Continue on reverse if necessary and identify by block number) The nonlinear, large amplitude free vibration of composite helicopter blades under large static deflection is investigated analytically. A new model capable of handling large amplitudes as well as large deflections was developed, based on the work in a previous report by Minguet. The model can deal with large displacements and rotations by use of Euler angle and can account for structural couplings such as bending-twist and extension-twist. The reduction of this large deflection model to a commonly used moderate deflection model is also shown. A Newton-Raphson type iterative solution technique based on numerical integration of the basic large deflection equations is seen effective for the present analysis. Two different lay-ups [0/90] ₃₅ , [45/0] ₅ , of graphite/epoxy flat beams have been selected to demonstrate the large amplitude analysis. The behavior of the first and second bending, the first fore-and aft, and the first torsional modes is presented as tip static deflection and tip amplitudes increase. It is found that both large static deflection and large amplitudes can affect the fore-and-aft and torsion modes significantly, but bending modes.			
CONTINUED ON OTHER SIDE -----			
20. DISTRIBUTION / AVAILABILITY OF ABSTRACT <input type="checkbox"/> UNCLASSIFIED/UNLIMITED <input type="checkbox"/> SAME AS RPT. <input type="checkbox"/> DTIC USERS		21. ABSTRACT SECURITY CLASSIFICATION Unclassified	
22a. NAME OF RESPONSIBLE INDIVIDUAL		22b. TELEPHONE (Include Area Code)	22c. OFFICE SYMBOL

UNCLASSIFIED

SECURITY CLASSIFICATION OF THIS PAGE

are not influenced much by the geometrical nonlinearities. γ

UNCLASSIFIED

SECURITY CLASSIFICATION OF THIS PAGE

TELAC REPORT 90-14

**NONLINEAR LARGE AMPLITUDE VIBRATION OF
COMPOSITE HELICOPTER ROTOR BLADE AT
LARGE STATIC DEFLECTION**

Taehyoun Kim

John Dugundji

July 1990

**Technology Laboratory for Advanced Composites
Department of Aeronautics and Astronautics
Massachusetts Institute of Technology
Cambridge, Massachusetts 02139**

**Interim Technical Report, prepared for:
U. S. Army Research Office
Contract No. DAAL 03-87-K-0024**

The view, opinions, and/or findings contained in this report are those of the authors and should not be construed as an official Department of the Army position, policy, or decision, unless so designated by other documentation.

Abstract

The nonlinear, large amplitude free vibration of composite helicopter blades under large static deflection is investigated analytically. A new model capable of handling large amplitudes as well as large deflections was developed, based on the work in a previous report by Minguet. The model can deal with large displacements and rotations by use of Euler angles and can account for structural couplings such as bending-twist and extension-twist. The reduction of this large deflection model to a commonly used moderate deflection model is also shown. A Newton-Raphson type iterative solution technique based on numerical integration of the basic large deflection equations is seen effective for the present analysis. Two different lay-ups $[0/90]_{3s}$, $[45/0]_s$, of graphite/epoxy flat beams have been selected to demonstrate the large amplitude analysis. The behavior of the first and second bending, the first fore-and aft, and the first torsional modes is presented as tip static deflection and tip amplitudes increase. It is found that both large static deflection and large amplitudes can affect the fore-and-aft and torsion modes significantly, but bending modes are not influenced much by the geometrical nonlinearities.

Accession For	
NTIS GRA&I	<input checked="" type="checkbox"/>
DTIC TAB	<input type="checkbox"/>
Unannounced	<input type="checkbox"/>
Justification	
By _____	
Distribution/	
Availability Codes	
Dist	Avail and/or Special
A-1	

Acknowledgement

This research was performed in the Technology Laboratory for Advanced Composite (TELAC) of the Department of Aeronautics and Astronautics at the Massachusetts Institute of Technology, supported under U. S. Army Research Office contract DAAL03-87-K-0024, with Dr. Gary Anderson as Technical Monitor.

Contents

1	Introduction	1
2	Analytic Modeling	4
2.1	Basic Equations	4
2.2	Reduction of Basic Equations for Moderate Deflections	8
2.3	Modeling of Large Amplitude Motion	17
3	Method of Solution	21
4	Results and Discussion	24
5	Conclusion	28
	References	30
	Appendices	
A	Calculation of Coefficients of Harmonic Quantities	32
B	Multiplication of Two Harmonic Quantities	35
C	Multiplication of Three Harmonic Quantities	37
	Tables and Figures	39

List of Figures

1	Definition of global and local axes	40
2	Definition of local internal forces and moments	41
3	First Bending Mode;[0/90] _{3s} ,0 mm tip deflection,Z _s =10 mm	42
4	" " " ;[0/90] _{3s} ,0 mm " " ,Z _s =200 mm	42
5	Second Bending Mode;[0/90] _{3s} ,0 mm tip deflection,Z _s =10 mm	43
6	" " " ;[0/90] _{3s} ,0 mm " " ,Z _s =100 mm	43
7	First Fore-and-Aft Mode;[0/90] _{3s} ,0 mm tip deflection,Y _s =10 mm	44
8	" " " ;[0/90] _{3s} ,0 mm " " ,Y _s =38 mm	44
9	First Torsion Mode;[0/90] _{3s} ,0 mm tip deflection, θ _s = 5 degree	45
10	" " " ;[0/90] _{3s} ,0 mm " " , θ _s = 20 degree	45
11	First Bending Mode;[0/90] _{3s} ,59 mm tip deflection,Z _s =10 mm	46
12	" " " ;[90/0] _{3s} ,59 mm " " ,Z _s =200 mm	46
13	Second Bending Mode;[0/90] _{3s} ,59 mm tip deflection,Z _s =10 mm	47
14	" " " ; [0/90] _{3s} ,59 mm " " ,Z _s =80 mm	47
15	First Fore-and-Aft Mode;[0/90] _{3s} ,59 mm tip deflection,Y _s =10 mm	48
16	" " " ;[0/90] _{3s} ,59 mm " " ,Y _s =80 mm	48
17	First Torsion Mode;[0/90] _{3s} ,59 mm tip deflection, θ _s = 5 degree	49
18	" " " ;[0/90] _{3s} ,59 mm " " , θ _s = 20 degree	49
19	First Bending Mode;[0/90] _{3s} ,210 mm tip deflection,Z _s =10 mm	50
20	" " " ;[0/90] _{3s} ,210 mm " " ,Z _s =200 mm	50
21	Second Bending Mode;[0/90] _{3s} ,210 mm tip deflection,Z _s =10 mm	51
22	" " " ; [0/90] _{3s} ,210 mm " " ,Z _s =48 mm	51

23	First Fore-and-Aft Mode;	$[0/90]_{3s}$,	210 mm tip deflection,	$Y_s=10$ mm	52
24	"	"	"	; $[0/90]_{3s}$,	210 mm " " , $Y_s=80$ mm 52
25	First Torsion Mode;	$[0/90]_{3s}$,	210 mm tip deflection,	$\theta_s=5$ degree	53
26	"	"	"	; $[0/90]_{3s}$,	210 mm " " , $\theta_s=40$ degree 53
27	Frequency vs. Amplitude;	$[0/90]_{3s}$,	0 mm tip deflection	54	
28	"	"	"	; $[0/90]_{3s}$,	59 mm " " 55
29	"	"	"	; $[0/90]_{3s}$,	210 mm " " 56
30	Centershift vs. Amplitude;	$[0/90]_{3s}$,	59 mm tip deflection	57	
31	"	"	"	; $[0/90]_{3s}$,	210 mm " " 58
32	Frequency vs. Amplitude w/o and w/ 2nd harmonics;	$[0/90]_{3s}$,	59 mm and 210 mm tip deflection	59	
33	Natural Frequencies of $[0/90]_{3s}$ Beam as a Function of Tip Deflection (from Ref. 1)			60	
34	First Bending Mode;	$[45/0]_s$,	0 mm tip deflection,	$Z_s=10$ mm	61
35	"	"	"	; $[45/0]_s$,	0 mm " " , $Z_s=200$ mm 61
36	Second Bending Mode;	$[45/0]_s$,	0 mm tip deflection,	$Z_s=10$ mm	62
37	"	"	"	; $[45/0]_s$,	0 mm " " , $Z_s=130$ mm 62
38	First Fore-and-Aft Mode;	$[45/0]_s$,	0 mm tip deflection,	$Y_s=1$ mm	63
39	"	"	"	; $[45/0]_s$,	0 mm " " , $Y_s=3.5$ mm 63
40	First Torsion Mode;	$[45/0]_s$,	0 mm tip deflection,	$\theta_s=5$ degree	64
41	"	"	"	; $[45/0]_s$,	0 mm " " , $\theta_s=12$ degree 64
42	First Bending Mode;	$[45/0]_s$,	70 mm tip deflection,	$Z_s=10$ mm	65
43	"	"	"	; $[45/0]_s$,	70 mm " " , $Z_s=200$ mm 65
44	Second Bending Mode;	$[45/0]_s$,	70 mm tip deflection,	$Z_s=10$ mm	66
45	"	"	"	; $[45/0]_s$,	70 mm " " , $Z_s=70$ mm 66
46	First Fore-and-Aft Mode;	$[45/0]_s$,	70 mm tip deflection,	$Y_s=10$ mm	67
47	"	"	"	; $[45/0]_s$,	70 mm " " , $Y_s=80$ mm 67
48	First Torsion Mode;	$[45/0]_s$,	70 mm tip deflection,	$\theta_s=5$ degree	68

49	" " " ;[45/0] _s ,70 mm " " , $\theta_s = 10$ degree . . .	68
50	First Bending Mode:[45/0] _s ,203 mm tip deflection, $Z_s=10$ mm	69
51	" " " ;[45/0] _s ,203 mm " " , $Z_s=200$ mm	69
52	Second Bending Mode:[45/0] _s ,203 mm tip deflection, $Z_s=20$ mm . . .	70
53	" " " ; [45/0] _s ,203 mm " " , $Z_s=45$ mm . . .	70
54	First Fore-and-Aft Mode:[45/0] _s ,203 mm tip deflection, $Y_s=10$ mm . .	71
55	" " " ;[45/0] _s ,203 mm " " , $Y_s=80$ mm . .	71
56	First Torsion Mode:[45/0] _s ,203 mm tip deflection, $\theta_s = 1$ degree	72
57	" " " ;[45/0] _s ,203 mm " " , $\theta_s = 5$ degree . . .	72
58	Frequency vs. Amplitude:[45/0] _s ,0 mm tip deflection	73
59	" " " ;[45/0] _s ,70 mm " "	74
60	" " " ;[45/0] _s ,203 mm " "	75
61	Centershift vs. Amplitude:[45/0] _s ,70 mm tip deflection	76
62	" " " ;[45/0] _s ,203 mm " "	77
63	Frequency vs. Amplitude w/o and w/ 2nd harmonics:[45/0] _s , 70 mm and 203 mm tip deflection	78
64	Natural Frequencies of [45/0] _s Beam as a Function of Tip Deflection (from Ref. 1)	79

Nomenclature

A	Beam cross-sectional area
C	Chord
$[E]$	Beam stress-strain stiffness matrix
E	Young's modulus
\vec{F}_G	Force resultant vector in global axes, x, y, z
\vec{F}_L	" " " " local axes, ξ, η, ζ
F_1, F_2, F_3	Force resultant components in local axes
F_x, F_y, F_z	" " " in global axes
G	Shear modulus
I_η	Beam area moment of inertia about ζ axis
I_ζ	" " " " " " η axis
I_p	Beam mass moment of inertia about ξ axis
J	Beam torsion constant
L	Beam length
m	Beam mass per unit length
\vec{M}_G	Moment resultant vector in global axes, x, y, z
\vec{M}_L	" " " " local axes, ξ, η, ζ
M_1, M_2, M_3	Moment resultant components in local axes
M_x, M_y, M_z	" " " " global axes
\vec{m}_G	Applied moment vector in global axes
m_x, m_y, m_z	" " components in global axes
\vec{m}_{GT}	Total applied moment vector in global axes
m_{xT}, m_{yT}, m_{zT}	" " " components in global axes
\vec{m}_L	Applied moment vector in local axes
m_1, m_2, m_3	" " components in local axes
\vec{p}_G	Applied load vector in global axes
p_x, p_y, p_z	" " components in global axes

\vec{p}_{GT}	Total applied load vector in global axes
p_{xT}, p_{yT}, p_{zT}	" " " components in global axes
\vec{p}_l	Applied load vector in local axes
p_1, p_2, p_3	" " components in local axes
s	arc length
$[T]$	Transformation matrix
u, v, w	Displacements along x, y, z axes
x, y, z	Global coordinates
$\gamma_{\xi\eta}, \gamma_{\xi\zeta}$	Beam shear strains
ϵ	Beam extension strain or a small parameter
θ_t	Built-in twist angle
$[\kappa]$	Curvature matrix
κ_ξ	Twist rate around ξ axis
κ_η	Bending curvature around η axis
κ_ζ	" " " ζ axis
ξ, η, ζ	Local coordinates
α, β, θ	Euler angles
ϕ	Total twist angle
ω	Frequency

Chapter 1

Introduction

The behavior of nonlinear, large amplitude free vibration of composite helicopter rotor blades under large static deflections is investigated. A previous report by Minguet, Ref. 1 indicates that under large static deflections, natural frequencies and mode shapes of the blade, particularly those of the fore-and-aft and torsion modes show interesting trends that are not apparent from the characteristics of undeformed cantilever beams. The influence of the large static deflections on the modes was found by linearizing the governing equations of motion around a given static position to yield the small amplitude vibrations of the beam around that large static position.

In the present analysis, the amplitudes of motion are also allowed to be large, and emphasis is given on how the vibrational behavior of the blades is affected by not only the static deflection but also the amplitude level at the tip. This type of free vibration analysis should give insight into more general aeroelastic problems where large amplitude motion is accompanied by nonlinear exciting forces such as nonlinear periodic forces due to gravity or aerodynamic loads due to dynamic stall. A simple such analysis, dealing only with geometrical nonlinearities of the rigid blade, was given by Chopra and Dugundji in Ref. 2. More recently Dunn and Dugundji have given another such analysis, this time dealing only with aerodynamic stall. A fully nonlinear aeroelastic analysis involving both structural and aerodynamic nonlinearities would be of interest. Flexible helicopter blades are good examples in which these nonlinearities play important roles, and the present analysis should serve as an introduction to the

understanding of such complex phenomenon.

There exist two types of nonlinear helicopter blade equations that can be readily available for the purpose of present analysis; the equations that are based on various geometrical ordering schemes, and the ones that are not based on ordering schemes. The former group of equations approximate large displacements and rotations mostly up to second order (e.g. Ref. 4, 5) while the latter group preserve the complete nonlinearities in them (e.g. Ref. 1). Since strong couplings between various static and dynamic parts of the equations are expected in the nonlinear large amplitude vibrations, the set of complete nonlinear equations of the latter group is preferred. The nonlinear equations derived by Minguet in Ref. 1 are used here for their simplicity and immediate availability for analysis of composite blades. However, to illustrate correspondency between these two different types of equations, an attempt is made to reduce the nonlinear equations by Minguet to the second order equations for moderate deflections that are given by Hodges and Dowell in Ref. 4, and Boyd in Ref. 5.

A new technique based on harmonic balance and iterative Newton-Raphson algorithm is introduced to solve for the modes and their frequencies as functions of amplitudes of interest under moderate to large static deflections. Results of numerical analysis are given for two lay-ups $[0/90]_{3s}$, and $[45/0]_s$ of graphite/epoxy composite beams under various static deflections.

All assumptions made earlier in Ref. 1 are retained throughout the analysis. They are, the blade itself is long enough to be treated as a one-dimensional model, shear deformation can be neglected, and warping of the cross section of the blade can be neglected. Also, material nonlinearity is not considered here. As indicated by Friedmann in Ref. 6, this model has some limitations since it does not include shear deformation and warping of the blades which may be present to a small extent in realistic helicopter blades. However, it is only a matter of refining to include such structural effects, and for the purposes of current analysis the model is found to be adequate to show the basic characteristics of large amplitude free vibration of

composite helicopter blades.

Chapter 2

Analytic Modeling

2.1 Basic Equations

There are twelve first-order, nonlinear differential equations that describe the statics and dynamics of composite blades completely. For thorough derivation of the equations see Ref. 1. All the equations are derived based on the following transformation matrix that transforms the global coordinate x, y, z into the local one ξ, η, ζ (see figure 1), i. e. ,

$$\begin{aligned} \begin{Bmatrix} \vec{i}_\xi \\ \vec{i}_\eta \\ \vec{i}_\zeta \end{Bmatrix} &= [T] \begin{Bmatrix} \vec{i}_x \\ \vec{i}_y \\ \vec{i}_z \end{Bmatrix} \\ [T] &= \begin{bmatrix} \cos \beta \cos \psi & \cos \beta \sin \psi & \sin \beta \\ -\cos \theta \sin \psi & \cos \theta \cos \psi & \sin \theta \cos \beta \\ -\sin \theta \sin \beta \cos \psi & -\sin \theta \sin \beta \sin \psi & \\ \sin \theta \sin \psi & -\sin \theta \cos \psi & \cos \theta \cos \beta \\ -\cos \theta \sin \beta \cos \psi & -\cos \theta \sin \beta \sin \psi & \end{bmatrix} \end{aligned} \quad (2.1)$$

Here ψ, β, θ are the local Euler angles. The transformation matrix is orthogonal and related to the rotation (or curvature) matrix as follows.

$$[T]^{-1} = [T]^T$$

$$\frac{\partial [T]}{\partial s} = [\kappa] [T] \quad (2.2)$$

with

$$[\kappa] = \begin{bmatrix} 0 & \kappa_\zeta & -\kappa_\eta \\ -\kappa_\zeta & 0 & \kappa_\xi \\ \kappa_\eta & -\kappa_\xi & 0 \end{bmatrix} \quad (2.3)$$

where

$$\kappa_\xi = \frac{\partial \theta}{\partial s} + \sin \beta \frac{\partial \psi}{\partial s} \quad (\text{twist rate})$$

$$\kappa_\eta = -\cos \theta \frac{\partial \beta}{\partial s} + \sin \theta \cos \beta \frac{\partial \psi}{\partial s} \quad (\text{bending about } \eta \text{ axis}) \quad (2.4)$$

$$\kappa_\zeta = \sin \theta \frac{\partial \beta}{\partial s} + \cos \theta \cos \beta \frac{\partial \psi}{\partial s} \quad (\text{bending about } \zeta \text{ axis})$$

Inverting the above differential equation yields

$$\begin{aligned} \frac{\partial \theta}{\partial s} &= \kappa_\xi - \sin \theta \tan \beta \kappa_\eta - \cos \theta \tan \beta \kappa_\zeta \\ \frac{\partial \beta}{\partial s} &= -\cos \theta \kappa_\eta + \sin \theta \kappa_\zeta \\ \frac{\partial \psi}{\partial s} &= \frac{\sin \theta}{\cos \beta} \kappa_\eta + \frac{\cos \theta}{\cos \beta} \kappa_\zeta \end{aligned} \quad (2.5)$$

The global displacements x, y, z are related to Euler angles via

$$\begin{aligned} \frac{\partial x}{\partial s} &= (1 + \epsilon) \cos \beta \cos \psi \\ \frac{\partial y}{\partial s} &= (1 + \epsilon) \cos \beta \sin \psi \\ \frac{\partial z}{\partial s} &= (1 + \epsilon) \sin \beta \end{aligned} \quad (2.6)$$

where ϵ is the axial strain along the reference line. In addition to the above six compatibility equations, one has to consider equilibrium of forces and moments of the

beam. The equilibrium equations can be written either in global or local coordinates. Here they are written in local coordinate in order to take into account the large deformation of the beam in space. The first three differential equations that describe the equilibrium of the local force resultants F_1, F_2, F_3 are

$$\begin{aligned} \frac{\partial F_1}{\partial s} - \kappa_\zeta F_2 + \kappa_\eta F_3 + T_{11} p_x + T_{12} p_y + T_{13} p_z + p_1 &= 0 \\ \frac{\partial F_2}{\partial s} + \kappa_\zeta F_1 - \kappa_\xi F_3 + T_{21} p_x + T_{22} p_y + T_{23} p_z + p_2 &= 0 \\ \frac{\partial F_3}{\partial s} - \kappa_\eta F_1 + \kappa_\xi F_2 + T_{31} p_x + T_{32} p_y + T_{33} p_z + p_3 &= 0 \end{aligned} \quad (2.7)$$

with

\vec{p}_L : applied load vector in local axis = p_1, p_2, p_3

\vec{p}_G : applied load vector in global axis = p_x, p_y, p_z

The other three differential equations describe the equilibrium of the local moment resultants M_1, M_2, M_3 .

$$\begin{aligned} \frac{\partial M_1}{\partial s} - \kappa_\zeta M_2 + \kappa_\eta M_3 + T_{11} m_x + T_{12} m_y + T_{13} m_z + m_1 &= 0 \\ \frac{\partial M_2}{\partial s} + \kappa_\zeta M_1 - \kappa_\xi M_3 + T_{21} m_x + T_{22} m_y + T_{23} m_z + m_2 - F_3 &= 0 \\ \frac{\partial M_3}{\partial s} - \kappa_\eta M_1 + \kappa_\xi M_2 + T_{31} m_x + T_{32} m_y + T_{33} m_z + m_3 + F_2 &= 0 \end{aligned} \quad (2.8)$$

with

\vec{m}_L : applied moment vector in local axis = m_1, m_2, m_3

\vec{m}_G : applied moment vector in global axis = m_x, m_y, m_z

In helicopter problems, generally two kinds of loadings are arised; inertial loads that include normal and angular acceleration, Coriolis acceleration, centrifugal and gravitational forces, and aerodynamic loads that include both steady and unsteady parts. The former group usually appears as the global \vec{p}_G, \vec{m}_G while the latter group appears

as the local \vec{p}_L , and \vec{m}_L . In the present analysis only the normal, angular acceleration and gravitational loads are considered. Hence for a blade without mass centroid offset

$$\begin{aligned}
 p_x &= -m \ddot{x} \\
 p_y &= -m \ddot{y} \\
 p_z &= -m \ddot{z} - mg \\
 m_x &= m_y = m_z = 0
 \end{aligned} \tag{2.9}$$

and

$$\begin{aligned}
 p_1 &= p_2 = p_3 = 0 \\
 m_1 &= -I_p \ddot{\theta} \\
 m_2 &= m_3 = 0
 \end{aligned} \tag{2.10}$$

Finally, a set of generalized stress-strain relations are incorporated via the following six linear equations.

$$\begin{bmatrix} F_1 \\ F_2 \\ F_3 \\ M_1 \\ M_2 \\ M_3 \end{bmatrix} = \begin{bmatrix} E_{11} & E_{12} & E_{13} & E_{14} & E_{15} & E_{16} \\ & E_{22} & E_{23} & E_{24} & E_{25} & E_{26} \\ & & E_{33} & E_{34} & E_{35} & E_{36} \\ & & & E_{44} & E_{45} & E_{46} \\ & \text{SYM} & & & E_{55} & E_{56} \\ & & & & & E_{66} \end{bmatrix} \begin{bmatrix} \epsilon \\ \gamma_{\xi\eta} \\ \gamma_{\xi\zeta} \\ \kappa_\xi \\ \kappa_\eta \\ \kappa_\zeta \end{bmatrix} \tag{2.11}$$

Here $\gamma_{\xi\eta}, \gamma_{\xi\zeta}$ represent the two transverse shear strains. In its most general case, the above stiffness matrix can be full, i. e. there can be couplings between all of three force resultants, three moment resultants and all of six strain components. However in consistency with the earlier assumptions of a Bernoulli-Euler beam, the calculations of the two shear strains are completely ignored during the current analysis.

2.2 Reduction of Basic Equations for Moderate Deflections

Before proceeding with the large amplitude vibration solution of the basic nonlinear equations presented in the previous section, the equations of motion in u , v , w , and ϕ that were derived by Hodges and Dowell, Ref. 4, and Boyd, Ref. 5, for moderate deflections will be rederived from the twelve general nonlinear equations 2.5 through 2.8. Only the case of isotropic blade with no mass centroid offset is considered here for illustration. In this way, the approximations of the moderate deflection analysis can be assessed.

The first step in the reduction process is to rewrite the force and moment equilibrium equations in global x , y , z directions instead of local ξ , η , ζ directions. One can write the local force equilibrium equations 2.7 in vector form as

$$\frac{\partial \vec{F}_L}{\partial s} + [\kappa]^T \vec{F}_L + [T] \vec{p}_G + \vec{p}_L = 0 \quad (2.12)$$

where L , and G refer to local and global components. Multiplying by $[T]^T$ and noting the basic kinematic relations given by equation 2.2 gives,

$$[T]^T \frac{\partial \vec{F}_L}{\partial s} + \frac{\partial [T]^T}{\partial s} \vec{F}_L + \vec{p}_G + [T]^T \vec{p}_L = 0 \quad (2.13)$$

and upon rearranging,

$$\frac{\partial \vec{F}_G}{\partial s} + \vec{p}_{GT} = 0 \quad (2.14)$$

where one has

$$\begin{aligned} \vec{p}_{GT} &= \vec{p}_G + [T]^T \vec{p}_L \\ \vec{F}_G &= [T]^T \vec{F}_L \\ \vec{F}_L &= [T] \vec{F}_G \end{aligned} \quad (2.15)$$

In scalar form, equation 2.14 becomes,

$$\begin{aligned}\frac{\partial F_x}{\partial s} &= -p_x T \\ \frac{\partial F_y}{\partial s} &= -p_y T \\ \frac{\partial F_z}{\partial s} &= -p_z T\end{aligned}\quad (2.16)$$

Similarly, one can write the local moment equilibrium equations 2.8 in vector form as,

$$\frac{\partial \vec{M}_L}{\partial s} + [\kappa]^T \vec{M}_L + [T] \vec{m}_G + \vec{m}_L + \begin{Bmatrix} 0 \\ -F_3 \\ F_2 \end{Bmatrix} = 0 \quad (2.17)$$

Applying the same transformations as for the force equilibrium equations results in,

$$\frac{\partial \vec{M}_G}{\partial s} + \vec{m}_{GT} + [T]^T \begin{Bmatrix} 0 \\ -F_3 \\ F_2 \end{Bmatrix} = 0 \quad (2.18)$$

where one has defined,

$$\begin{aligned}\vec{m}_{GT} &= \vec{m}_G + [T]^T \vec{m}_L \\ \vec{M}_G &= [T]^T \vec{M}_L \\ \vec{M}_L &= [T] \vec{M}_G\end{aligned}\quad (2.19)$$

In scalar form, equation 2.18 becomes

$$\begin{aligned}\frac{\partial M_x}{\partial s} + m_{xT} - T_{21} F_3 + T_{31} F_2 &= 0 \\ \frac{\partial M_y}{\partial s} + m_{yT} - T_{22} F_3 + T_{32} F_2 &= 0 \\ \frac{\partial M_z}{\partial s} + m_{zT} - T_{23} F_3 + T_{33} F_2 &= 0\end{aligned}\quad (2.20)$$

The local force components are related to the global components from equations 2.15 as

$$\begin{aligned}
F_1 &= T_{11} F_x + T_{12} F_y + T_{13} F_z \\
F_2 &= T_{21} F_x + T_{22} F_y + T_{23} F_z \\
F_3 &= T_{31} F_x + T_{32} F_y + T_{33} F_z
\end{aligned} \tag{2.21}$$

One places the above into equations 2.20 and simplifies by using the following relations obtained from noting that $[T]^{-1} = [T]^T$ and applying Cramer's rule with $|T| = 1$.

$$\begin{aligned}
T_{11} &= T_{22} T_{33} - T_{23} T_{32} \\
T_{12} &= T_{23} T_{31} - T_{21} T_{33} \\
T_{13} &= T_{21} T_{32} - T_{22} T_{31}
\end{aligned} \tag{2.22}$$

This will result in the three scalar equations,

$$\begin{aligned}
\frac{\partial M_x}{\partial s} + m_{xT} - T_{13} F_y + T_{12} F_z &= 0 \\
\frac{\partial M_y}{\partial s} + m_{yT} + T_{13} F_x - T_{11} F_z &= 0 \\
\frac{\partial M_z}{\partial s} + m_{zT} - T_{12} F_x + T_{11} F_y &= 0
\end{aligned} \tag{2.23}$$

Taking the derivatives of the last two equations and introducing the force equilibrium equations 2.16 gives

$$\begin{aligned}
\frac{\partial^2 M_y}{\partial s^2} + \frac{\partial m_{yT}}{\partial s} + \frac{\partial}{\partial s}(T_{13} F_x) + T_{11} p_{zT} - F_z \frac{\partial T_{11}}{\partial s} &= 0 \\
\frac{\partial^2 M_z}{\partial s^2} + \frac{\partial m_{zT}}{\partial s} - \frac{\partial}{\partial s}(T_{12} F_x) - T_{11} p_{yT} + F_y \frac{\partial T_{11}}{\partial s} &= 0
\end{aligned} \tag{2.24}$$

In addition to these, it is convenient to keep the local moment equilibrium in the ξ direction,

$$\frac{\partial M_1}{\partial s} - \kappa_\zeta M_2 + \kappa_\eta M_3 + m_{1T} = 0 \tag{2.25}$$

The above moment equations together with the three global force equations 2.16 are the equivalent of equations (71 b, c) (74), and (69 a, b, c) of Hodges and Dowell, Ref.

5. No approximations have been made as yet in equations 2.16, 2.24, 2.25.

The second step in the reduction process is to look at the kinematics and to approximate the Euler angles, ψ and β in terms of global deflections, v and w in the x and y directions respectively. From the kinematic relations equations 2.6, one has

$$\begin{aligned} v' &= \frac{\partial y}{\partial s} = \cos \beta \sin \psi \\ w' &= \frac{\partial z}{\partial s} = \sin \beta \end{aligned} \quad (2.26)$$

where

$$(\quad)' \equiv \frac{\partial(\quad)}{\partial s}$$

and the axial strain ϵ has been neglected relative to unity. These equations give rise to the trigonometric relations, to second order,

$$\begin{aligned} \sin \beta &= w' \\ \cos \beta &\simeq 1 - w'^2/2 \\ \sin \psi &\simeq v' \\ \cos \psi &\simeq 1 - v'^2/2 \end{aligned} \quad (2.27)$$

so that effectively, the two Euler angles β and ψ are approximated to second order as

$$\begin{aligned} \beta &\simeq w' \\ \psi &\simeq v' \end{aligned} \quad (2.28)$$

By differentiating equations 2.27, then solving for β' and ψ' keeping terms only to second order, one obtains the same expressions as would have been obtained by simply differentiating equations 2.28 directly. Finally, substituting the β' and ψ' into the three curvature strains κ_ξ , κ_η , κ_ζ given by equations 2.4 and keeping terms to second order, results in,

$$\begin{aligned}
\kappa_\xi &\simeq \theta' + w' v'' \\
\kappa_\eta &\simeq v'' \sin \theta - w'' \cos \theta \\
\kappa_\zeta &\simeq v'' \cos \theta + w'' \sin \theta
\end{aligned} \tag{2.29}$$

The three curvature strains are now expressed, to second order, in terms of global deflections v , w and Euler rotation angle θ . Often, it is more convenient to express the twisting behavior of the blade in terms of a total twist angle ϕ which is defined as,

$$\phi = \int_0^s \kappa_\xi ds = \theta + \int_0^s w' v'' ds \tag{2.30}$$

In this case, the curvature strain κ_ξ and the Euler angle θ are replaced in equations 2.29 by,

$$\begin{aligned}
\kappa_\xi &= \phi' \\
\theta &= \phi - \int_0^s w' v'' ds
\end{aligned} \tag{2.31}$$

Since the correction to the Euler angle is a small nonlinear term, it is often neglected and the relation $\theta \simeq \phi$ is used.

The second order approximations to the Euler angles as given by equations 2.27 are also used for the general transformation matrix $[T]$. Placing these trigonometric relations into the basic transformation matrix $[T]$, equation 2.1 gives to second order,

$$[T] \simeq \begin{bmatrix} 1 - v'^2/2 - w'^2/2 & v' & w' \\ -(v' \cos \theta + w' \sin \theta) & \cos \theta (1 - v'^2/2) & \sin \theta (1 - w'^2/2) \\ (v' \sin \theta - w' \cos \theta) & -\sin \theta (1 - v'^2/2) & \cos \theta (1 - w'^2/2) \end{bmatrix} \tag{2.32}$$

The third step in the reduction process is to relate the moment resultants to the curvature strains, and then to the coordinates v , w , θ . Using the generalized linear stress-strain relations given in equation 2.11 and introducing the strain-displacement relations of equations 2.29, one may write,

$$\begin{aligned} M_1 &= E_{44} \kappa_\xi \simeq GJ(\theta' + w'v'') \\ M_2 &= E_{55} \kappa_\eta \simeq EI_\eta(v'' \sin \theta - w'' \cos \theta) \\ M_3 &= E_{66} \kappa_\zeta \simeq EI_\zeta(v'' \cos \theta + w'' \sin \theta) \end{aligned} \quad (2.33)$$

The above are for a blade principal axis system located along the elastic axis, where there is no coupling between the ξ , η , and ζ axes. For non-principal axes, there may be additional couplings between η and ζ and for non-elastic axis, such as in composite blades, there may be additional couplings between the ξ and η and ξ and ζ curvatures. For use in the equilibrium equations 2.24, it is also required to express the moments in global x , y , z directions in addition to the local ξ , η , ζ directions given by equations 2.33. From equations 2.19, one has

$$\begin{aligned} M_x &\equiv T_{11}M_1 + T_{21}M_2 + T_{31}M_3 \\ M_y &\equiv T_{12}M_1 + T_{22}M_2 + T_{32}M_3 \\ M_z &\equiv T_{13}M_1 + T_{23}M_2 + T_{33}M_3 \end{aligned} \quad (2.34)$$

This gives, to second order,

$$\begin{aligned} M_y &= GJ\theta'v' - (EI_\zeta \sin^2 \theta + EI_\eta \cos^2 \theta)w'' \\ &\quad - (EI_\zeta - EI_\eta) \cos \theta \sin \theta v'' \\ M_x &= GJ\theta'w' + (EI_\zeta \cos^2 \theta + EI_\eta \sin^2 \theta)v'' \\ &\quad + (EI_\zeta - EI_\eta) \cos \theta \sin \theta w'' \end{aligned} \quad (2.35)$$

M_x is not given above, since in the present formulation, the local moment M_1 is used rather than the global moment M_x .

Finally, to complete the reduction process, one places the moments equations 2.35, 2.33 and curvature strains equation 2.29 into the equilibrium equations 2.24, 2.25 to obtain,

$$\begin{aligned}
 & [GJ \theta' v' - (EI_\zeta \sin^2 \theta + EI_\eta \cos^2 \theta) w'' - (EI_\zeta - EI_\eta) \cos \theta \sin \theta v'']'' \\
 & + (w' F_x)' + (1 - v'^2/2 - w'^2/2) p_{zT} - F_z (v' v'' + w' w'') + m'_{yT} = 0 \\
 & [GJ \theta' w' + (EI_\zeta \cos^2 \theta + EI_\eta \sin^2 \theta) v'' + (EI_\zeta - EI_\eta) \cos \theta \sin \theta w'']'' \\
 & - (v' F_x)' + (1 - v'^2/2 - w'^2/2) p_{yT} + F_y (v' v'' + w' w'') + m'_{zT} = 0 \quad (2.36) \\
 & [GJ (\theta' + w' v'')] - (EI_\zeta - EI_\eta) [(w''^2 - v''^2) \cos \theta \sin \theta + v'' w'' \cos 2\theta] \\
 & + m_{1T} = 0
 \end{aligned}$$

The force loadings F_x , F_y , F_z in the above are found from integrating the global force equations 2.16. For free vibrations, the inertial loadings p_x , p_y , p_z and m_1 are given by equations 2.9 and 2.10.

Although the above equations have been reduced formally to second order, some further simplifications are still made to reduce them to a simpler form. First, as mentioned in Ref. 4, by integrating the third equation, then multiplying it by v' , then subtracting it from the first equation, one can eliminate the $GJ \theta' v'$ term, introducing only new third order terms from the third equation. Hence, to second order, the $GJ \theta' v'$ term can be neglected. Similarly for the $GJ \theta' w'$ term in the second equation. Next, the v'^2 and w'^2 terms can be neglected compared to unity for moderate deflection slopes. This would also eliminate the F_y and F_z terms since they were multiplied by $\frac{\partial T_{11}}{\partial s}$ and T_{11} is now set equal to unity as seen in equation 2.32. Along the same lines, all derivatives

$$\frac{\partial}{\partial s}$$

in these equations can be replaced by

$$\frac{\partial}{\partial x}$$

since from the kinematic relations, equations 2.6,

$$\frac{\partial}{\partial s} = \frac{\partial}{\partial x} \frac{\partial x}{\partial s} \simeq (1 - w^2/2 - v^2/2) \frac{\partial}{\partial x} \simeq \frac{\partial}{\partial x} \quad (2.37)$$

Also, it is convenient to introduce the total twist variable ϕ as defined by equation 2.30 rather than deal with the Euler angle θ . With these simplifications, the previous equations can be rewritten as,

$$\begin{aligned} w : \quad & [(EI_\zeta \sin^2 \theta + EI_\eta \cos^2 \theta) w'' + (EI_\zeta - EI_\eta) \cos \theta \sin \theta v'']'' \\ & -(w' F_x)' = p_{xT} + m'_{vT} \\ v : \quad & [(EI_\zeta \cos^2 \theta + EI_\eta \sin^2 \theta) v'' + (EI_\zeta - EI_\eta) \cos \theta \sin \theta w'']'' \\ & -(v' F_x)' = p_{vT} - m'_{vT} \end{aligned} \quad (2.38)$$

$$\begin{aligned} \phi : \quad & -(GJ \phi')' + (EI_\zeta - EI_\eta) [(w''^2 - v''^2) \cos \theta \sin \theta + v'' w'' \cos 2\theta] \\ & = m_{1T} \end{aligned}$$

where one has,

$$\begin{aligned} \theta & \simeq \phi - \int_0^x w' v'' dx \\ F_x & \simeq + \int_x^L p_{xT} dx \\ \epsilon & \simeq u' + v^2/2 + w^2/2 = 0 \end{aligned} \quad (2.39)$$

Equations 2.38 are effectively the nonlinear moderate deflection equations presented by Hodges and Dowell, Ref. 4, Boyd, Ref. 5, and others. They have been shown to arise from a straightforward reduction of the general nonlinear, large deflection equations given by Minguet and Dugundji, Ref. 1, and presented here in section 2.1. Often, the relation $\theta \simeq \phi$ is used in place of the more accurate relation given by equations 2.39. The $\epsilon = 0$ relation of equations 2.39 represents an effective no stretch condition and is used to determine the axial deflection u since v and w deflections have been determined. For vibration problems the inertia loadings are given by equations 2.9 and 2.10 with $-I_p \ddot{\theta}$ replaced by $-I_p \ddot{\phi}$.

One last item of reductions of these equations comes about by eliminating the trigonometric functions in them. For a flat blade without built-in twist, $\theta_i = 0$, the trigonometric functions can be expanded to second order as,

$$\begin{aligned}\sin \theta &\simeq \theta \\ \cos \theta &\simeq 1 - \theta^2/2\end{aligned}\quad (2.40)$$

Placing these into the previous equations 2.38 gives the more useful form,

$$\begin{aligned}w : & [(EI_\eta w'' + (EI_\zeta - EI_\eta)(v''\theta + w''\theta^2)]'' \\ & -(w' F_x)' = p_{zT} + m'_{vT} \\ v : & [EI_\zeta v'' + (EI_\zeta - EI_\eta)(w''\theta - v''\theta^2)]'' \\ & -(v' F_x)' = p_{vT} - m'_{zT}\end{aligned}\quad (2.41)$$

$$\begin{aligned}\phi : & -(GJ \phi')' + (EI_\zeta - EI_\eta)[(w''^2 - v''^2)\theta + v'' w''] \\ & = m_{1T}\end{aligned}$$

This form shows more clearly the type of nonlinear couplings involved between the w , v , and ϕ motions. These nonlinear couplings depend on the difference in bending stiffness, $(EI_\zeta - EI_\eta)$, and would give rise to linear couplings by the presence of an initial static deflection in w and v . Similar equations can be obtained for blades with an initial twist θ_i , by replacing equations 2.40 with,

$$\begin{aligned}\sin(\theta_i + \theta) &\simeq \sin \theta_i + \theta \cos \theta_i - (\theta^2/2)\sin \theta_i \\ \cos(\theta_i + \theta) &\simeq \cos \theta_i - \theta \sin \theta_i - (\theta^2/2)\cos \theta_i\end{aligned}\quad (2.42)$$

Although the moderate deflection equations 2.41 lend themselves well to Galerkin solution, one should be careful to use a sufficient number of modes to capture the nonlinear effects when static deflections are present. They can always be checked against the general solution of the twelve nonlinear differential equations presented by Minguet and Dugundji, Ref. 1.

Before leaving this section, it might be interesting to note that the moderate deflection equations can also be derived from an energy formulation by minimizing the total potential energy Π of the functional,

$$\begin{aligned}
 \Pi = & \frac{1}{2} \int_0^L EI_\eta (w'' \cos \theta - v'' \sin \theta)^2 dx \\
 & + \frac{1}{2} \int_0^L EI_\zeta (w'' \sin \theta + v'' \cos \theta)^2 dx \\
 & + \frac{1}{2} \int_0^L GJ (\theta' + w' v'')^2 dx \\
 & + \frac{1}{2} \int_0^L F_x (w'^2 + v'^2) dx \\
 & - \int_0^L (p_{vT} v + p_{xT} w - m_{vT} w' + m_{xT} v' + m_{1T} \phi) dx
 \end{aligned} \tag{2.43}$$

A simple application of variational methods will lead to the moderate deflection equations given by equations 2.38 and 2.41.

2.3 Modeling of Large Amplitude Motion

In Ref. 1, the basic equations given in section 2.1 were linearized around a given static position to yield a small, perturbed free vibration. An appropriate eigenvalue problem was then solved to find the various mode shapes and their associated natural frequencies. This eigenanalysis is not useful for large amplitude motion because once structural nonlinearities are present in both static and dynamic sense, the natural frequency of a particular mode becomes a function of amplitude of that mode. Furthermore, it is also expected that certain amount of couplings exist between the static and dynamic components in the various variables. Thus two basic characteristics that distinguish the nonlinear, large amplitude vibration from the linear, small vibration can be summarized as follows.

- (1) The natural frequency of a particular mode changes as its amplitude increases.
- (2) The static mean position of the beam can also change as a function of amplitude.

Two popular methods for the solution of general nonlinear dynamic problems are direct numerical time integration of the basic equations, and the harmonic balance

method. The former method will give the exact solution which shows the effects of all possible harmonics, while the latter method will yield a solution with only few harmonics. The direct time integration requires a set of governing equations that contain only time t as independent variable. By performing appropriate modal analysis, one has to reduce the equations of motion into a modal form, expressing them as functions of generalized coordinates. Usually, a large amount of computing time is used until the solutions reach their final steady states.

In the present analysis, the harmonic balance method is used because we do not want to begin with a set of approximate modal equations which are based on an ordering scheme, but rather use the large deflection equations of section 2.1. These twelve differential equations contain all the twelve variables, i. e. three Euler angles, three force resultants and three moment resultants, in addition to the usual three displacements x, y, z as their independent variables. In such a situation, it is more insightful to assume the time dependency of the solution in the the form $\sin \omega t$, and use numerical integration in space rather than in time. In doing so one loses, of course, the effects of higher harmonics, but the key arguement is that in most of the nonlinear analysis, amplitudes associated with the first harmonic take the largest quotient, and therefore are most critical in determining its response or stability.

Thus for the purpose of present analysis, all quantities are assumed to be of the following form

$$X(\omega, t) = X_0(\omega) + X_s(\omega) \sin \omega t$$

where X_0, X_s represent the static part and the associated amplitude (not a small quantity) around that static part, respectively. The fact that X_s is not a small quantity is reflected in the frequency dependency of both X_0 and X_s . Hence, unlike small vibration problem, there exists one-to-one correspondence between amplitude and frequency.

The analytic modeling consists of substituting the above expression for each variable into the twelve governing equations. As a result of multiplications involving

$\sin \omega t$, this will produce many higher order terms containing higher harmonics such as $\sin 2\omega t$, $\sin 3\omega t$. For details of how these multiplications are performed and what the resulting coefficients are, see the Appendices. A harmonic balance method is then employed to retain only two kinds of terms; the ones that are constants and the ones that are coefficients of $\sin \omega t$. All the higher harmonic terms are left out. Some of the remaining terms will contain higher order of magnitude terms, for example, $\sin^4 \omega t$ produces the constant $3/8$ even after neglecting its higher harmonic components $\cos 2\omega t$ and $\cos 4\omega t$. It is clear that keeping all these higher order of magnitude terms will make the equations extremely long and unwieldy. Hence, an ordering scheme that keeps magnitudes of up to third order is employed to maintain a consistent level of nonlinearities in all of the equations. See the Appendices. It is emphasized that this ordering scheme does not mean

$$\cos \theta \sim 1 - \frac{\theta^2}{2} + \text{H. O. T.}$$

but rather

$$\begin{aligned} \cos \theta \sim & \cos \theta_0 - \sin \theta_0 \Delta\theta - \frac{1}{2} \cos \theta_0 (\Delta\theta)^2 \\ & + \frac{1}{6} \sin \theta_0 (\Delta\theta)^3 + \text{H. O. T.} \end{aligned}$$

where $\theta = \theta_0 + \Delta\theta$, and the θ_0 and $\Delta\theta = \theta, \sin \omega t$ represent the static and dynamic components of θ . So the complete nonlinearity in the large rotations is still kept in a static sense, but as a strategy, terms only up to third order are kept in the dynamic counterparts.

One point is noted here; applying the harmonic balance followed by the approximating schemes will not render the final twenty four equations completely compatible with each other. More specifically, these coupled equations would not satisfy equilibrium, geometric compatibilities, and stress-strain relations perfectly as their original

twelve versions would. Therefore, one should expect deterioration in the degree of compatibility as amplitudes increase. Normally this would mean loss of accuracy in the solutions, or in the worst case, even the loss of convergence. However, as shown later in this report, this does not impose serious computational limits in most of practical range of amplitudes.

Chapter 3

Method of Solution

Having obtained all the necessary formulations for the large amplitude, nonlinear free vibration model, one can express the equations of section 2.1 in vector form

$$\frac{dX_0}{ds} = g_0(X_0, X_s, \omega) \quad (3.1)$$

(12 × 1) (12 × 1)

and

$$\frac{dX_s}{ds} = g_s(X_0, X_s, \omega) \quad (3.2)$$

(12 × 1) (12 × 1)

where

$$X_0 = [F_{10} F_{20} F_{30} M_{10} M_{20} M_{30} x_0 y_0 z_0 \theta_0 \beta_0 \psi_0]^T$$
$$X_s = [F_1, F_2, F_3, M_1, M_2, M_3, x, y, z, \theta, \beta, \psi_s]^T$$

The two vector function arrays g_0 and g_s contain many product terms involving multiplications of two, or three harmonic quantities. They, of course, originate from the twelve basic equations that are presented in section 2.1. Multiplications of harmonics and calculations of the coefficients of the resulting new harmonics can be easily implemented according to the formulae in the Appendices.

To solve this system, all of the twenty four equations (now twelve for the static part, twelve for the dynamic part) are first integrated from the tip to the root of the

blade once. In the previous TELAC report Ref. 1, Minguet used a finite-difference iteration method for the solution of static deformation, sweeping from the tip to the root and vice versa a few times until all the residues become very small. When applying this scheme to the solution of mode shapes and their frequencies, one has to be cautious because this finite-difference iteration will usually converge to the first mode only. To obtain higher modes, one must consider other integration techniques which do not sweep back and forth along the span but are more appropriate for boundary value type problems. Among such, Runge-Kutta integration is frequently used and very effective. Currently fourth order Runge-Kutta algorithm is used.

In the early step of numerical integration, one has to guess boundary values of displacements and rotations at the tip as well as the frequency that will make, for a given mode shape, all the displacements and rotations at the root as close to the prescribed values as possible. For instance, a linear solution by Minguet can provide such a good guess for tip values X_t . The functional relationships between these two sets of boundary values at the root and at the tip can be written as

$$X_r = f(X_t, \omega) \quad (3.3)$$

$$(12 \times 1) \quad (12 \times 1)$$

where

$$X_t = [x_0 \ x, y_0 \ y, z_0 \ z, \theta_0 \ \theta, \beta_0 \ \beta, \psi_0 \ \psi_s]^T$$

at the tip, and

$$X_r = [0 \ 0 \ 0 \ 0 \ 0 \ \theta_0 \ 0 \ \beta_0 \ 0 \ \psi_0 \ 0]^T$$

at the root.

Here $\theta_0, \beta_0, \psi_0$ are prescribed values at the root (they are zero for flat cantilever blades). Since the initial guess for the twelve components of X_t can not be perfect, there will be nonzero residues R by the time the integration reaches the root. A Newton-Raphson type algorithm can then be used to produce a better set of boundary

values based on the current values. This will produce a series of the following set of boundary values.

$$X_i^{n+1} = X_i^n - J(X_i^n, \omega^n)^{-1} R^n \quad (3.4)$$

where

$$R^n \equiv f(X_i^n, \omega^n) - X_r$$

and

J : (12 × 12) Jacobian matrix

Here the superscript n refers to the n th iterative values, and X_r refers to the desired values at the root. The n th boundary values X_i^n at the tip will eventually march to the true solution, provided it exists. Currently two algorithms called F. D. G. (finite difference Gauss' method) and F. D. L. M. (finite difference Levenberg-Marquardt method) (Ref. 7), respectively are used. The former is simply a numerical version of Newton-Raphson method, and in the latter case, an efficient relaxation scheme is added.

It is noted that whatever algorithm is used, it must take iterations on the frequency as well as the boundary values, since it is not known in advance at which frequency a mode will happen for a given amplitude level. Therefore, one of the six boundary amplitudes at the tip $x_s, y_s, z_s, \theta_s, \beta_s, \psi_s$, is replaced by the frequency ω , and the replaced displacement is fixed throughout iterations. Which one has to be fixed depends on which mode is being sought. For instance, if bending modes are of concern it will be z_s ; if it is torsional modes then θ_s is fixed. The iteration will march until the boundary conditions at the root are met, i. e. , the residues R^n are zeros or at least less than some preset ϵ where $\epsilon \ll 1$.

As a final notion, the above solution procedure, when applied to linear problems, is similar to the so called transfer matrix technique used to obtain helicopter blade vibration modes by Isakson and Eisley in Ref. 8.

Chapter 4

Results and Discussion

The prescribed algorithms have been used to investigate the first and second bending modes, first fore-and-aft modes, and first torsion modes of cantilevered blades with the lay-ups $[0/90]_{3s}$, $[45/0]_s$ of graphite/epoxy for various tip deflections. These modes were chosen because they have the lowest natural frequencies and hence should be easily converged. Furthermore, they pose much importance from a aeroelastic point of view. The configurations of the blades investigated are those used by Minguet in Ref. 1 (560 mm long, 30 mm wide). Beam material properties of these lay-ups are listed on Table 1. To see how these coefficients are calculated, refer to section 2.6 of Ref. 1.

The static deflections were varied by imposing and adjusting uniform gravity level throughout the blade. As stated earlier, one of the six boundary amplitudes at the tip was replaced by ω , and the replaced amplitude was fixed throughout the iterations. The z_s , y_s , and θ_s were fixed for bending, fore-and-aft, and torsional modes, respectively. Also, $\theta_0, \beta_0, \psi_0$, at the root were all set equal to zero since the blade is a flat cantilever beam. A total of 16 node points were used along the blades. Note that the same number of nodes was also used in Ref. 1. All of the cases were guided by the linear results by Minguet. That is, the linear mode shapes and their natural frequencies provide reasonable trial values which, after a few iterations, would lead to nontrivial solutions. All the runs were made on a DEC Microvax computer with typical number of iterations from 5 to 10 for convergence. Each iteration took

approximately between 15 to 30 seconds of CPU time, longer times being required for cases with strong structural couplings. Very often, it was necessary to use under-relaxation to lead iterations smoothly to the final solution without causing divergence or any sudden jump into another nonlinear solution (In fact, both F. D. G. and F. D. L. M. algorithms assume use of certain under-relaxations). Each analysis was continued until the amplitude could not be further increased. At this point, the Jacobian matrix became almost singular and the solution did not converge.

Before illustrating the results in detail it is worthwhile to mention that in linear problems where perturbations are very small, the present analysis would be slightly superior to Ref. 1. The present analysis is based on a continuous model while Ref. 1 is based on a lumped, finite difference model.

The first example is that of the $[0/90]_{3s}$ specimen. Figure 3 through figure 26 show mode shapes at two amplitude levels under three different static tip deflections. It is seen that for most of the amplitude range, the nonlinear modes remain almost the same as linear modes in their shapes even though their frequencies change. Next, figure 27 through 29 show change of natural frequencies as functions of amplitudes $z_s, y_s,$ and θ_s at the tip. Also Figure 30 and 31 represent the variations of the centershifts z_0 at the tip of various modes as functions of the tip amplitudes. From the figures the following two observations can be made.

(1) Increasing amplitude level has slight stiffening effects in 1B, 2B (or any bending modes, presumably) whereas it has significant softening effects in 1F, 1T modes, particularly for moderate range of static tip deflections. As a result, the natural frequencies of bending modes rise slightly with amplitude level while those of 1F and 1T modes always drop.

(2) The above frequency changes are accompanied by centershift changes. Increasing amplitude levels has slight effects on the centershifts of bending modes except for the 2B mode, whereas it has significant centershift increase for the 1F mode and a centershift decrease for the 1T mode, particularly for moderate static tip deflections.

The behavior of these centershift changes seem relevant to the linear findings in Ref. 1 (see figure 33).

Figure 32 presents the effects of second harmonics on the natural frequencies of 1F modes. It was found that including terms involving the second harmonic $\cos 2\omega t$ in two-dimensional sense was enough to capture the missing second harmonics in 1F modes. In other words, only F_1, F_3, M_2 , and β, x, z were expressed in the form

$$X(\omega, t) = X_0(\omega) + X_s(\omega) \sin \omega t + X_{2c}(\omega) \cos 2\omega t$$

with all other variables containing only the first harmonics as before. This was done based on the intuition that second harmonics will mostly appear in x_s, z , and their motion should be initially 90 degrees out of phase with the rest of amplitudes. Then a new set of formulae that performs multiplications of harmonics was implemented in the computer program. These are different from the previous ones in the appendix in that they now have to deal with $\cos 2\omega t$ as well. The resulting Jacobian is then (15×15) instead of (18×18) which would result if $\cos 2\omega t$ were introduced in all of the variables. As can be seen from the plots, 1F modes exhibit significant second harmonic contents in z_s motion for moderate range of static tip deflections (roughly, from 20 mm to 80 mm.) as amplitude is increased. On the other hand, at either zero or very large tip deflection the second harmonics are almost unrecognizable. In fact, z_s has no first harmonic content in 1F modes. An effort was also made to seek for any second harmonics in 1T, 1B and 2B bending modes, but they have been found very weak and are not presented here.

Next example is that of $[45/0]_s$, which, unlike the previous case, exhibit bending-torsion coupling. Due to the structural coupling, computer time was increased and the convergence became more sensitive. This resulted in earlier breakdown of nonsingularity of Jacobian matrix which in turn caused shorter range of solutions available as functions of amplitudes. Figure 34 through 57 show mode shape changes at two amplitude levels under three different tip deflections. Once again, the mode shapes do not change significantly from the linear modes. Figure 58 through 62 show the

frequency and centershift changes as the amplitudes of various modes increase. The two former observations (1) and (2) can also be made in these figures; a similar analogy about the relationship between frequency and centershift changes can be also made. The effects of second harmonics on the natural frequencies of 1F modes is shown in figure 63. Unlike the previous case of $[0/90]_{3s}$, the presence of second harmonics is relatively weak. In particular, due to the existing bending-torsion coupling, the static tip deflection will not lie on the z axis, and the 1F motion is not symmetric about the z axis even though the root angles here are again zeros.

Finally, it is interesting to consider what makes the Jacobian matrix singular at a certain point along the way of increasing amplitude. Except for the cases of 1B, there seem to be certain limits on the largest amplitudes that can be solved by the current algorithms. These limits were even more severe if second harmonics were included. In section 2.3, it was suggested that one should expect deterioration in the degree of compatibility as amplitudes increase. This could be one possibility. Apart from that, other factors may attribute to the singularity of solution; the round-off errors associated with the large size of Jacobian matrix, and the interaction of several modes as amplitudes increase, with possible resulting chaotic vibration.

Chapter 5

Conclusion

Throughout the research period, it has been demonstrated that the nonlinear analysis derived from work by Minguet in Ref. 1, and iteration methods based on harmonic balance and numerical integration of the basic equations seems efficient for large amplitude vibration problems of composite rotor blades. These include the nonlinear free vibration problem which is presented here, and nonlinear limit cycle problems with dynamic stall in hover and possibly in forward flight, which will be investigated as parts of future work.

For the free vibration part, it has been shown that both large static deflection and large amplitude can affect significantly the fore-and-aft modes and torsion modes, but not much the bending modes. More specific conclusions are as follows.

- (1) Increasing amplitude level has slight stiffening effects in bending modes whereas it has significant softening effects in 1F, 1T modes, particularly for moderate range of static tip deflections. As a result, the natural frequencies of bending modes rise slightly while those of 1F and 1T modes always drop.
- (2) Increasing amplitude level of a particular mode also results in centershift changes that are small for the bending modes but significant for the 1F and 1T modes, particularly for moderate static tip deflections. The 1F centershift seems to increase considerably with amplitude level. The behavior of these centershift changes seem to stem from the linear findings in Ref. 1.
- (3) The flat $[90/0]_3$, or any isotropic blade with zero root angle has significant second

harmonic contents in the 1F mode for moderate static tip deflections. These appear mostly in the bending amplitude z_s . If the root angle is not zero, or there is bending-torsion coupling however, the second harmonics are not as strong.

The conclusions made during the research period should give insight into more general nonlinear, large amplitude analysis such as proposed by Dugundji (Ref. 9) for future investigation.

Regarding the future work which is specified in Ref. 9, nonlinear limit cycle analysis of composite blades in the presence of dynamic stall is currently being pursued. The structural nonlinearities are well represented by the current model, and for the aerodynamic nonlinearity, the ONERA model developed by Tran and Petot in Ref. 10 is used. The analysis begins with a simple two-dimensional motion with bending modes only (called "bending stall"), and later will go into three-dimensional motion with additional torsion and fore-and-aft modes as well as centrifugal forces, Coriolis acceleration, and coning angles also present.

Bibliography

- [1] Minguet, P.J., "Static and Dynamic Behavior of Composite Helicopter Rotor blades under Large deflection", TELAC Report 89-7A, Department of Aeronautics and Astronautics, M.I.T., Cambridge, Massachusetts, May 1989. Also, Minguet, P.J., and Dugundji, J., "Experiments and Analysis for Composite Blades Under Large Deflections. Part 1: Static Behavior, Part 2: Dynamic Behavior" to be published in AIAA Journal, about September 1990.
- [2] Chopra, I., and Dugundji, J., "Non-linear Dynamic Response of a Wind Turbine Blade", Journal of Sound and Vibration, Vol. 63, 1979, pp. 265-286.
- [3] Dunn, P.E., "Stall Flutter of Graphite/Epoxy Wings with Bending-Torsion Coupling", TELAC Report 89-5, Department of Aeronautics and Astronautics, M.I.T., Cambridge, Massachusetts, May 1989. Also, Dunn, P.E., and Dugundji, J., "Nonlinear Stall Flutter and Divergence Analysis of Cantilevered Graphite/Epoxy Wings", 31st AIAA/ASME/ASCE/AHS/ACE Structures, Structural Dynamics and Material Conference, Long Beach, CA, April 2-4 1990 AIAA Paper No. 90-0983.
- [4] Hodges, D.H., and Dowell, E.H., "Nonlinear Equations of Motion for the Elastic Bending and Torsion of Twisted Non-uniform Rotor Blades", NASA TN D-7818, December 1974.
- [5] Boyd, W.N., "Effect of Chordwise Forces and Deformations and Deformations due to Steady Lift on Wing Flutter", SUDAAR No. 508, Department of

Aeronautics and Astronautics, Stanford University, Stanford, California, December 1977.

- [6] Friedmann, P.P., "Helicopter Rotor Dynamics and Aeroelasticity: Some Key Ideas and Insights", Vertica, Vol. 14, No. 1, 1990, pp. 101-121
- [7] Brown, K.M., and Dennis, J.E., "Derivative Free Analogues of the Levenberg-Marquardt and Gauss Algorithms for Nonlinear Least Squares Approximation", Numerische Mathematik, 18, pp 289-297, 1972.
- [8] Isakson, G., and Eisley, J.G., "Natural Frequencies in Coupled Bending and Torsion of Twisted Rotating and Nonrotating Blades", NASA CR-65, July 1964.
- [9] Dugundji, J., "Basic Research into Nonlinear Aeroelasticity and Stall Properties of Composite Helicopter Blades", TELAC Proposal submitted to U.S. Army Research Office, Department of Aeronautics and Astronautics, M.I.T., April, 1990.
- [10] Tran, C.T., and Petot, D., "Semi-Empirical Model for the Dynamic Stall of Airfoils in View of their Application to the Calculation of Responses of a Helicopter Rotor in Forward Flight," Vertica, Vol. 5, No. 1, 1981, pp. 35-53.

Appendix A

Calculation of Coefficients of Harmonic Quantities

In section 2.3 it was suggested that for large amplitude motion, every variable be expressed as

$$X(\omega, t) = X_0(\omega) + X_s(\omega) \sin \omega t$$

where X_0, X_s represent the static and dynamic components of a particular variables. As a result, all the quantities in the original twelve governing equations will take the above form immediately. Recall, however, that many of the terms in the equations involve trigonometric functions and their arguments are the three Euler angles ψ, β, θ . Then it is clear that one can not apply harmonic balance method with the Euler angles expressed as above and themselves inside the trigonometric functions. So, it is useful to rely on series expansion versions of these trigonometric functions. In order to get the series expressions, let x represent any of the three Euler angles, and let $X(x)$ be any trigonometric function, i. e. $\cos x$, $\sin x$, $\tan x$, or $1/\cos x$. Then substituting

$$x = x_0 + x_s \sin \omega t$$

into the function X and expanding in a Taylor series about x_0 yields

$$\begin{aligned}
X(x) &= X(x_0) + \frac{dX}{ds}(x_0) x_s \sin \omega t \\
&\quad + 1/2! \frac{d^2 X}{dx^2}(x_0) x_s^2 \sin^2 \omega t + 1/3! \frac{d^3 X}{dx^3}(x_0) x_s^3 \sin^3 \omega t \quad (\text{A.1}) \\
&= X_0 + X_s \sin \omega t \\
&\quad + X_{s,2} \sin^2 \omega t + X_{s,3} \sin^3 \omega t + \text{H. O. T.}
\end{aligned}$$

where

$$X_0 \equiv X(x_0) \quad (\text{A.2})$$

$$X_s \equiv \frac{dX}{dx}(x_0) x_s \quad (\text{A.3})$$

$$X_{s,2} \equiv 1/2! \frac{d^2 X}{dx^2}(x_0) x_s^2 \quad (\text{A.4})$$

$$X_{s,3} \equiv 1/3! \frac{d^3 X}{dx^3}(x_0) x_s^3 \quad (\text{A.5})$$

Here according to our ordering scheme only terms up to third order are kept in the expansion (see section 2.3). Then, when applying harmonic balance methods, the $\sin^2 \omega t$ and $\sin^3 \omega t$ can be expanded into constant and $\sin \omega t$ type terms after multiplication with other harmonic quantities, as shown in Appendices B and C.

In the current analysis four different trigonometric functions are encountered. They are $\cos x$, $\sin x$, $\tan x$, and $1/\cos x$. According to above expansion rules then each trigonometric function can be expressed, up to third order, as

$$\begin{aligned}
\cos x &= \cos x_0 - (\sin x_0) x_s \sin \omega t - 1/2 (\cos x_0) x_s^2 \sin^2 \omega t \\
&\quad + 1/6 (\sin x_0) x_s^3 \sin^3 \omega t \quad (\text{A.6})
\end{aligned}$$

$$\begin{aligned}
\sin x &= \sin x_0 + (\cos x_0) x_s \sin \omega t - 1/2 (\sin x_0) x_s^2 \sin^2 \omega t \\
&\quad - 1/6 (\cos x_0) x_s^3 \sin^3 \omega t \quad (\text{A.7})
\end{aligned}$$

$$\begin{aligned} \tan x = & \tan x_0 + (1/\cos^2 x_0) x_1 \sin \omega t + (\tan x_0/\cos^2 x_0) x_1^2 \sin^2 \omega t \\ & + 1/3((2 \tan^2 x_0 + 1/\cos^2 x_0)/\cos^2 x_0) x_1^3 \sin^3 \omega t \end{aligned} \quad (\text{A.8})$$

$$\begin{aligned} 1/\cos x = & 1/\cos x_0 + (\tan x_0/\cos x_0) x_1 \sin \omega t + 1/2(1/\cos^3 x_0 + \tan^2 x_0/\cos x_0) \\ & \cdot x_1^2 \sin^2 \omega t + 1/6(5 \tan x_0/\cos^3 x_0 + \tan^3 x_0/\cos x_0) x_1^3 \sin^3 \omega t \end{aligned} \quad (\text{A.9})$$

Appendix B

Multiplication of Two Harmonic Quantities

In the previous section it was seen that any harmonic quantity can be expressed, up to third order, as

$$X = X_0 + X_s \sin \omega t + X_{s2} \sin^2 \omega t + X_{s3} \sin^3 \omega t \quad (\text{B.1})$$

where X_0, X_s, X_{s2}, X_{s3} are determined by the formula A.2. $X(x)$ could be either a harmonic variable itself (e.g. F, M, x, \dots etc.) or a trigonometric function. If it is a harmonic variable X_{s2}, X_{s3} are identically zero. Now let's consider a product of two quantities, X and Y which are expressed as above. It can be shown that

$$\begin{aligned} XY &= (X_0 + X_s \sin \omega t + X_{s2} \sin^2 \omega t + X_{s3} \sin^3 \omega t) \\ &\quad \cdot (Y_0 + Y_s \sin \omega t + Y_{s2} \sin^2 \omega t + Y_{s3} \sin^3 \omega t) \\ &= (XY)_0 + (XY)_s \sin \omega t + (XY)_{s2} \sin^2 \omega t + (XY)_{s3} \sin^3 \omega t \end{aligned} \quad (\text{B.2})$$

where

$$\begin{aligned} (XY)_0 &\equiv X_0 Y_0 \\ (XY)_s &\equiv X_0 Y_s + X_s Y_0 \\ (XY)_{s2} &\equiv X_0 Y_{s2} + X_s Y_s + X_{s2} Y_0 \\ (XY)_{s3} &\equiv X_0 Y_{s3} + X_s Y_{s2} + X_{s2} Y_s + X_{s3} Y_0 \end{aligned}$$

When applying harmonic balance method only the static and the first harmonic terms are retained. For this purpose note that

$$\sin^2 \omega t = 1/2 - 1/2 \cos 2\omega t \quad (\text{B.3})$$

$$\sin^3 \omega t = 3/4 \sin \omega t - 1/4 \sin 3\omega t \quad (\text{B.4})$$

So after neglecting higher harmonics one gets

$$XY = [(XY)_0 + 1/2 (XY)_{s2}] + [(XY)_s + 3/4 (XY)_{s3}] \sin \omega t \quad (\text{B.5})$$

Appendix C

Multiplication of Three Harmonic Quantities

Some of the governing equations contain products of three harmonic quantities. Multiplication of three harmonics X, Y, Z can then be performed as a series of two multiplications involving two harmonic quantities as follows.

$$\begin{aligned}XYZ &= (XY)Z \\ &= [(XY)_0 + (XY)_s \sin \omega t + (XY)_{s2} \sin^2 \omega t + (XY)_{s3} \sin^3 \omega t] \\ &\quad \cdot (Z_0 + Z_s \sin \omega t + Z_{s2} \sin^2 \omega t + Z_{s3} \sin^3 \omega t) \quad (C.1) \\ &= (XYZ)_0 + (XYZ)_s \sin \omega t + (XYZ)_{s2} \sin^2 \omega t + (XYZ)_{s3} \sin^3 \omega t\end{aligned}$$

where

$$\begin{aligned}(XYZ)_0 &\equiv (XY)_0 Z_0 \\ (XYZ)_s &\equiv (XY)_0 Z_s + (XY)_s Z_0 \\ (XYZ)_{s2} &\equiv (XY)_0 Z_{s2} + (XY)_s Z_s + (XY)_{s2} Z_0 \\ (XYZ)_{s3} &\equiv (XY)_0 Z_{s3} + (XY)_s Z_{s2} + (XY)_{s2} Z_s + (XY)_{s3} Z_0\end{aligned}$$

and

$$\begin{aligned}(XY)_0 &= X_0 Y_0 \\ (XY)_s &= X_0 Y_s + X_s Y_0\end{aligned}$$

$$(XY)_{s2} = X_0 Y_{s2} + X_s Y_s + X_{s2} Y_0$$

$$(XY)_{s3} = X_0 Y_{s3} + X_s Y_{s2} + X_{s2} Y_s + X_{s3} Y_0$$

as before. Once again, neglecting higher harmonics one gets

$$XYZ = [(XYZ)_0 + 1/2(XYZ)_{s2}] + [(XYZ)_s + 3/4(XYZ)_{s3}] \sin \omega t \quad (C.2)$$

Table 1: Beam Material Properties (AS4/3501-6)

[0/90] ₃ , Laminate			$t = 1.49 \times 10^{-3} \text{ m}$
$m = 0.0683 \text{ kg/m}$	$I_p = 5.13 \times 10^{-6} \text{ kg. m}$		
$E_{11} = 3.68 \times 10^6 \text{ N}$	$E_{22} = 0.26 \times 10^6 \text{ N}$	$E_{33} = 2.9 \times 10^5 \text{ N}$	
$E_{44} = 0.183 \text{ N. m}^2$	$E_{55} = 0.707 \text{ N. m}^2$	$E_{66} = 276 \text{ N. m}^2$	
[45/0] ₃ , Laminate			$t = 1.49 \times 10^{-3} \text{ m}$
$m = 0.0238 \text{ kg/m}$	$I_p = 1.66 \times 10^{-6} \text{ kg. m}$		
$E_{11} = 1.32 \times 10^6 \text{ N}$	$E_{22} = 0.27 \times 10^6 \text{ N}$	$E_{33} = 1.0 \times 10^5 \text{ N}$	
$E_{44} = 0.0195 \text{ N. m}^2$	$E_{55} = 0.0143 \text{ N. m}^2$	$E_{66} = 99.1 \text{ N. m}^2$	
$E_{12} = 1.0 \times 10^6 \text{ N}$	$E_{45} = 0.00632 \text{ N. m}^2$		

Note: in more conventional terms,

$$E_{11} \simeq EA \quad E_{22} \simeq GA_\eta \quad E_{33} \simeq GA_\zeta$$

$$E_{44} \simeq GJ \quad E_{55} \simeq EI_\eta \quad E_{66} \simeq EI_\zeta$$

$$E_{12} \simeq \text{Extension-shear coupling}$$

$$E_{14} \simeq \text{Extension-twist coupling}$$

$$E_{45} \simeq \text{Bending-twist coupling}$$

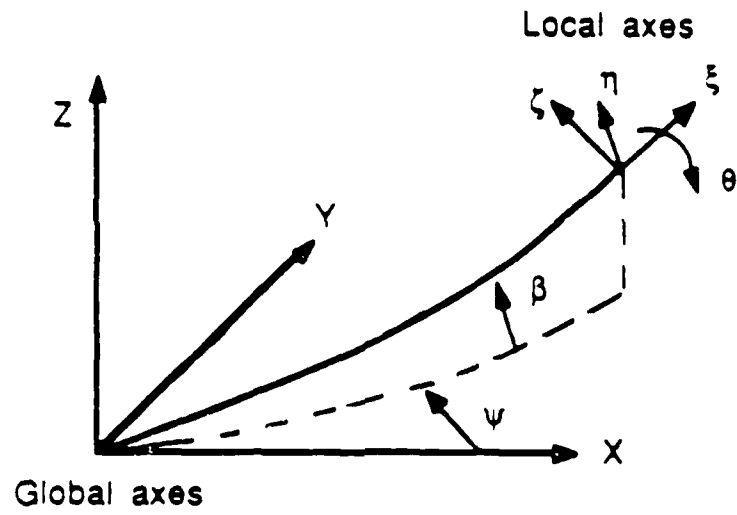


Figure 1: Definition of global and local axes

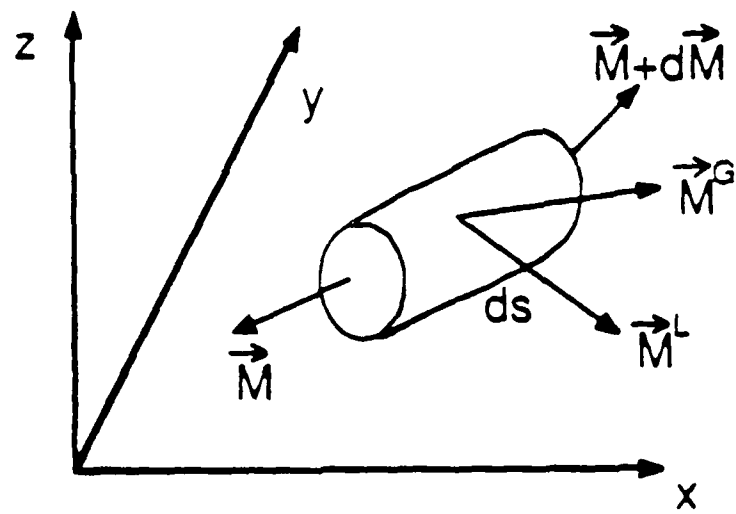
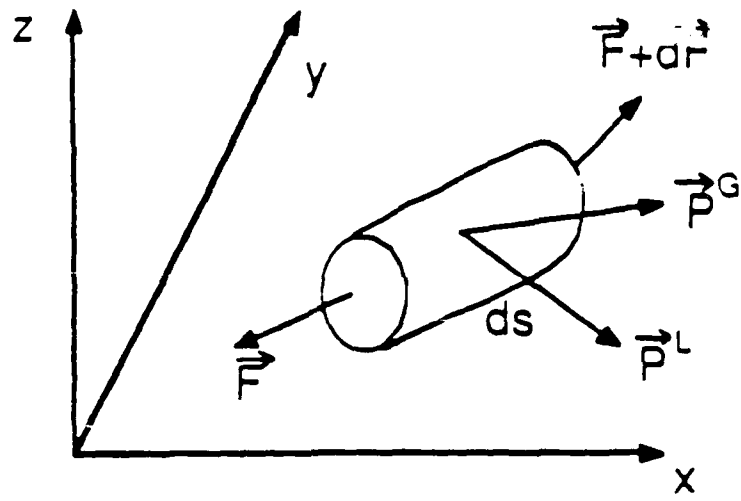


Figure 2: Definition of local internal forces and moments

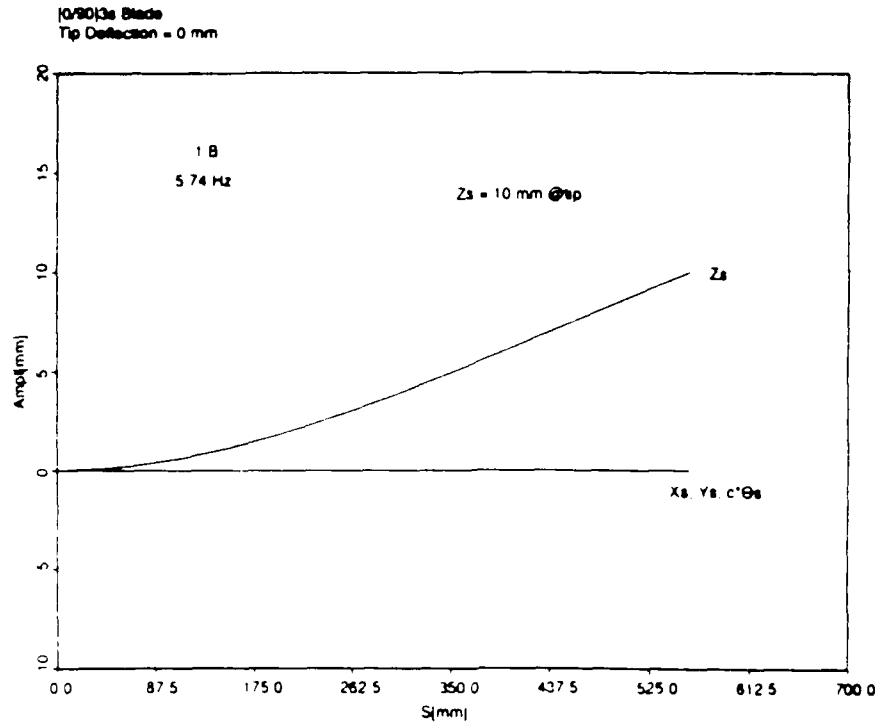


Figure 3: First Bending Mode; [0/90]_{3s}, 0 mm tip deflection, Z_s=10 mm

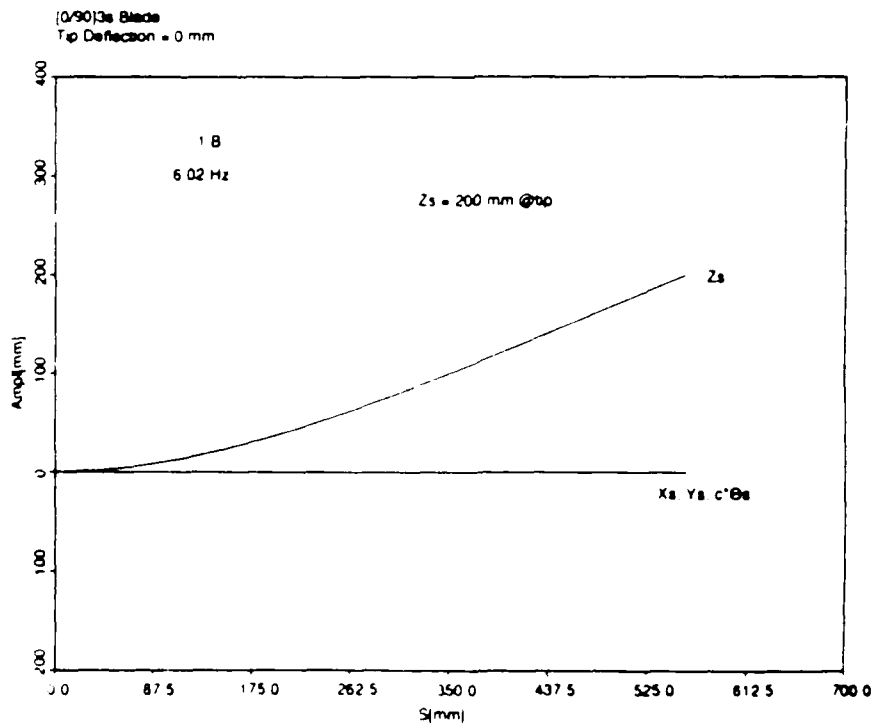


Figure 4: First Bending Mode; [0/90]_{3s}, 0 mm tip deflection, Z_s=200 mm

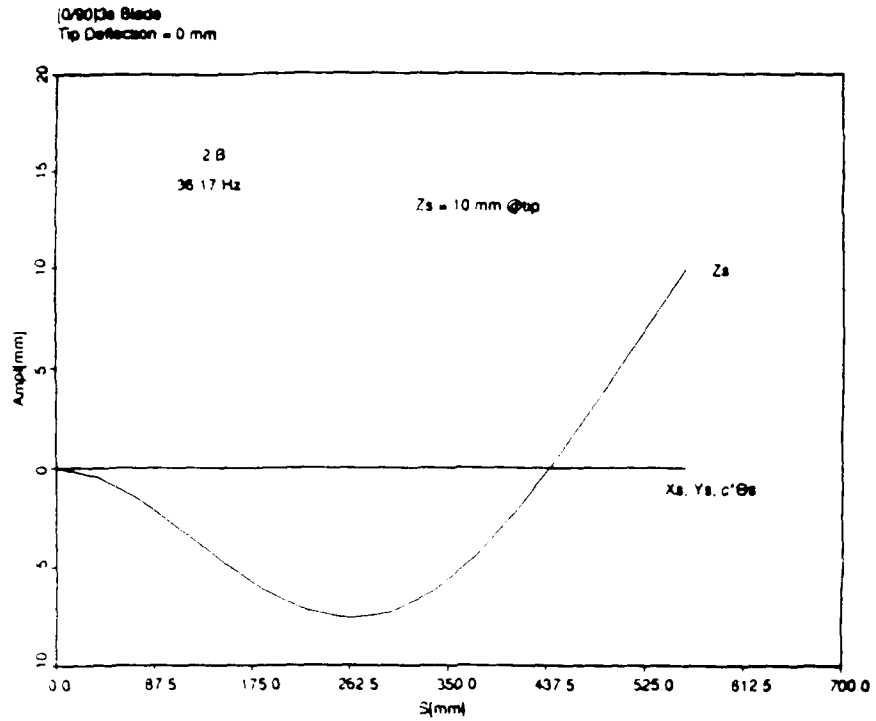


Figure 5: Second Bending Mode; (0/90)_{3s}, 0 mm tip deflection, Zs=10 mm

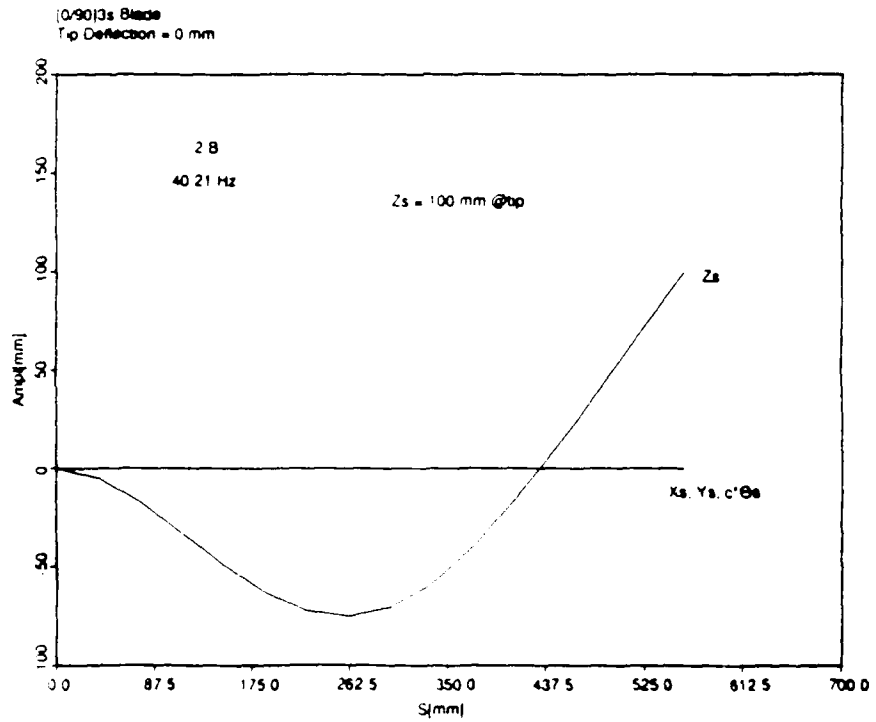


Figure 6: Second Bending Mode; (0/90)_{3s}, 0 mm tip deflection, Zs=100 mm

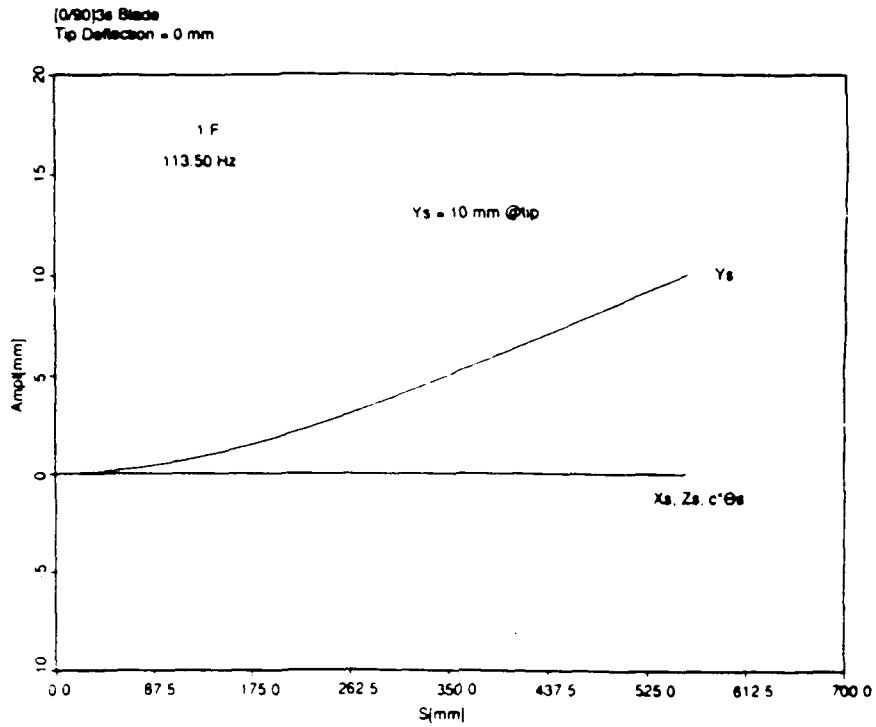


Figure 7: First Fore-and-Aft Mode; [0/90]_{3s}, 0 mm tip deflection, Ys = 10 mm

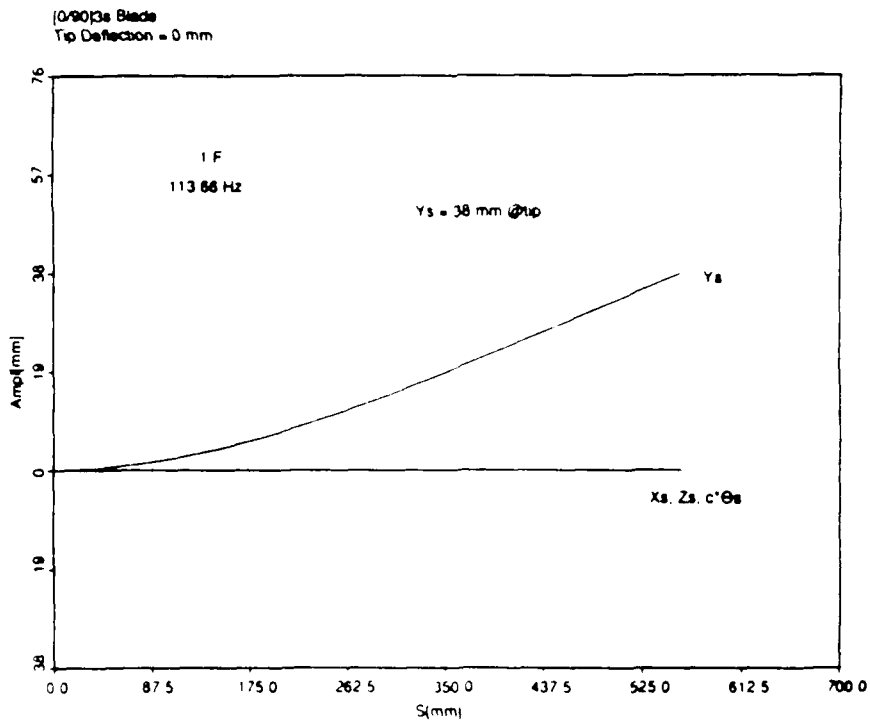


Figure 8: First Fore-and-Aft Mode; [0/90]_{3s}, 0 mm tip deflection, Ys = 38 mm

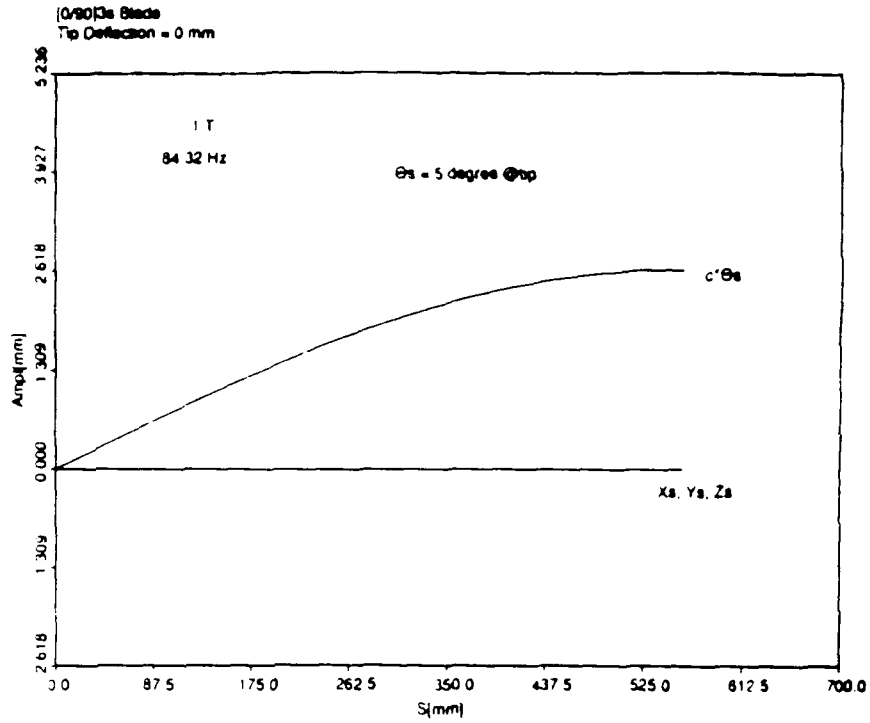


Figure 9: First Torsion Mode; [0/90]_{3s}, 0 mm tip deflection, $\theta_s = 5$ degree

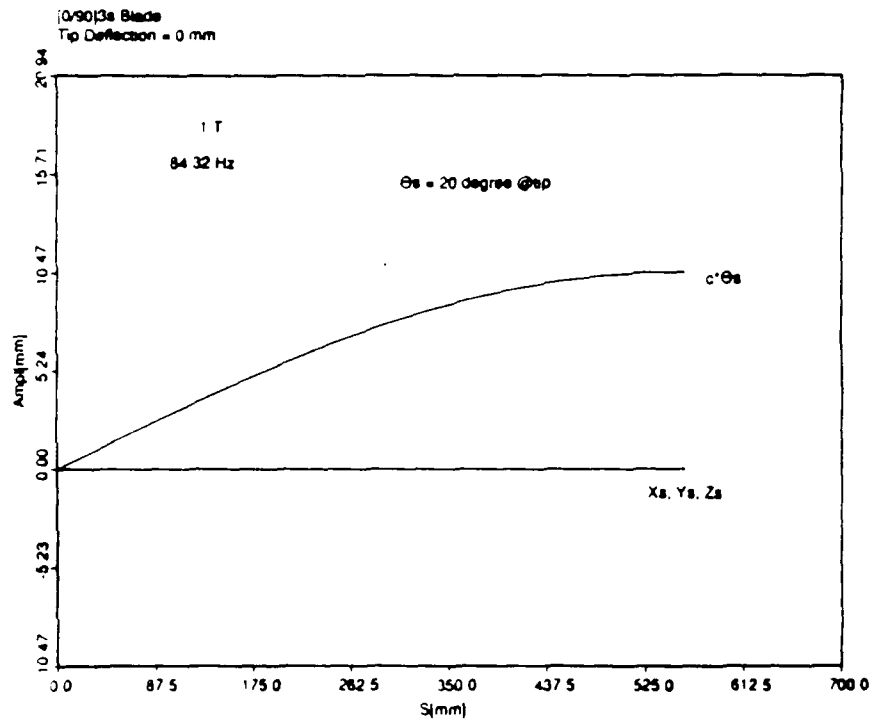


Figure 10: First Torsion Mode; [0/90]_{3s}, 0 mm tip deflection, $\theta_s = 20$ degree

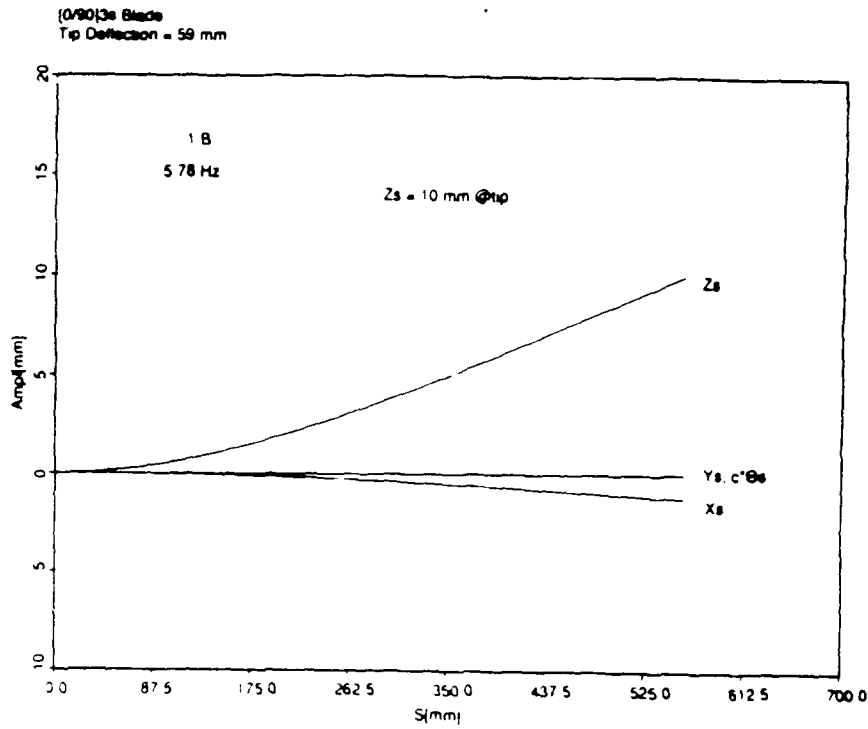


Figure 11: First Bending Mode; [0/90]_{3s}, 59 mm tip deflection, Zs=10 mm

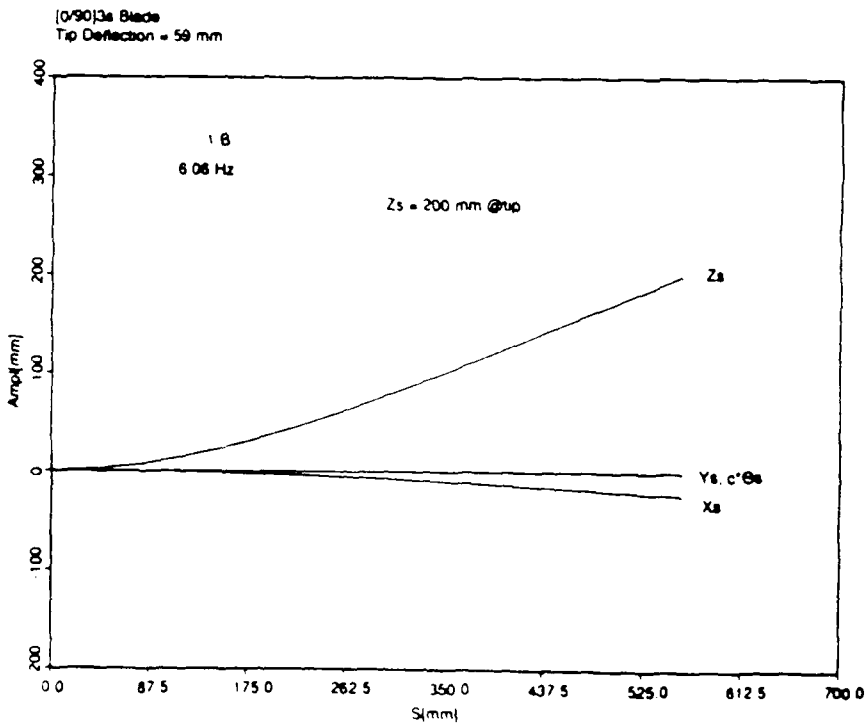


Figure 12: First Bending Mode; [0/90]_{3s}, 59 mm tip deflection, Zs=200 mm

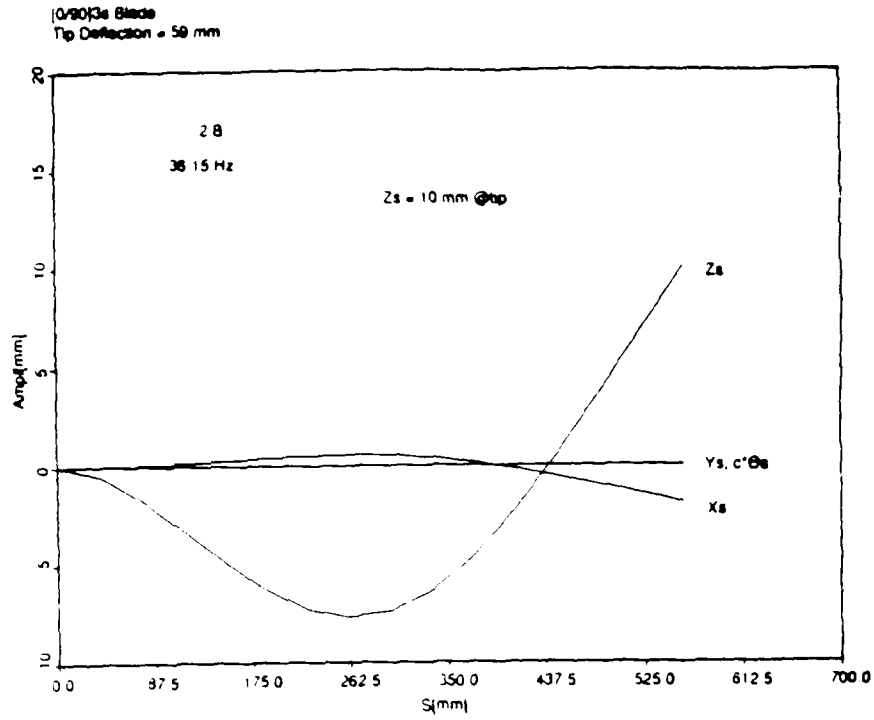


Figure 13: Second Bending Mode; [0/90]_{3s}, 59 mm tip deflection, Zs = 10 mm

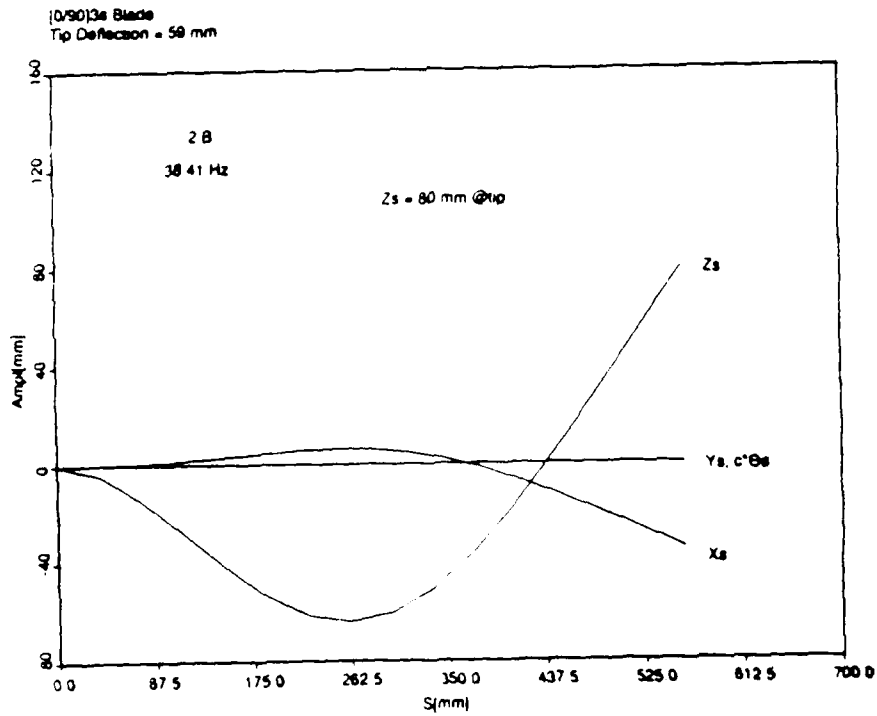


Figure 14: Second Bending Mode; [0/90]_{3s}, 59 mm tip deflection, Zs = 80 mm

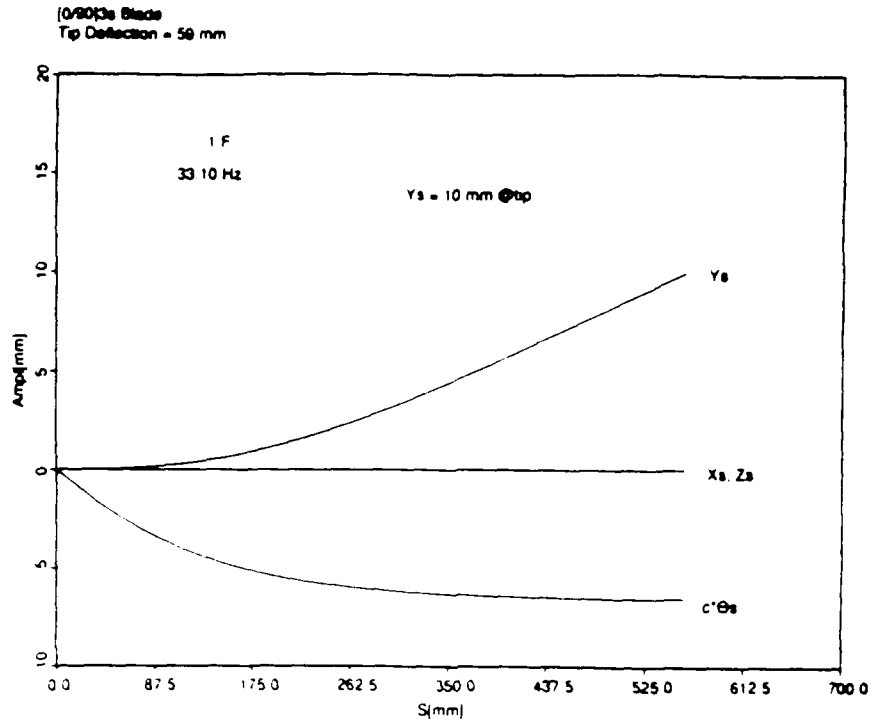


Figure 15: First Fore-and-Aft Mode; (0/90)_{3s}, 59 mm tip deflection, Ys=10 mm

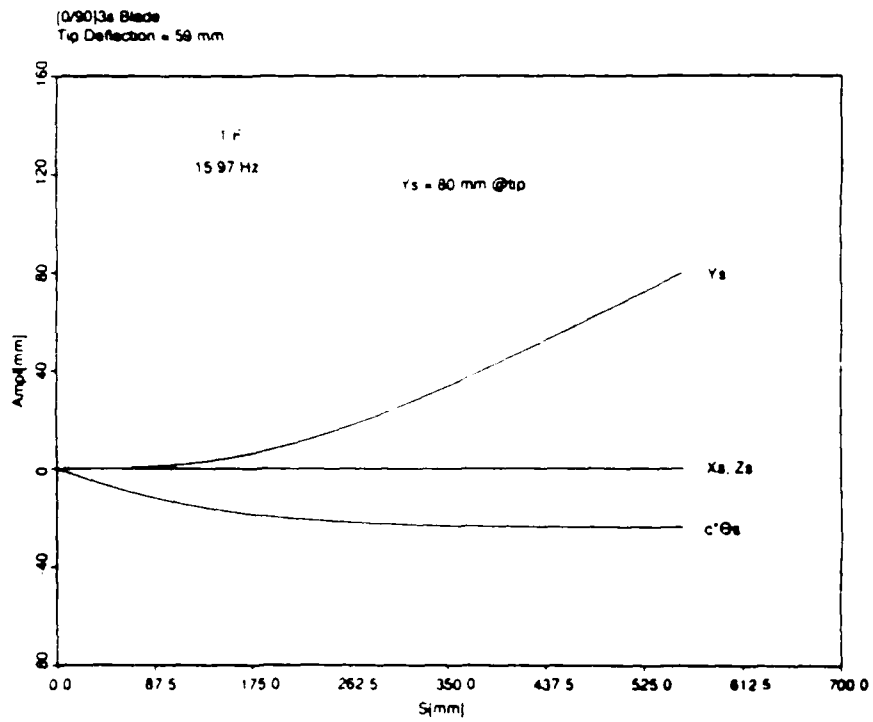


Figure 16: First Fore-and-Aft Mode; (0/90)_{3s}, 59 mm tip deflection, Ys=80 mm

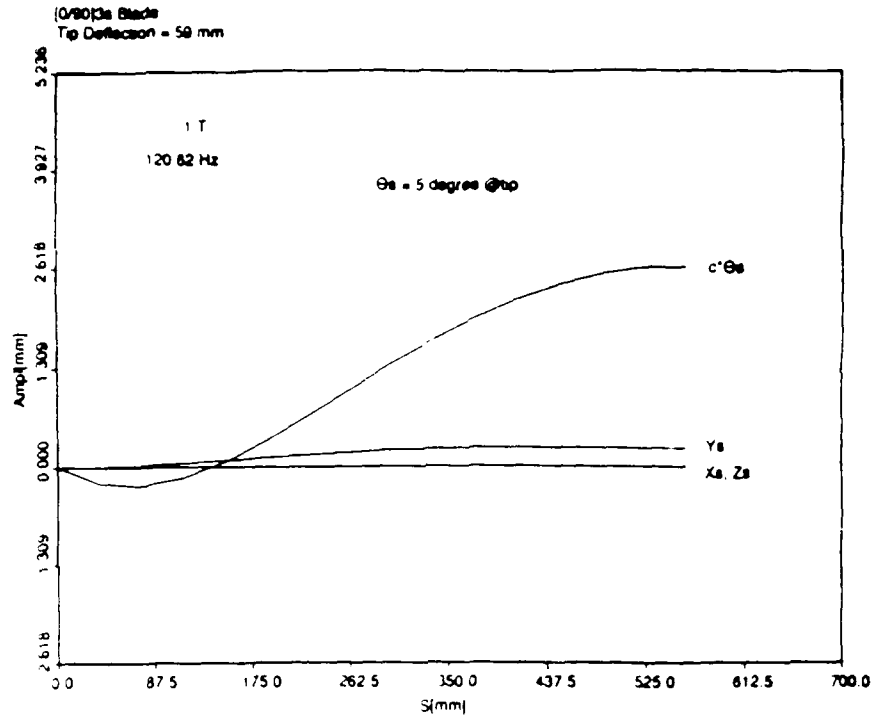


Figure 17: First Torsion Mode; [0/90]_{3s}, 59 mm tip deflection, $\theta_s = 5 \text{ degree}$

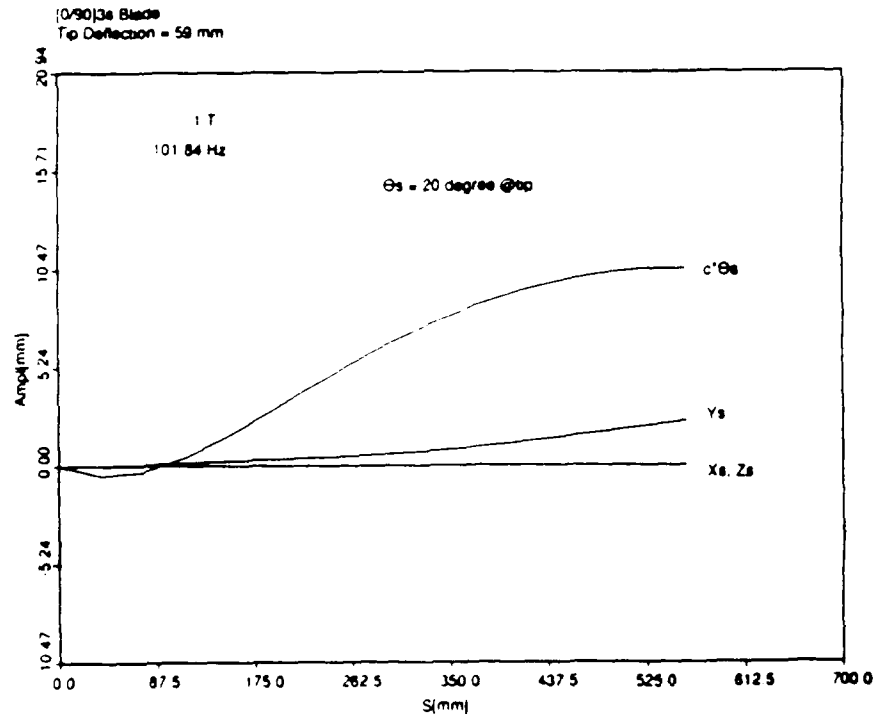


Figure 18: First Torsion Mode; [0/90]_{3s}, 59 mm tip deflection, $\theta_s = 20 \text{ degree}$

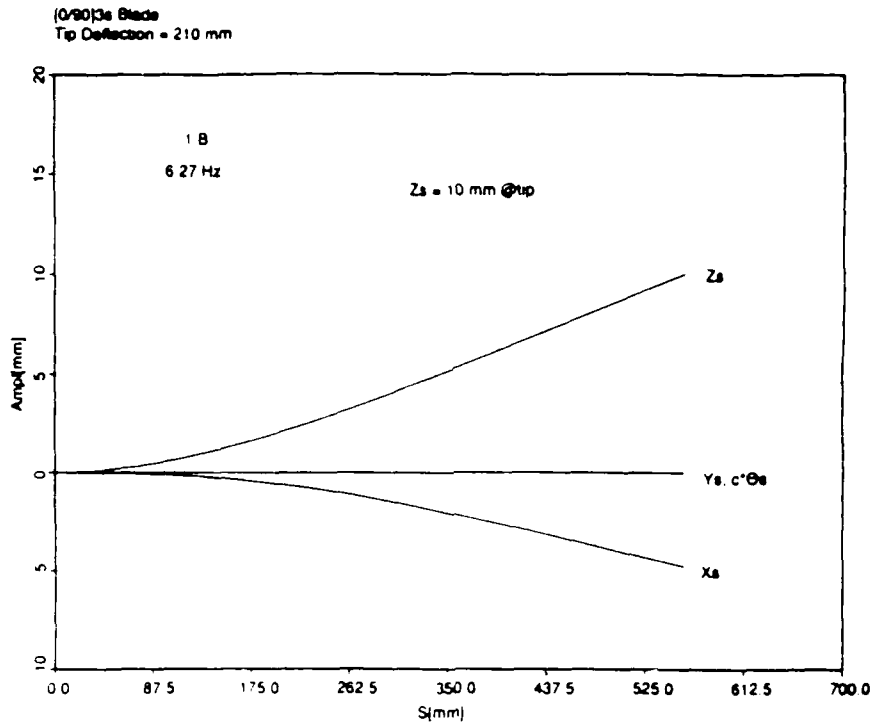


Figure 19: First Bending Mode; (0/90)_{3s}, 210 mm tip deflection, $Z_s=10$ mm

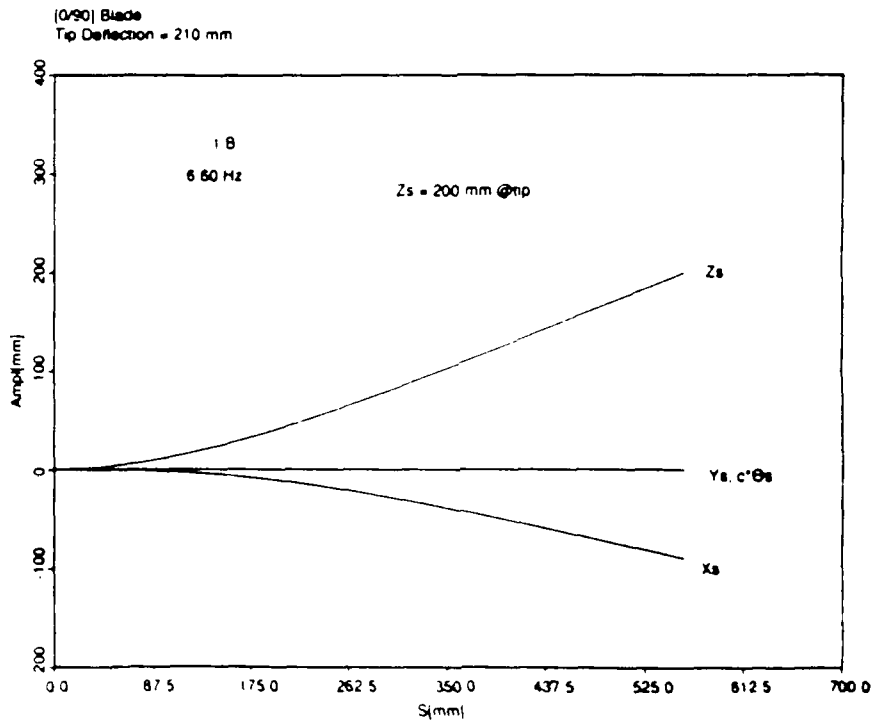


Figure 20: First Bending Mode; (0/90)_{3s}, 210 mm tip deflection, $Z_s=200$ mm

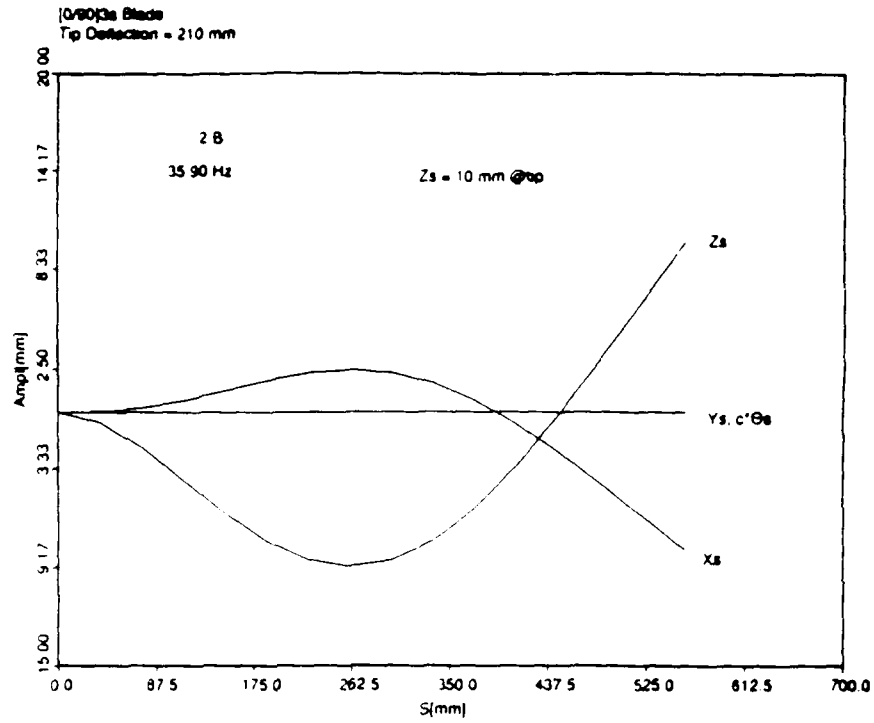


Figure 21: Second Bending Mode;[0/90]_{3s},210 mm tip deflection,Zs=10 mm

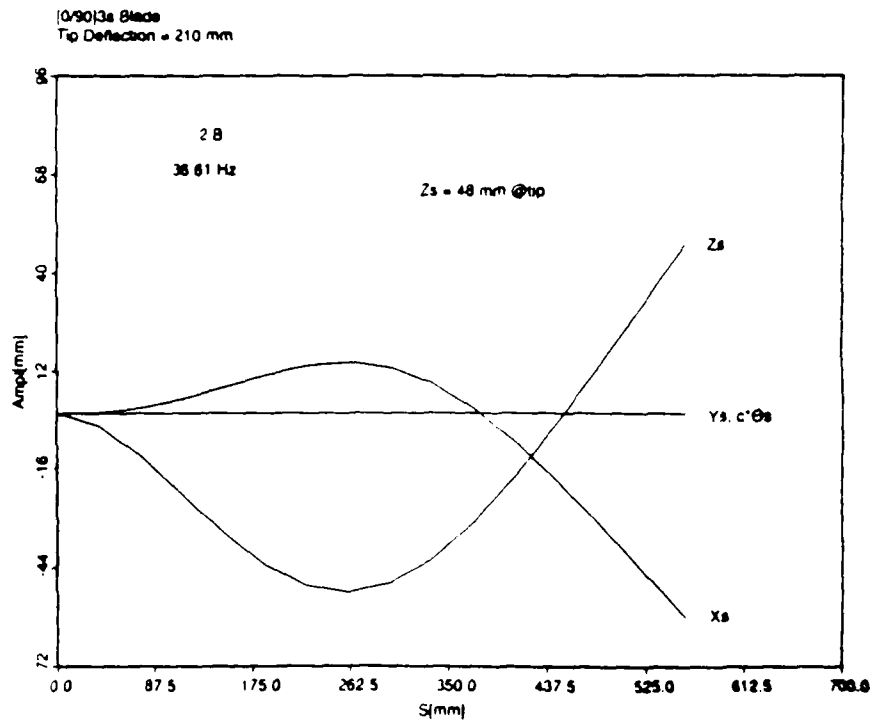


Figure 22: Second Bending Mode;[0/90]_{3s},210 mm tip deflection,Zs= 48 mm

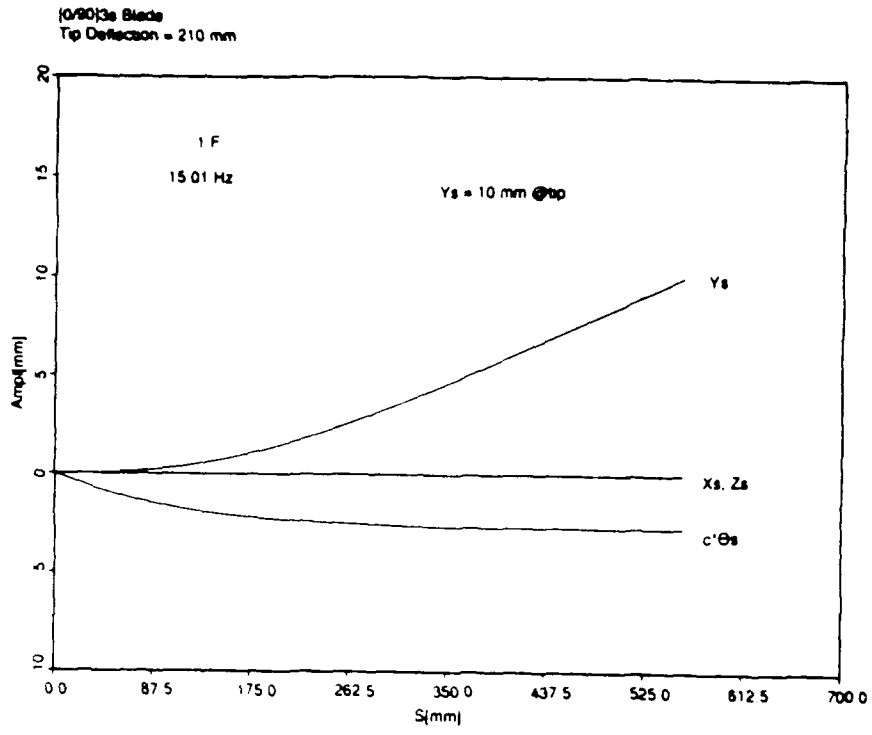


Figure 23: First Fore-and-Aft Mode; [0/90]_{3s}, 210 mm tip deflection, $Y_s = 10 \text{ mm}$

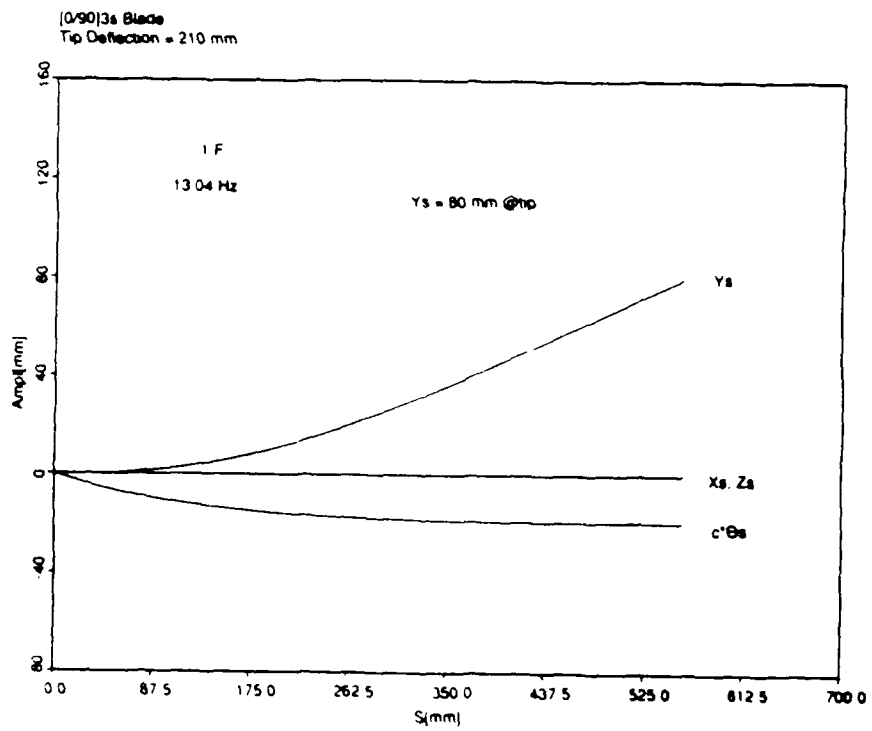


Figure 24: First Fore-and-Aft Mode; [0/90]_{3s}, 210 mm tip deflection, $Y_s = 80 \text{ mm}$

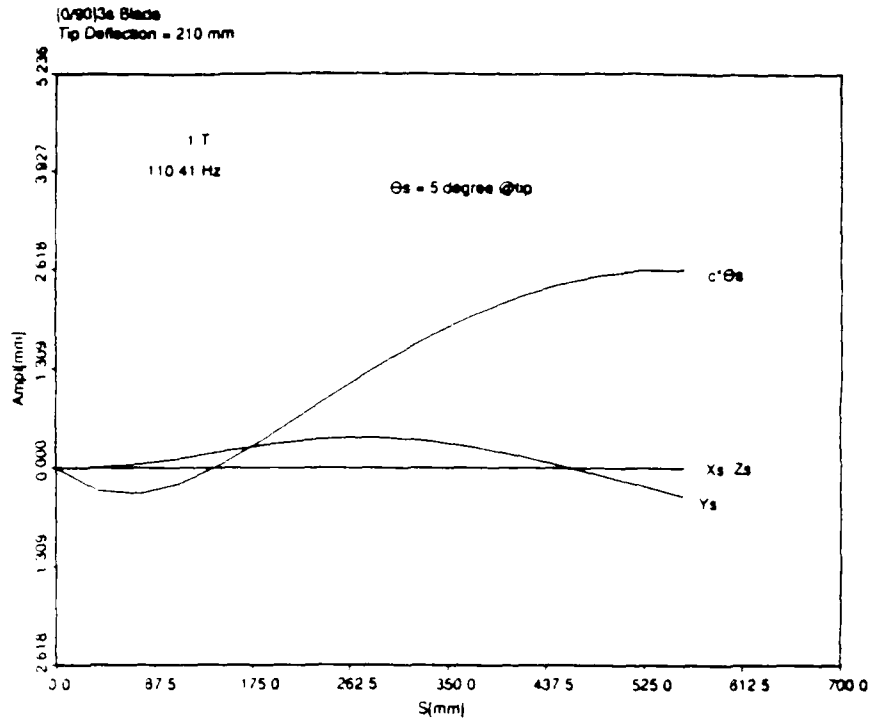


Figure 25: First Torsion Mode; [0/90]_{3s}, 210 mm tip deflection, $\theta_s = 5$ degree

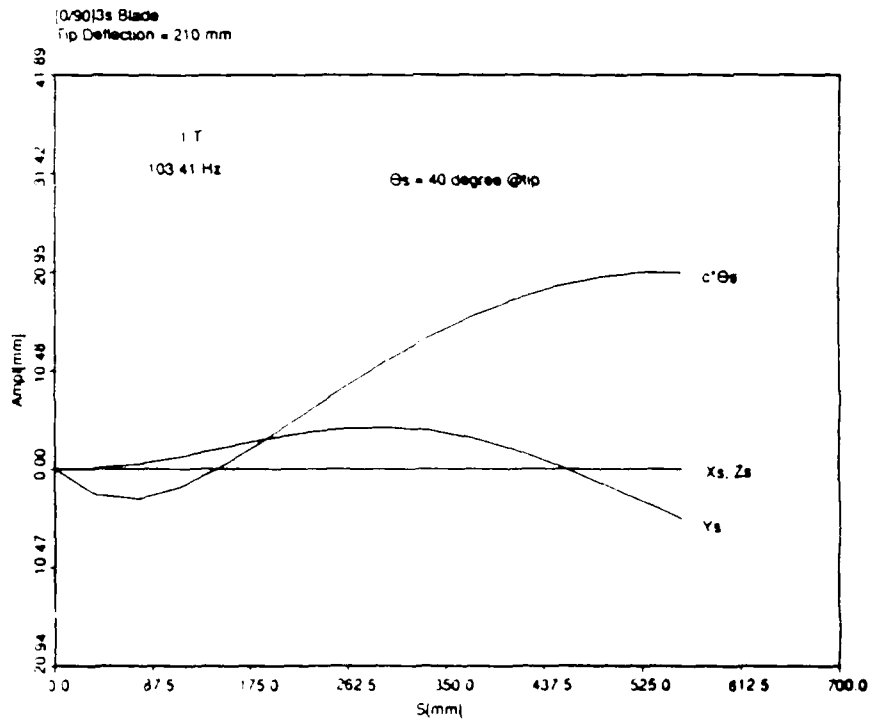


Figure 26: First Torsion Mode; [0/90]_{3s}, 210 mm tip deflection, $\theta_s = 40$ degree

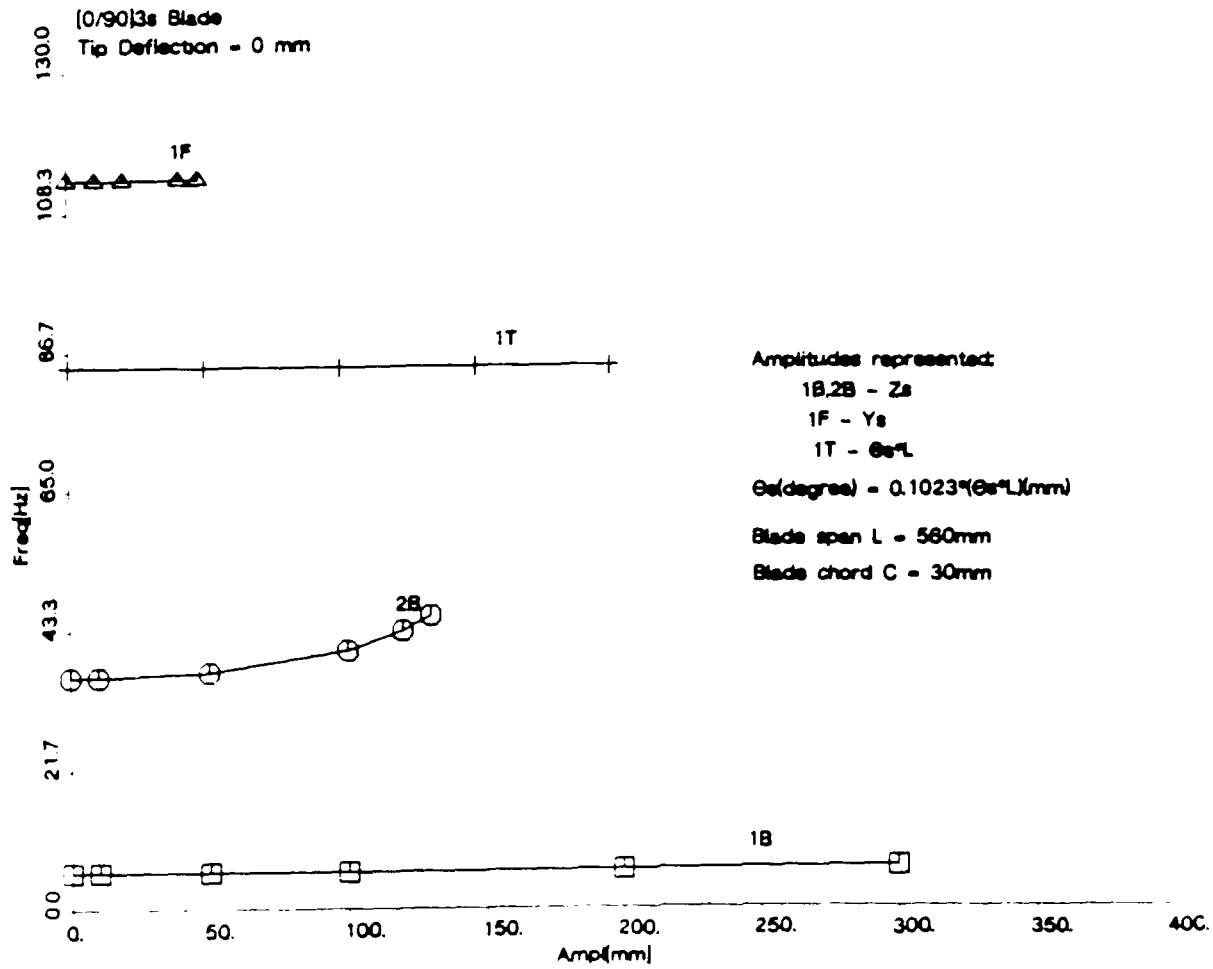


Figure 27: Frequency vs. Amplitude; [0/90]3s, 0 mm tip deflection

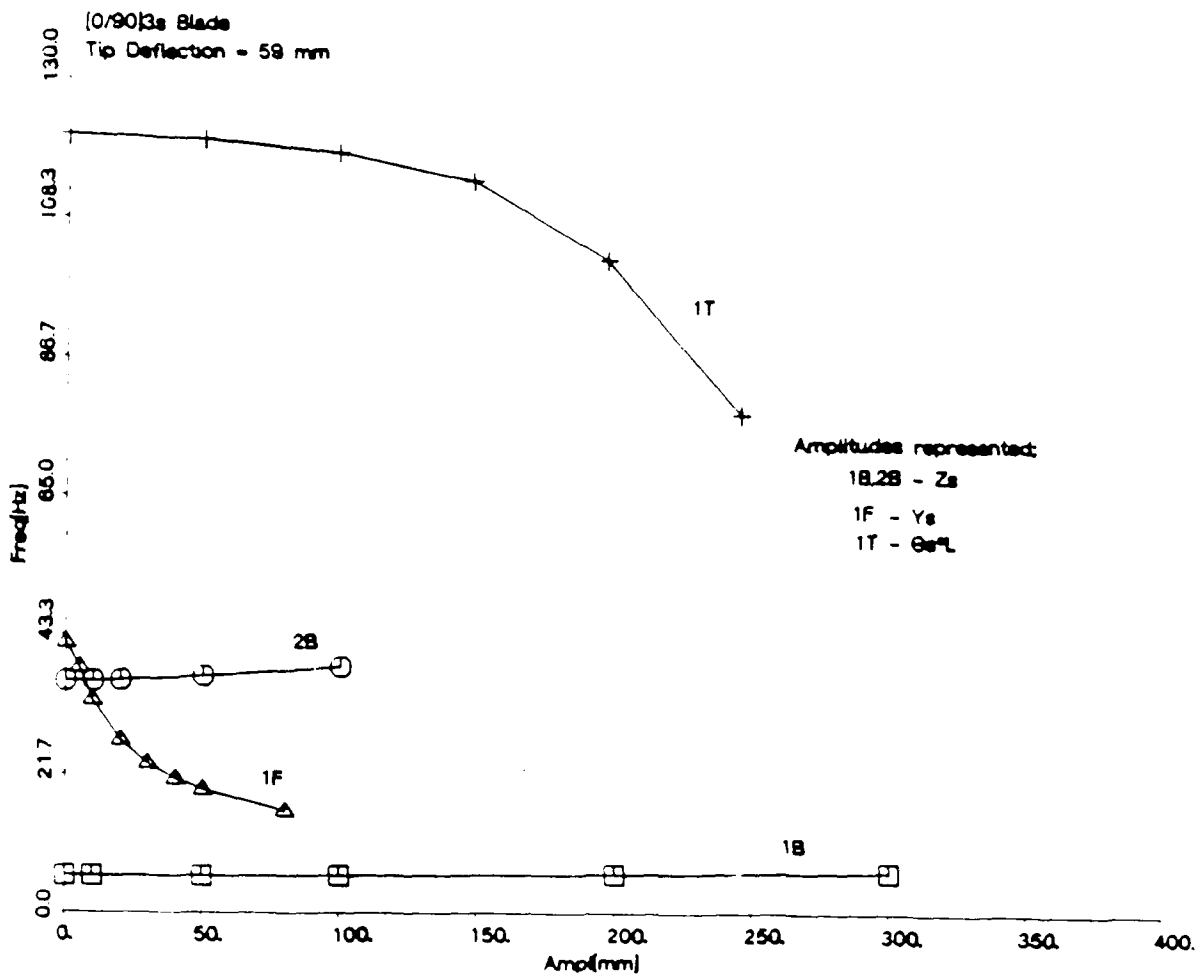


Figure 28: Frequency vs. Amplitude: [0/90]_{3s}, 59 mm tip deflection

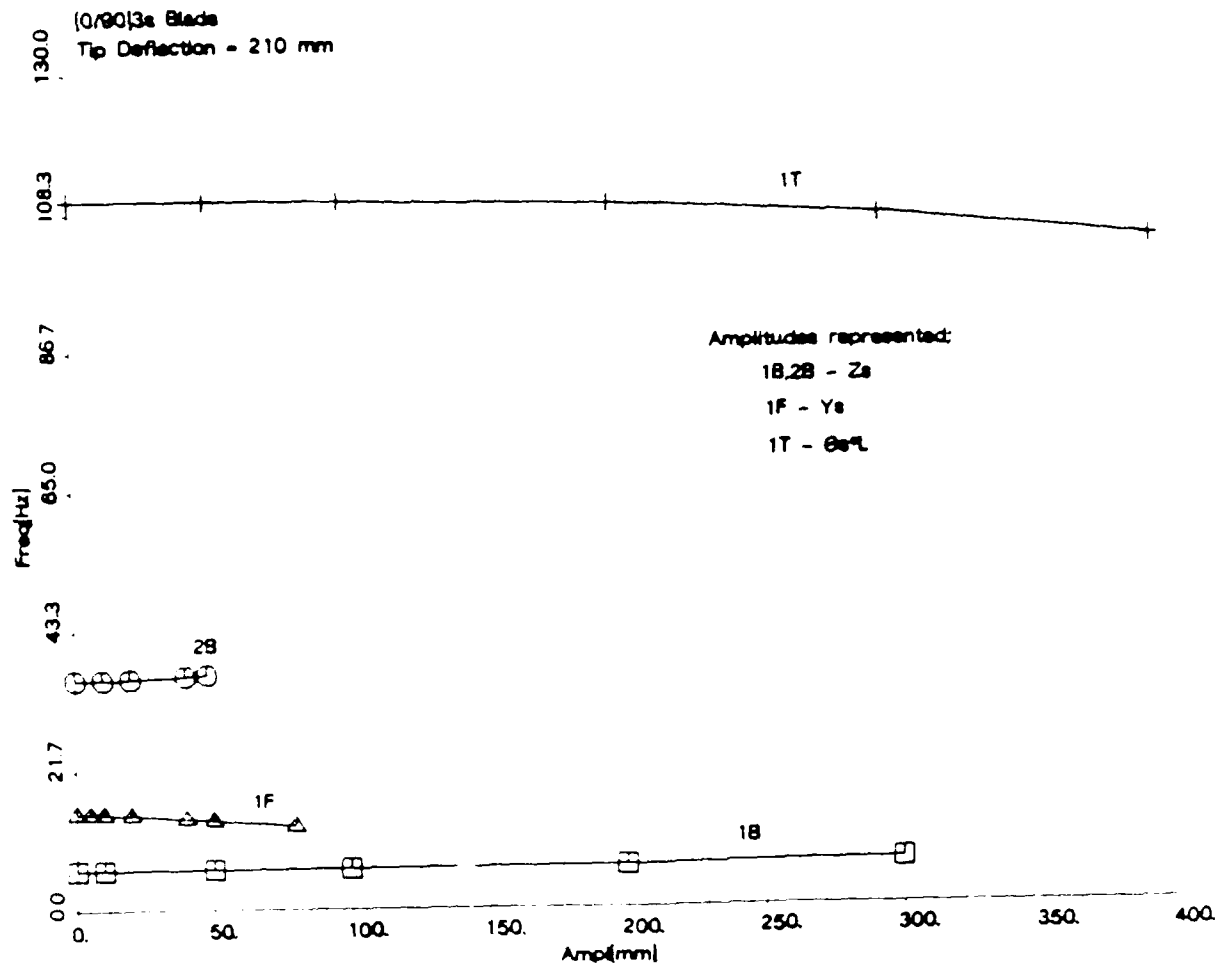


Figure 29: Frequency vs. Amplitude; (0/90)_{3s}, 210 mm tip deflection

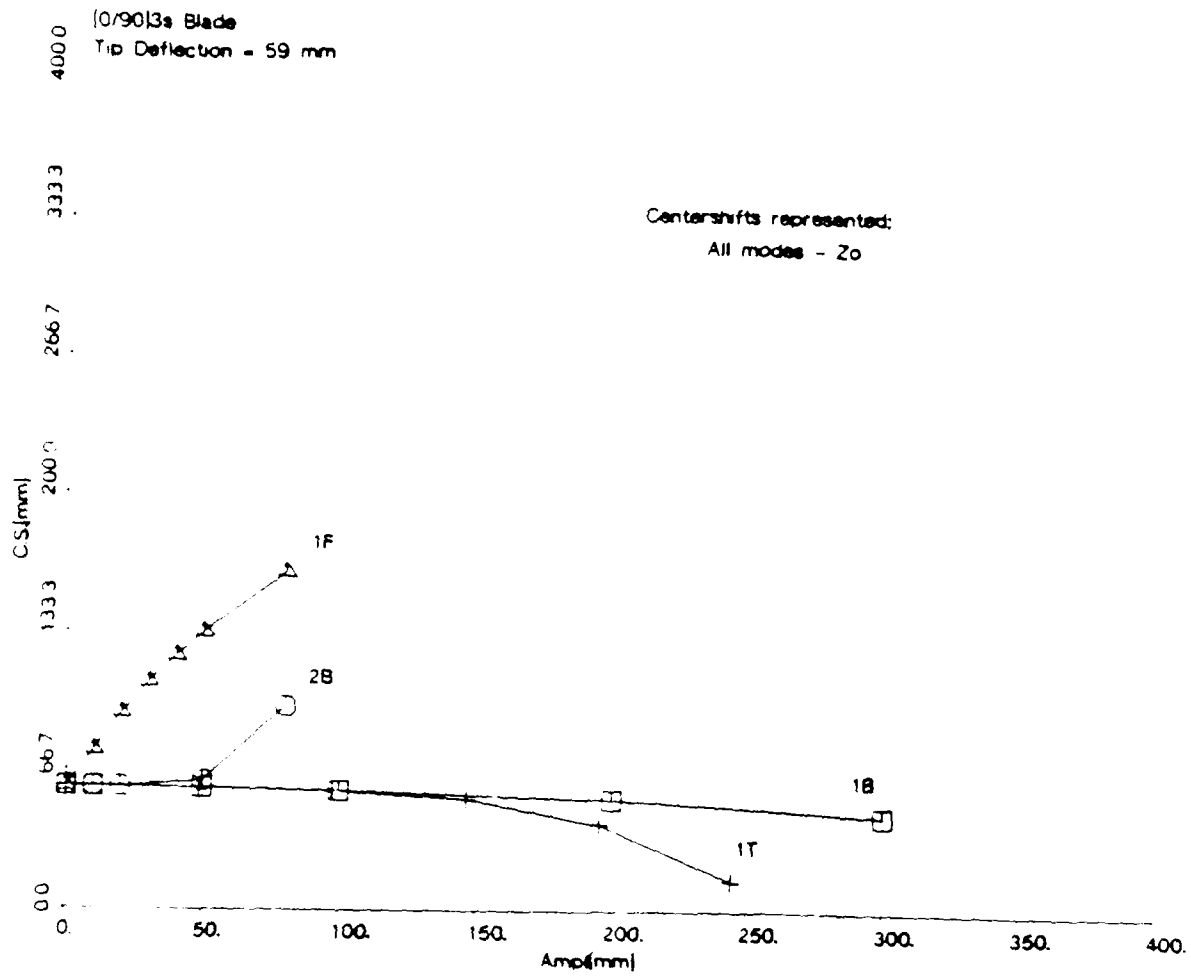


Figure 30: Centershift vs. Amplitude: [0/90]_{3s}, 59 mm tip deflection

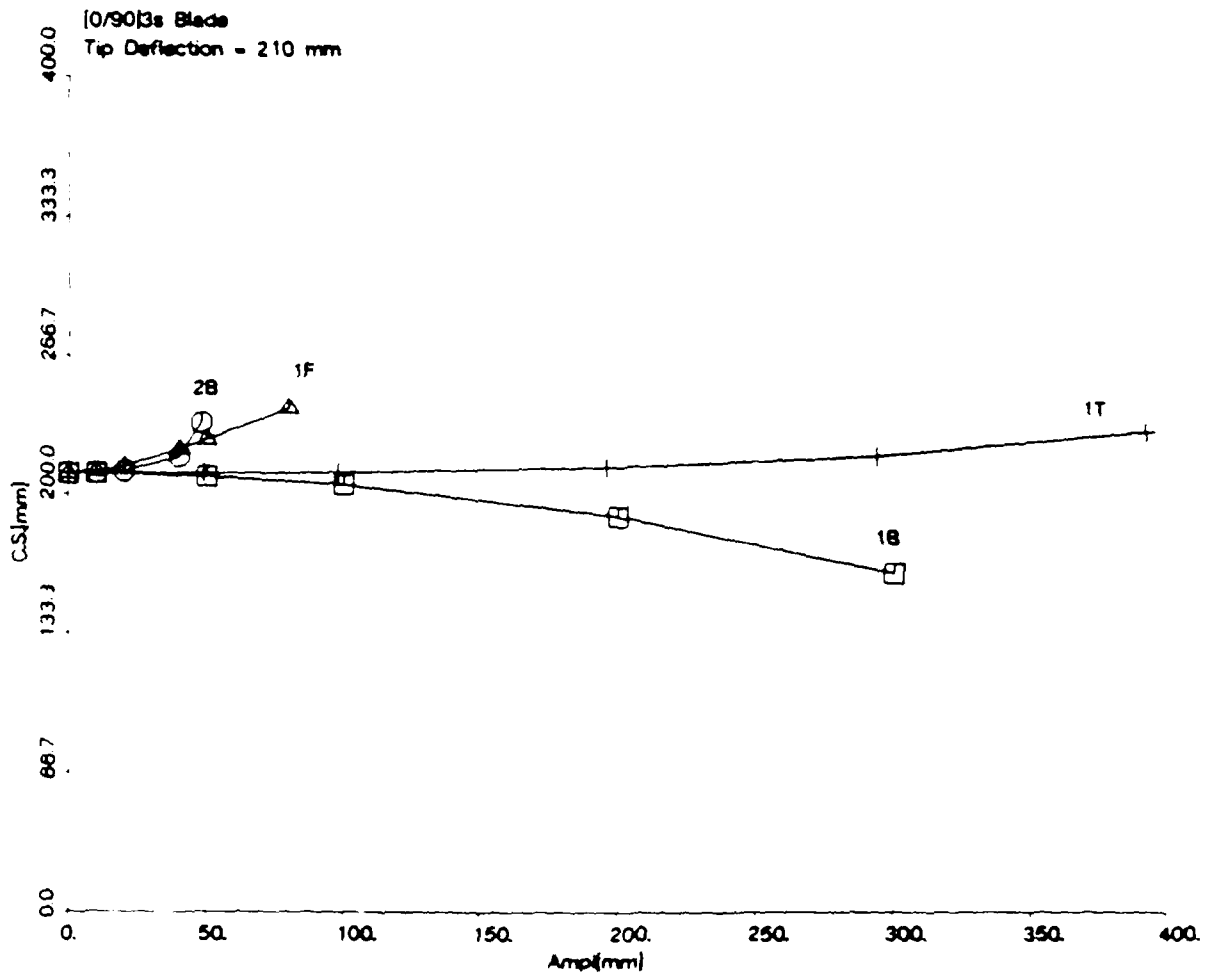


Figure 31: Centershift vs. Amplitude; [0/90]3s, 210 mm tip deflection

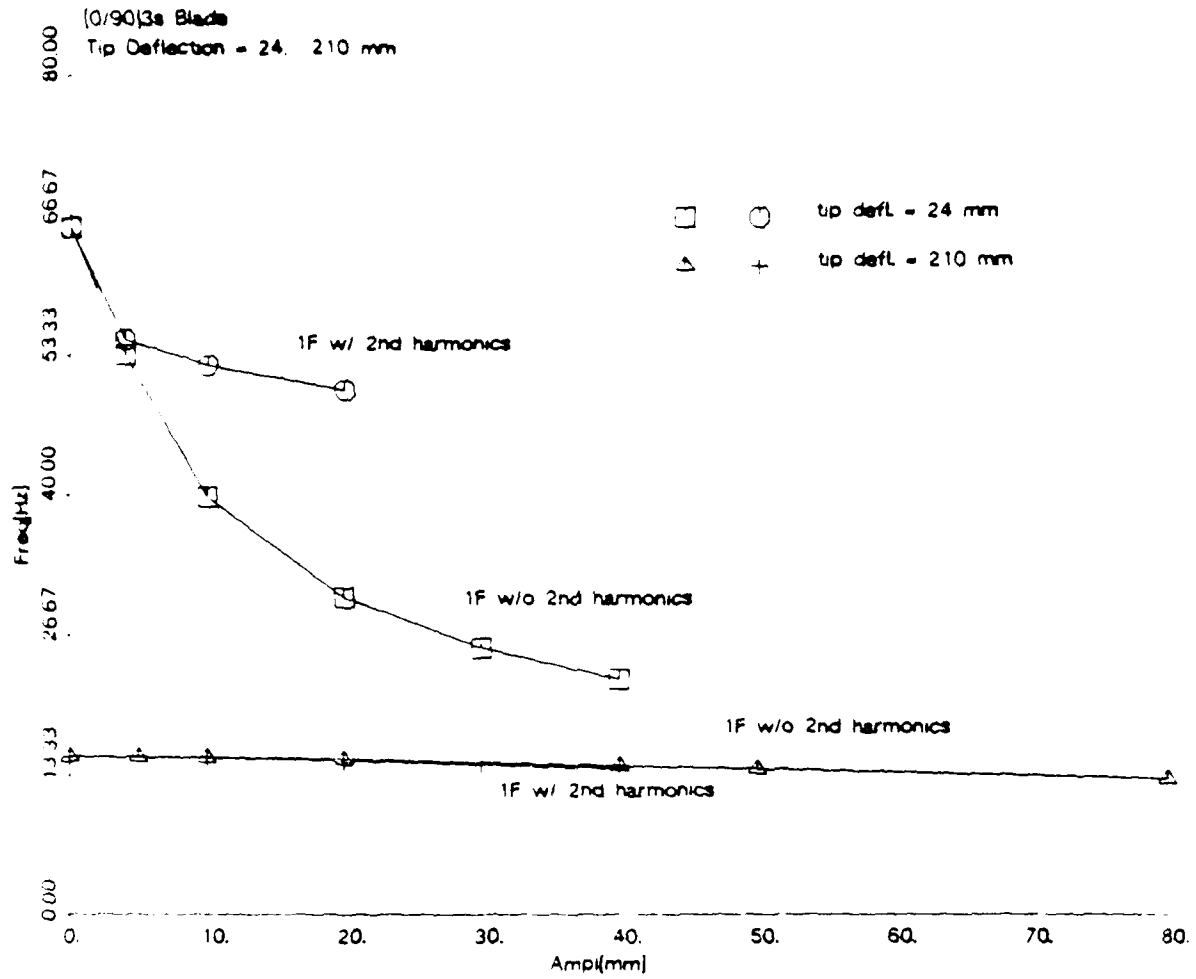


Figure 32: Frequency vs. Amplitude w/o and w/ 2nd harmonics; (0/90)_{3s}, 24 mm and 210 mm tip deflection

[0/90]_{3s} Beam

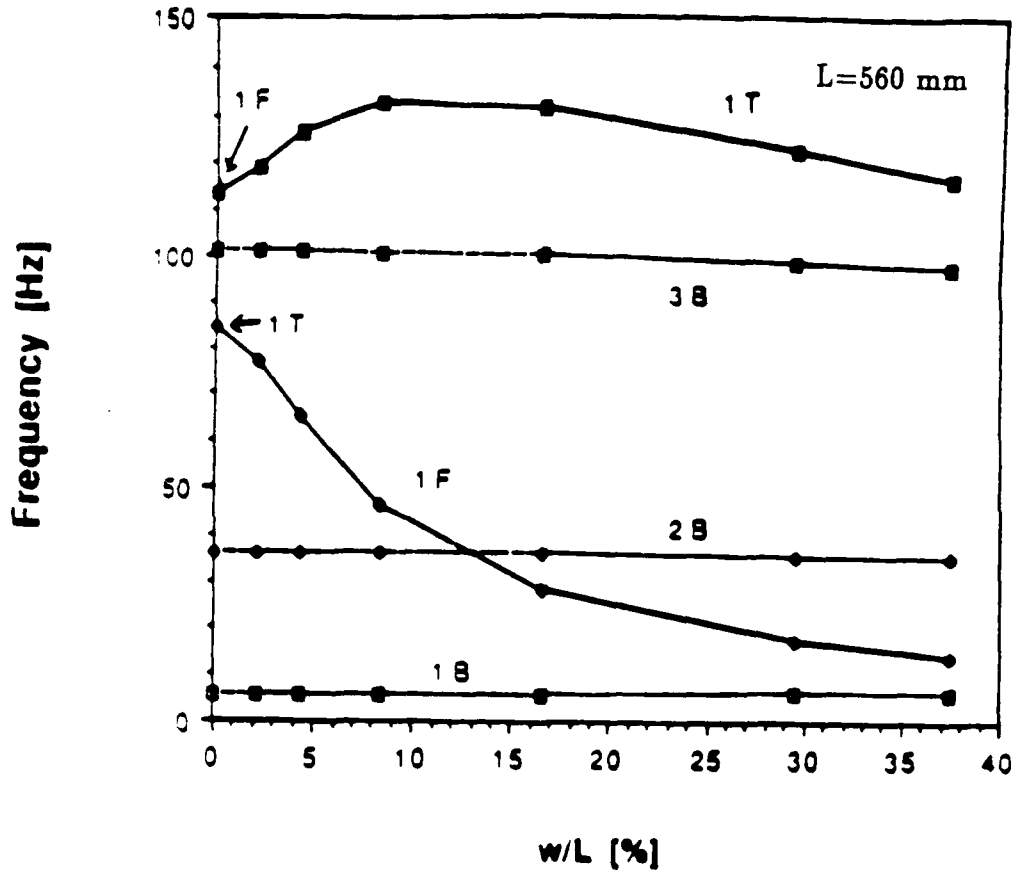


Figure 33: Natural Frequencies of [0/90]_{3s} Beam as a Function of Tip Deflection (from Ref. 1)

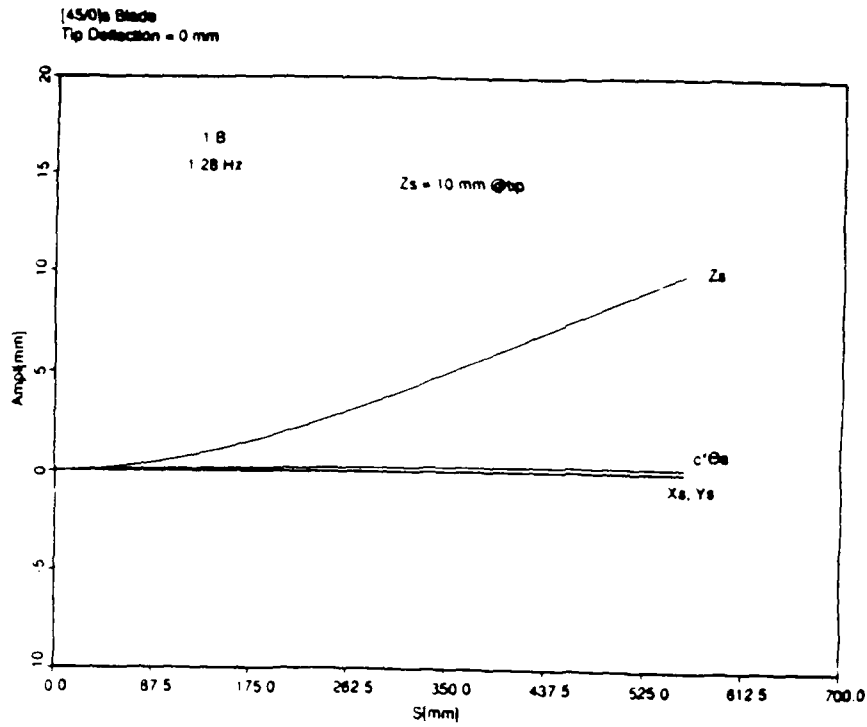


Figure 34: First Bending Mode;[45/0]s,0 mm tip deflection,Zs=10 mm

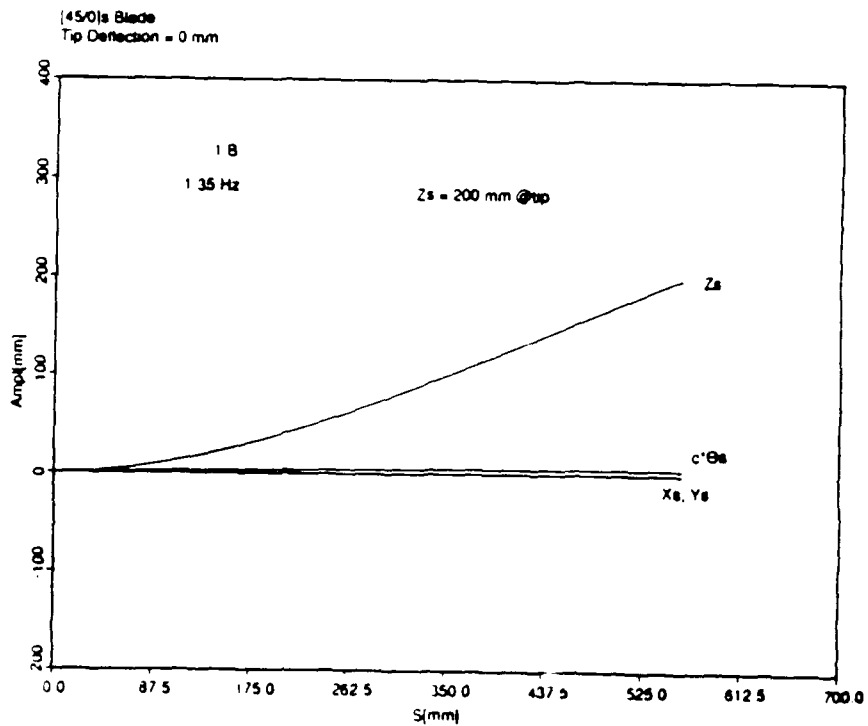


Figure 35: First Bending Mode;[45/0]s,0 mm tip deflection,Zs=200 mm

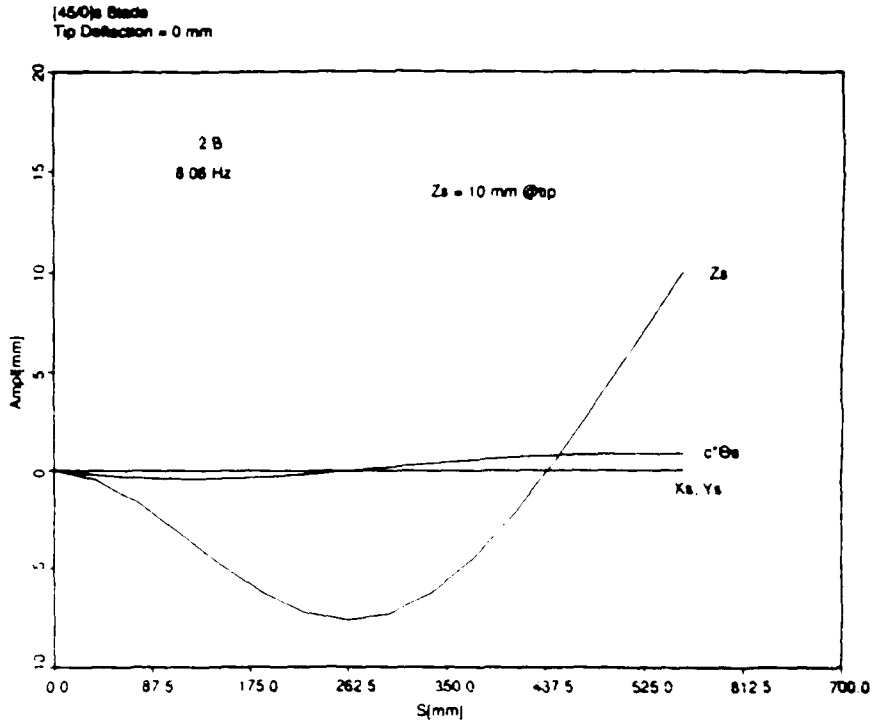


Figure 36: Second Bending Mode; [45/0]_s, 0 mm tip deflection, Zs = 10 mm

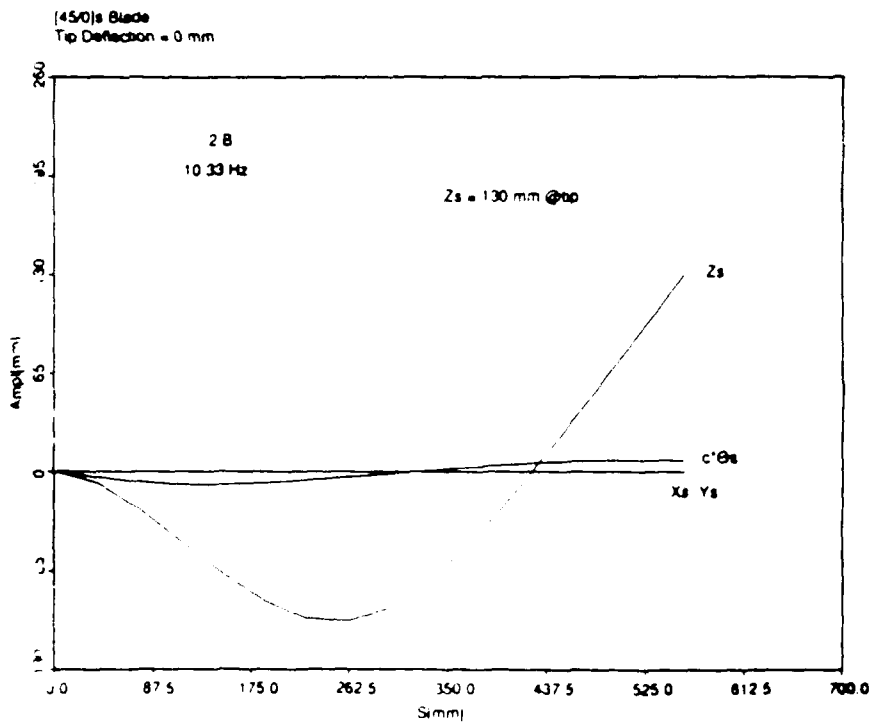


Figure 37: Second Bending Mode; [45/0]_s, 0 mm tip deflection, Zs = 130 mm

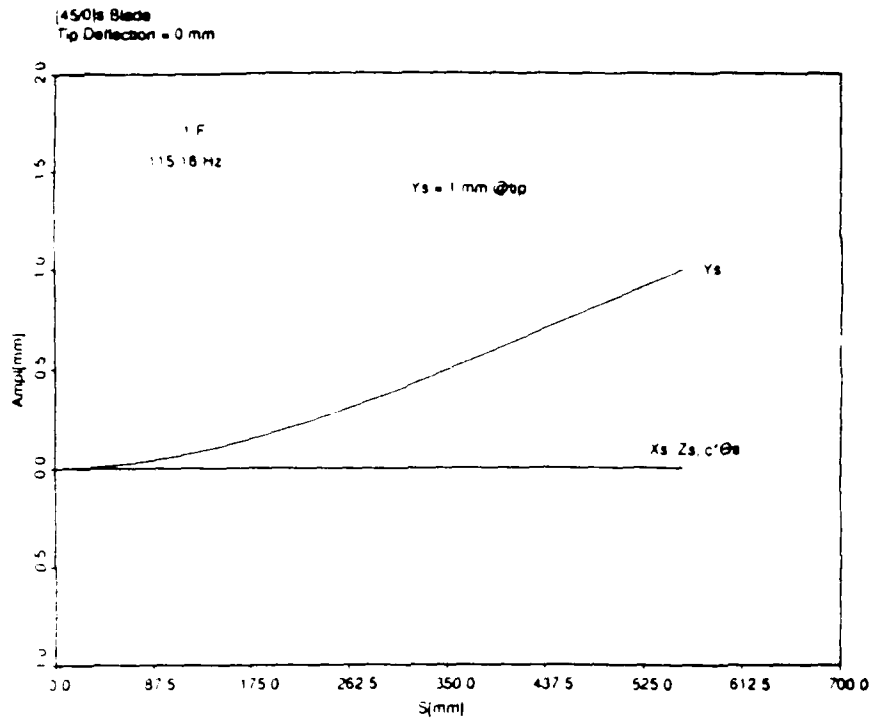


Figure 38: First Fore-and-Aft Mode; [45/0]_s, 0 mm tip deflection, Y_s = 1 mm

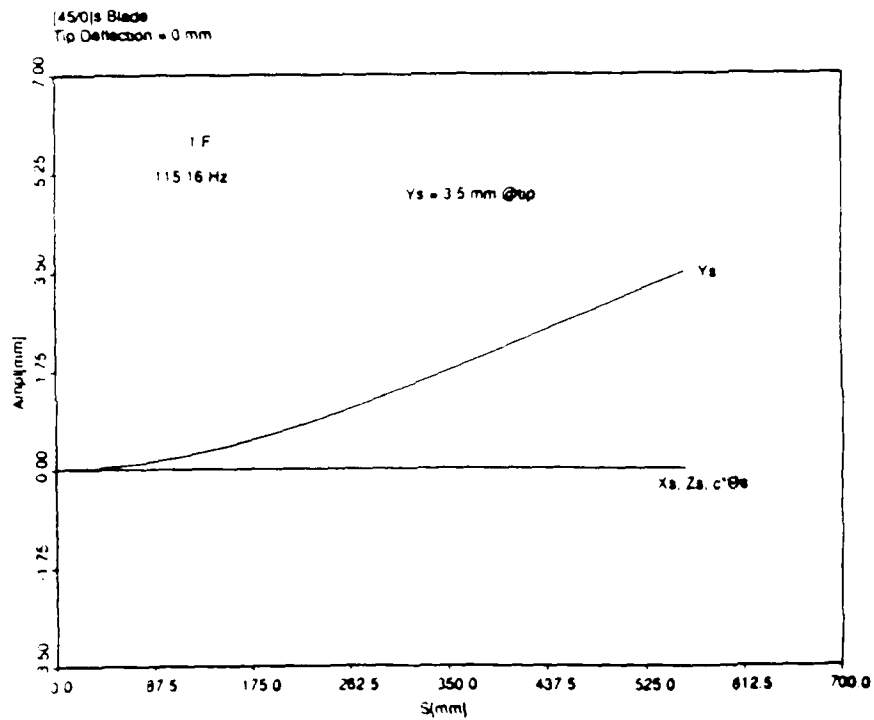


Figure 39: First Fore-and-Aft Mode; [45/0]_s, 0 mm tip deflection, Y_s = 3.5 mm

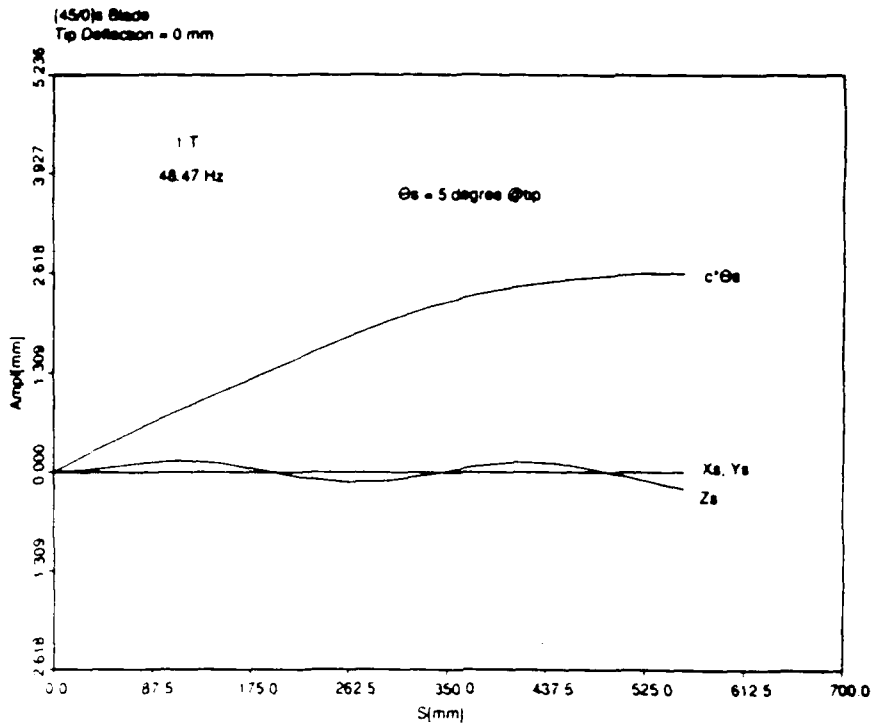


Figure 40: First Torsion Mode; [45/0]_s, 0 mm tip deflection, $\theta_s = 5$ degree

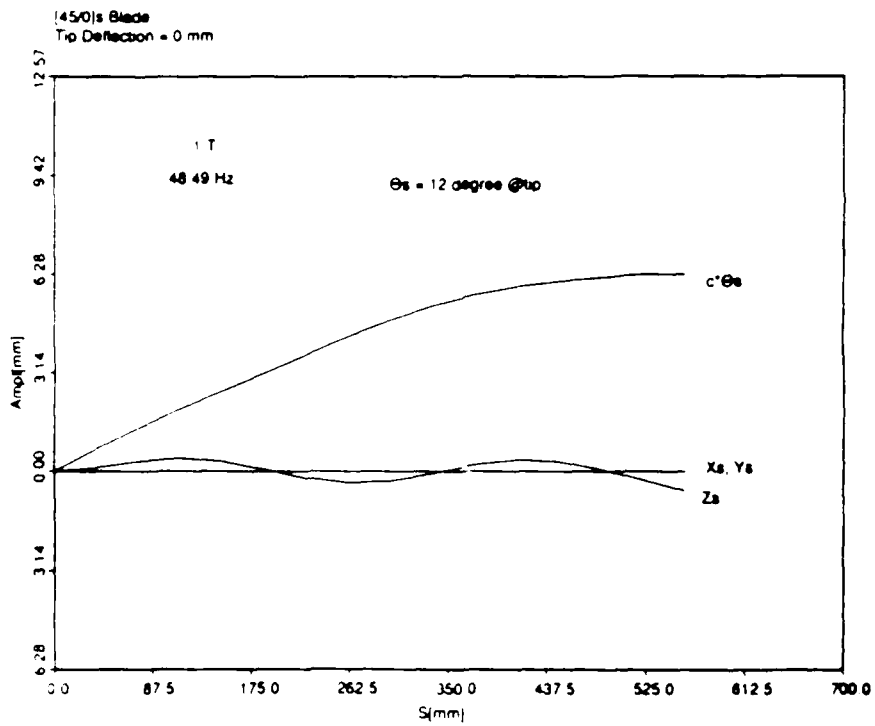


Figure 41: First Torsion Mode; [45/0]_s, 0 mm tip deflection, $\theta_s = 12$ degree

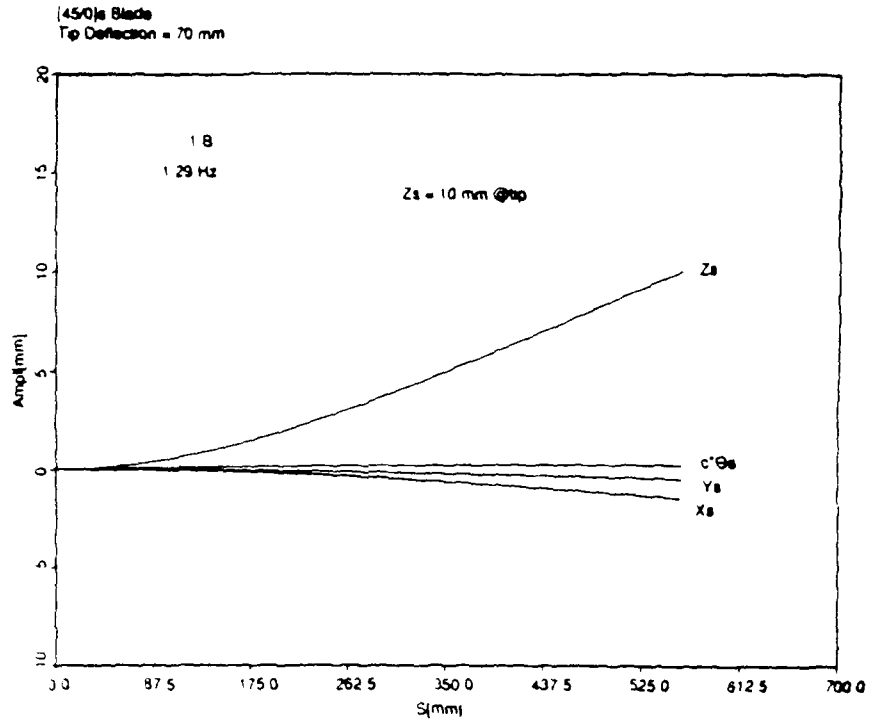


Figure 42: First Bending Mode;[45/0]_s,70 mm tip deflection,Zs=10 mm

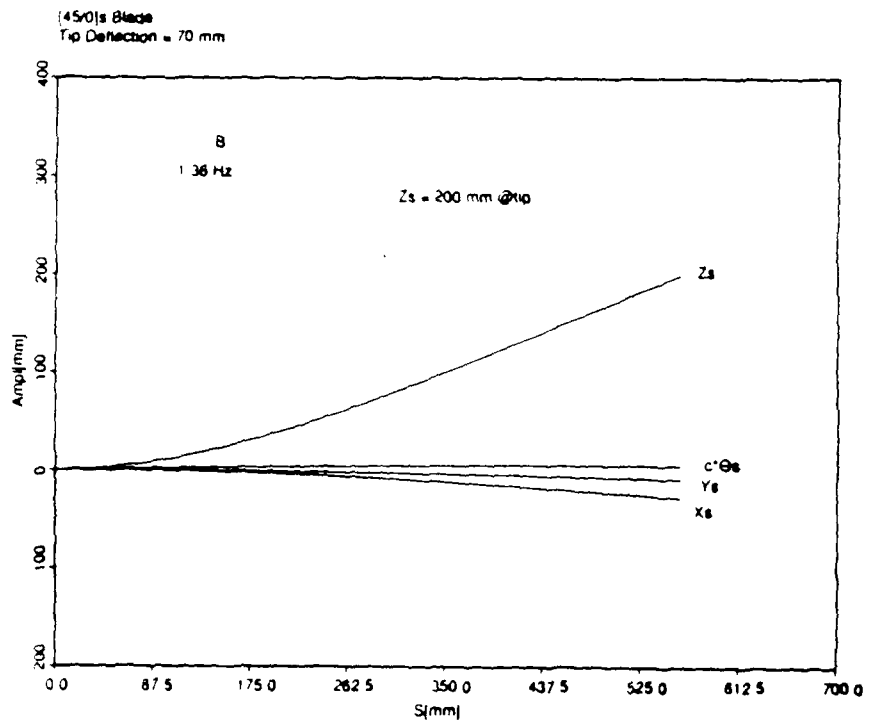


Figure 43: First Bending Mode;[45/0]_s,70 mm tip deflection,Zs=200 mm

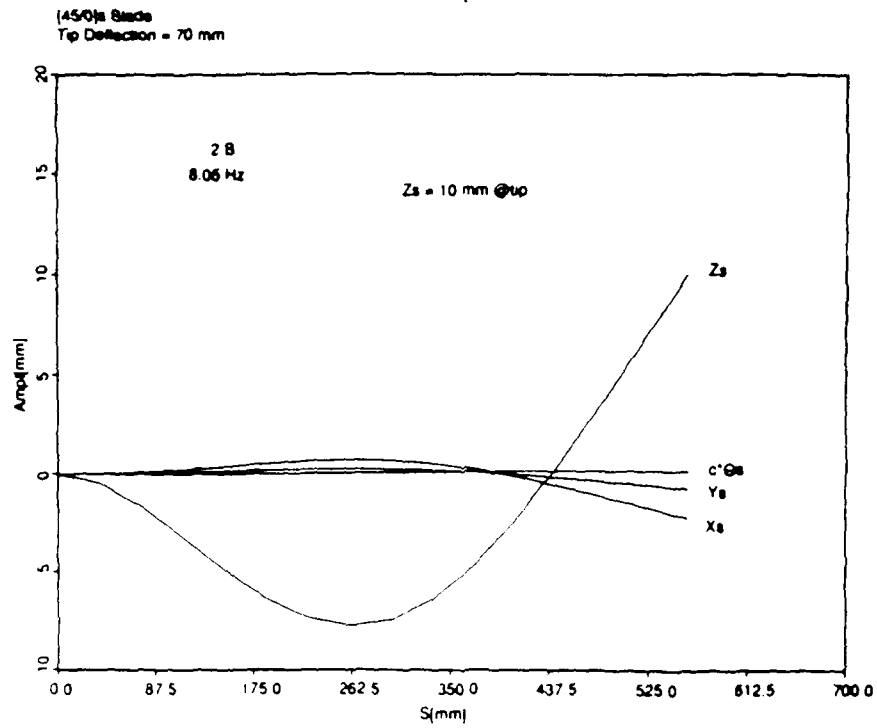


Figure 44: Second Bending Mode; [45/0]_s, 70 mm tip deflection, Zs = 10 mm

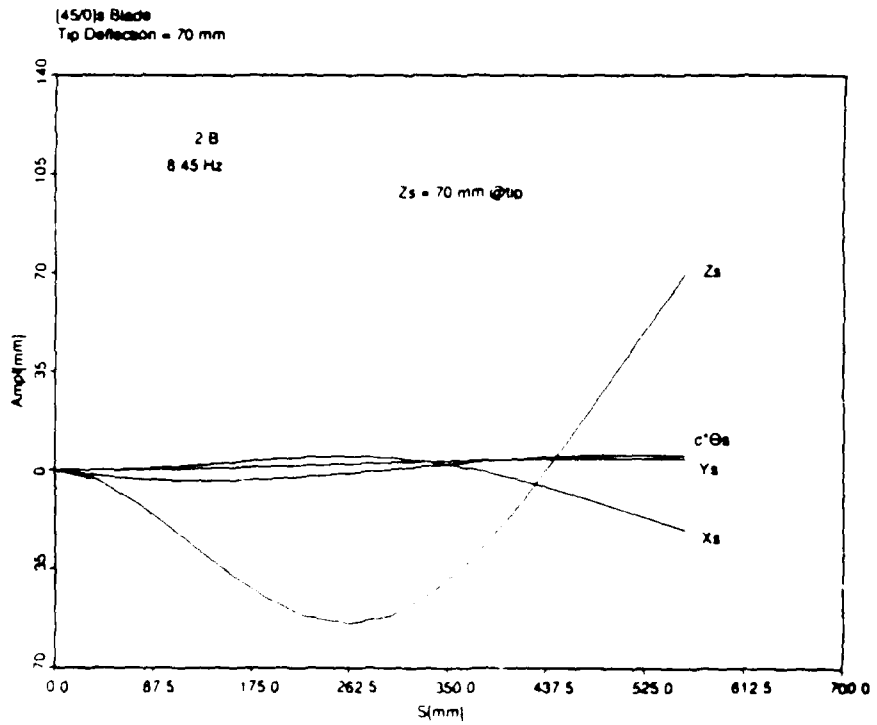


Figure 45: Second Bending Mode; [45/0]_s, 70 mm tip deflection, Zs = 70 mm

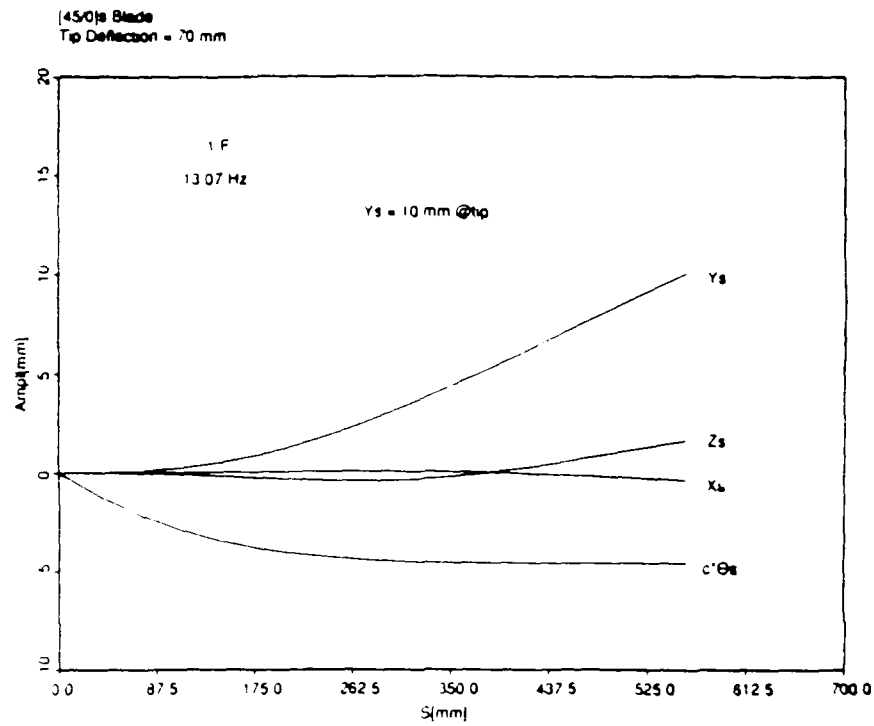


Figure 46: First Fore-and-Aft Mode; [45/0]_s, 70 mm tip deflection, $Y_s = 10 \text{ mm}$

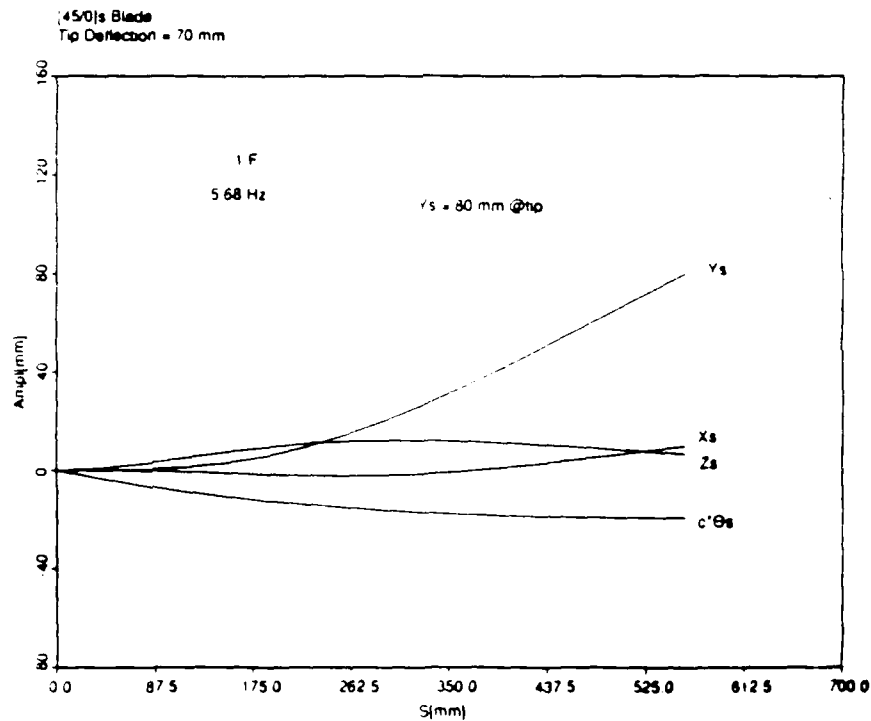


Figure 47: First Fore-and-Aft Mode; [45/0]_s, 70 mm tip deflection, $Y_s = 80 \text{ mm}$

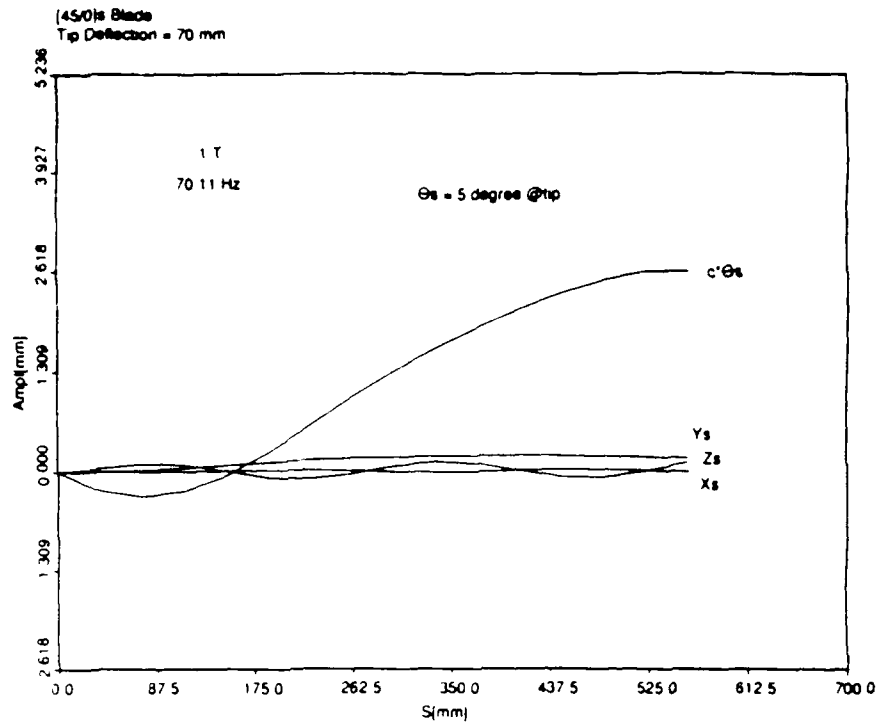


Figure 48: First Torsion Mode; [45/0]_s, 70 mm tip deflection, $\theta_s = 5$ degree

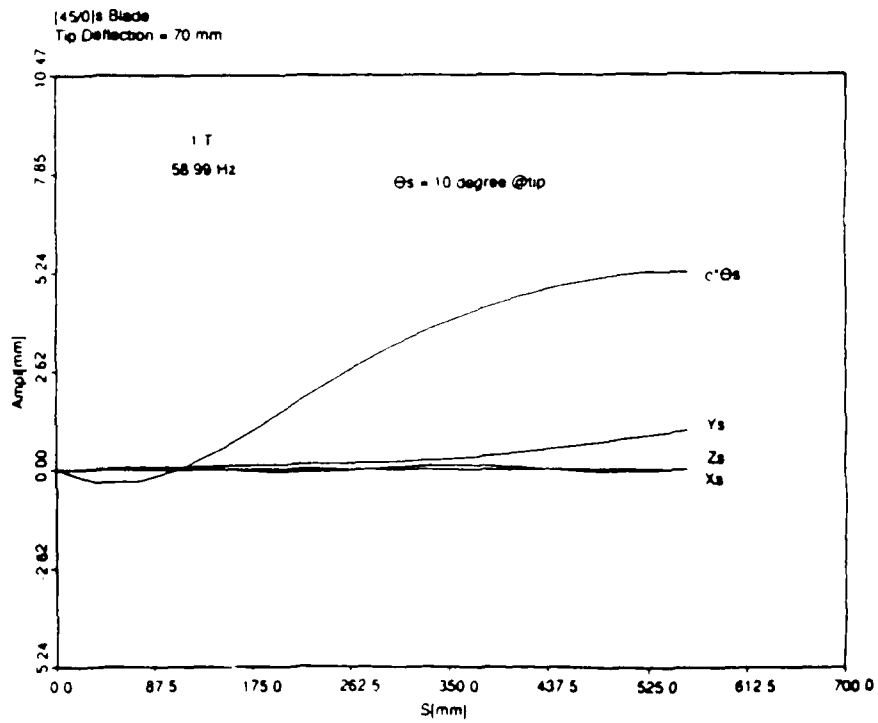


Figure 49: First Torsion Mode; [45/0]_s, 70 mm tip deflection, $\theta_s = 10$ degree

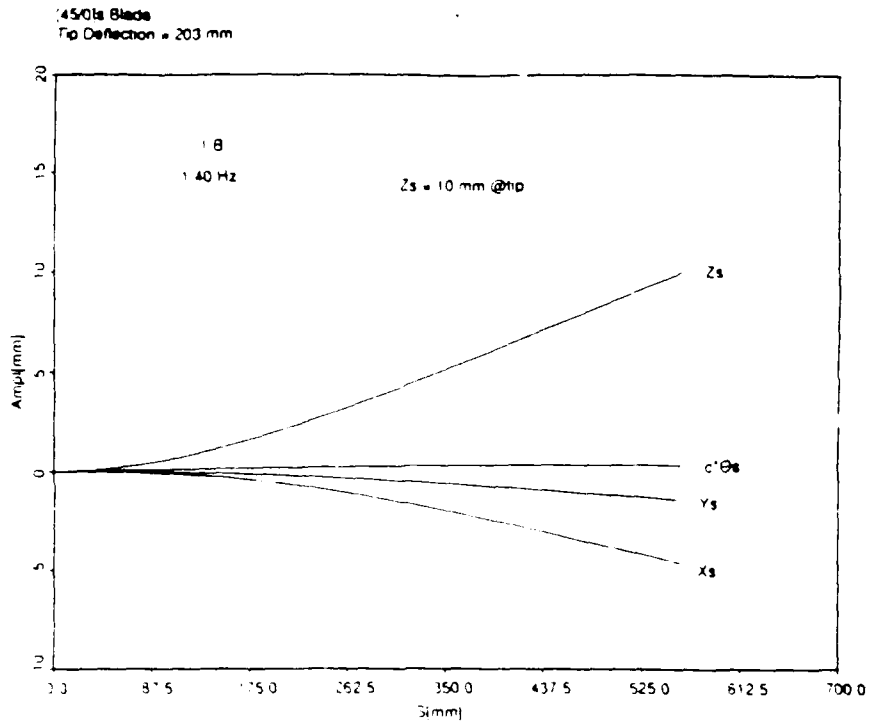


Figure 50: First Bending Mode;[45/0]s,203 mm tip deflection,Zs=10 mm

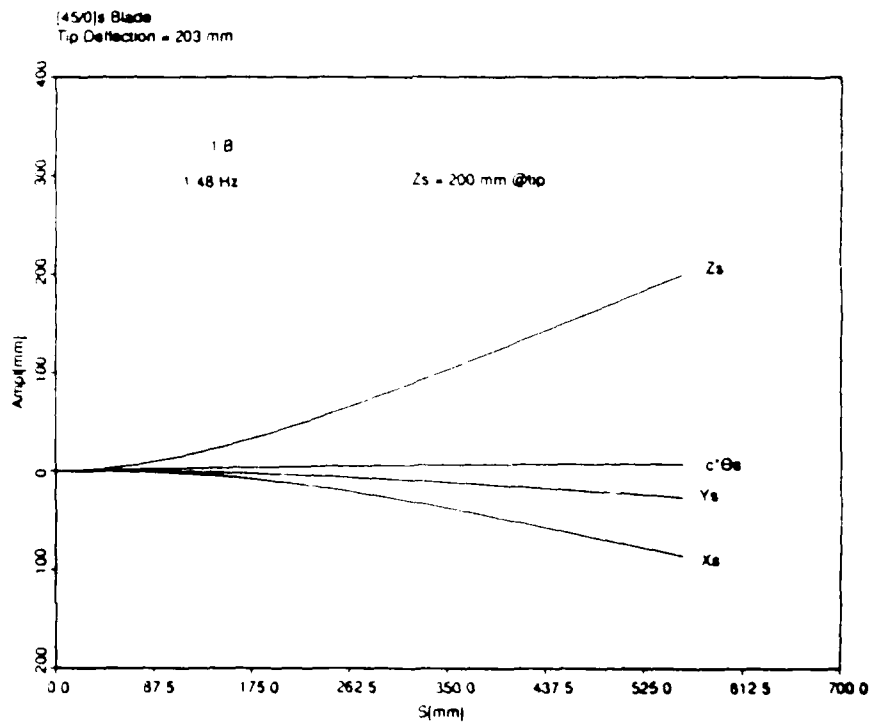


Figure 51: First Bending Mode;[45/0]s,203 mm tip deflection,Zs=200 mm

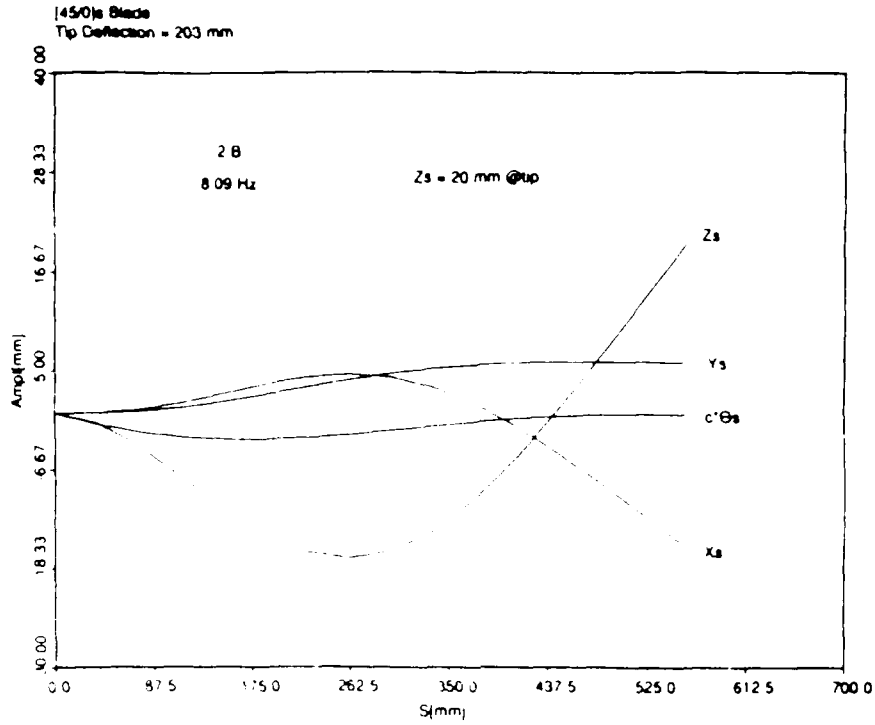


Figure 52: Second Bending Mode; $[45/0]_s$, 203 mm tip deflection, $Z_s = 20$ mm

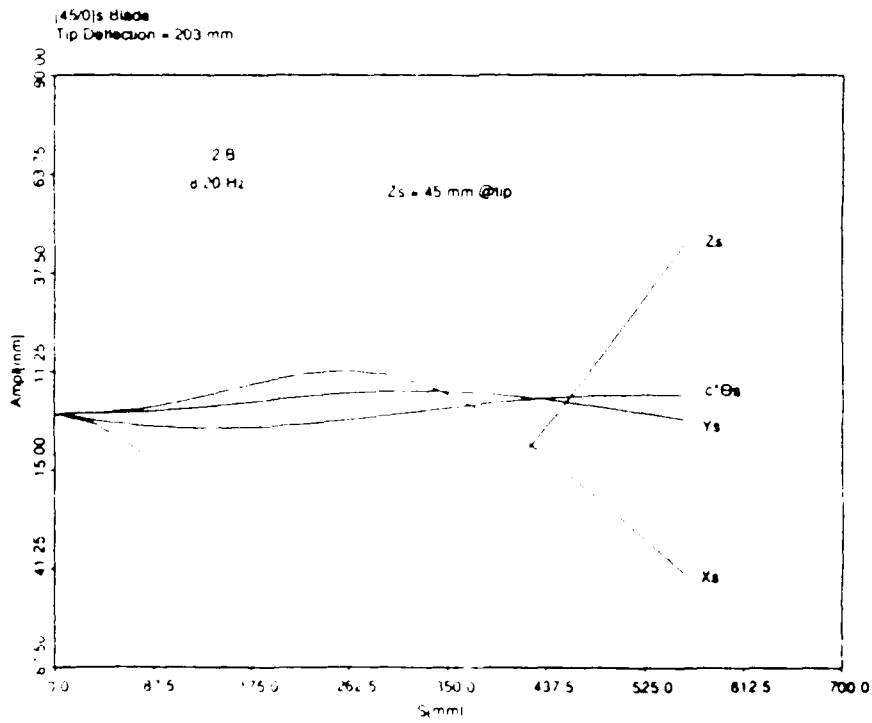


Figure 53: Second Bending Mode; $[45/0]_s$, 203 mm tip deflection, $Z_s = -45$ mm

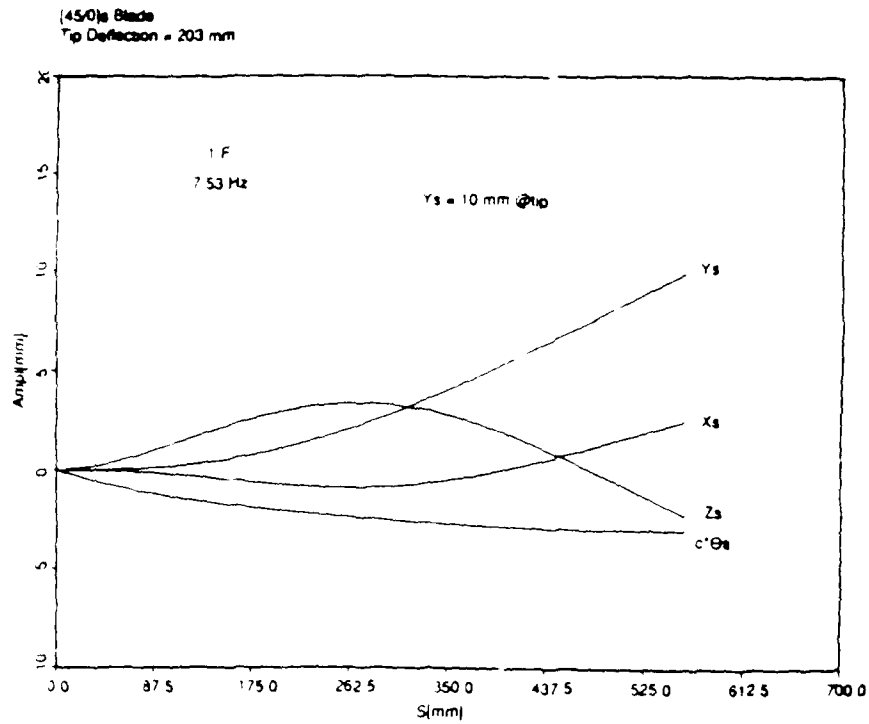


Figure 54: First Fore-and-Aft Mode; [45/0]_s, 203 mm tip deflection, Ys=10 mm

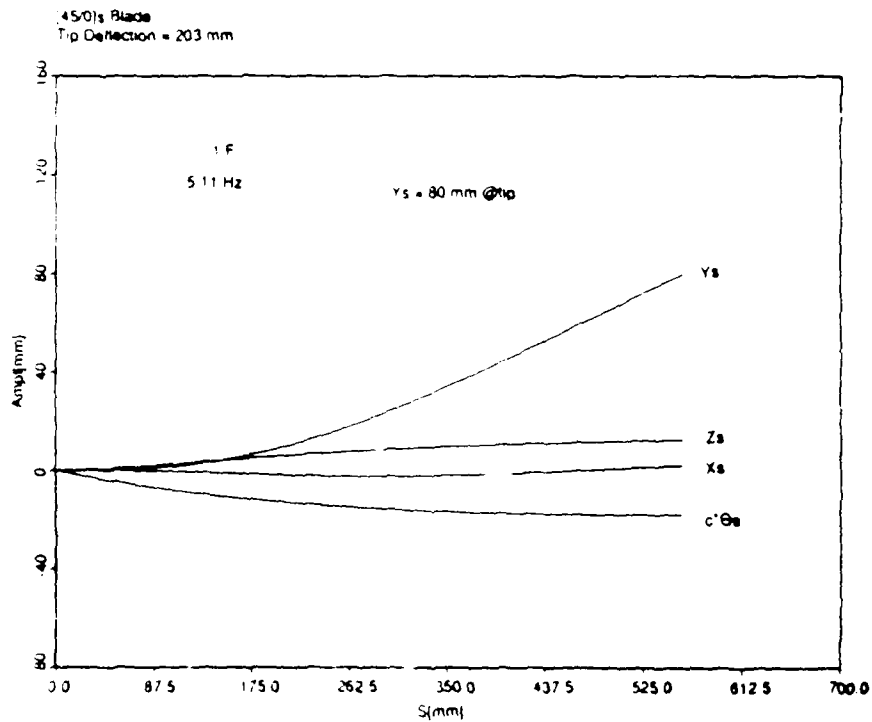


Figure 55: First Fore-and-Aft Mode; [45/0]_s, 203 mm tip deflection, Ys=80 mm

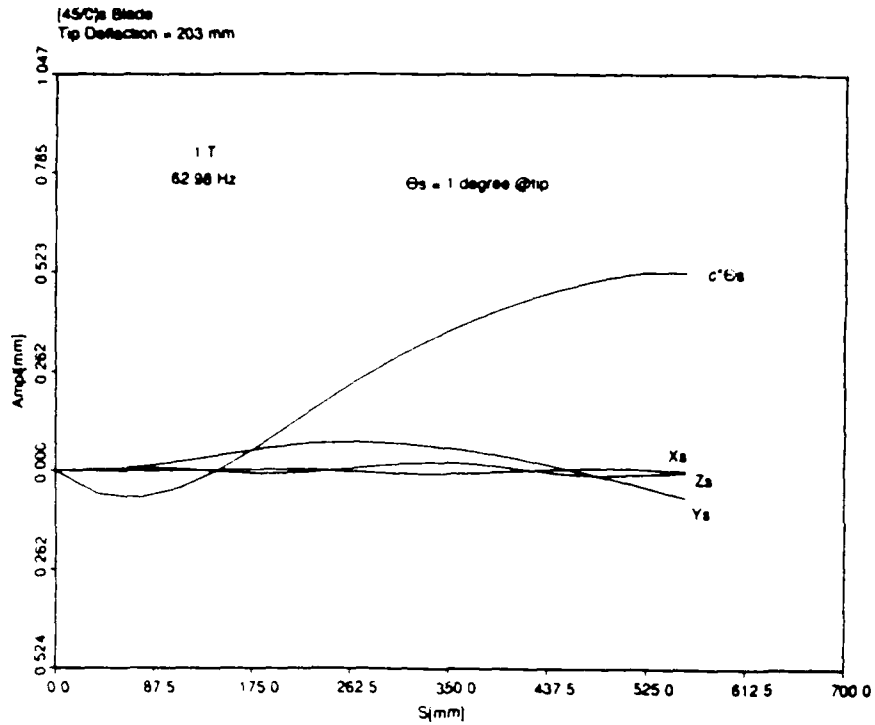


Figure 56: First Torsion Mode; [45/0]_s, 203 mm tip deflection, $\theta_s = 1$ degree

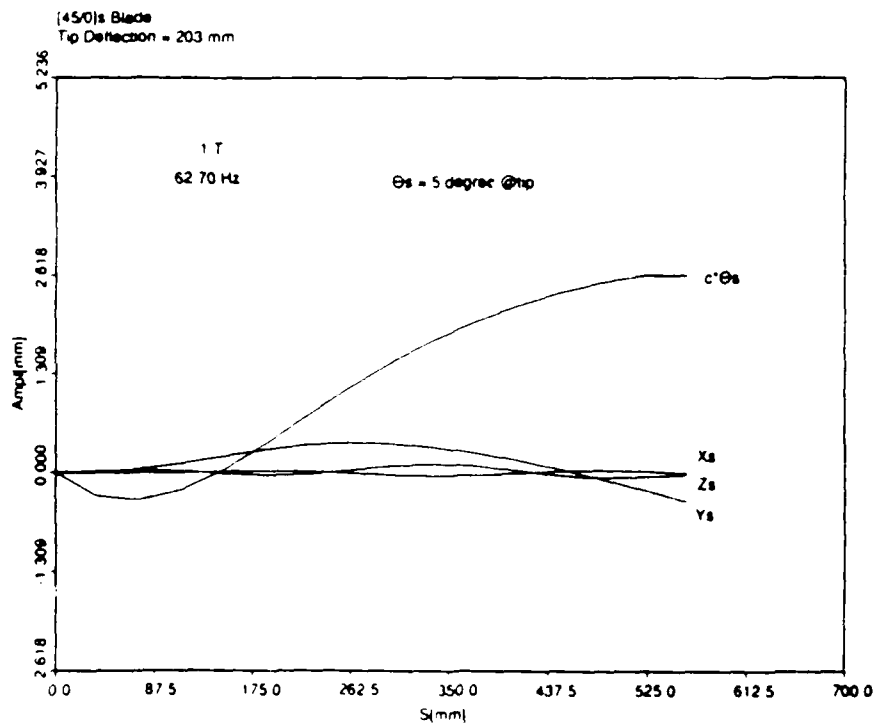


Figure 57: First Torsion Mode; [45/0]_s, 203 mm tip deflection, $\theta_s = 5$ degree

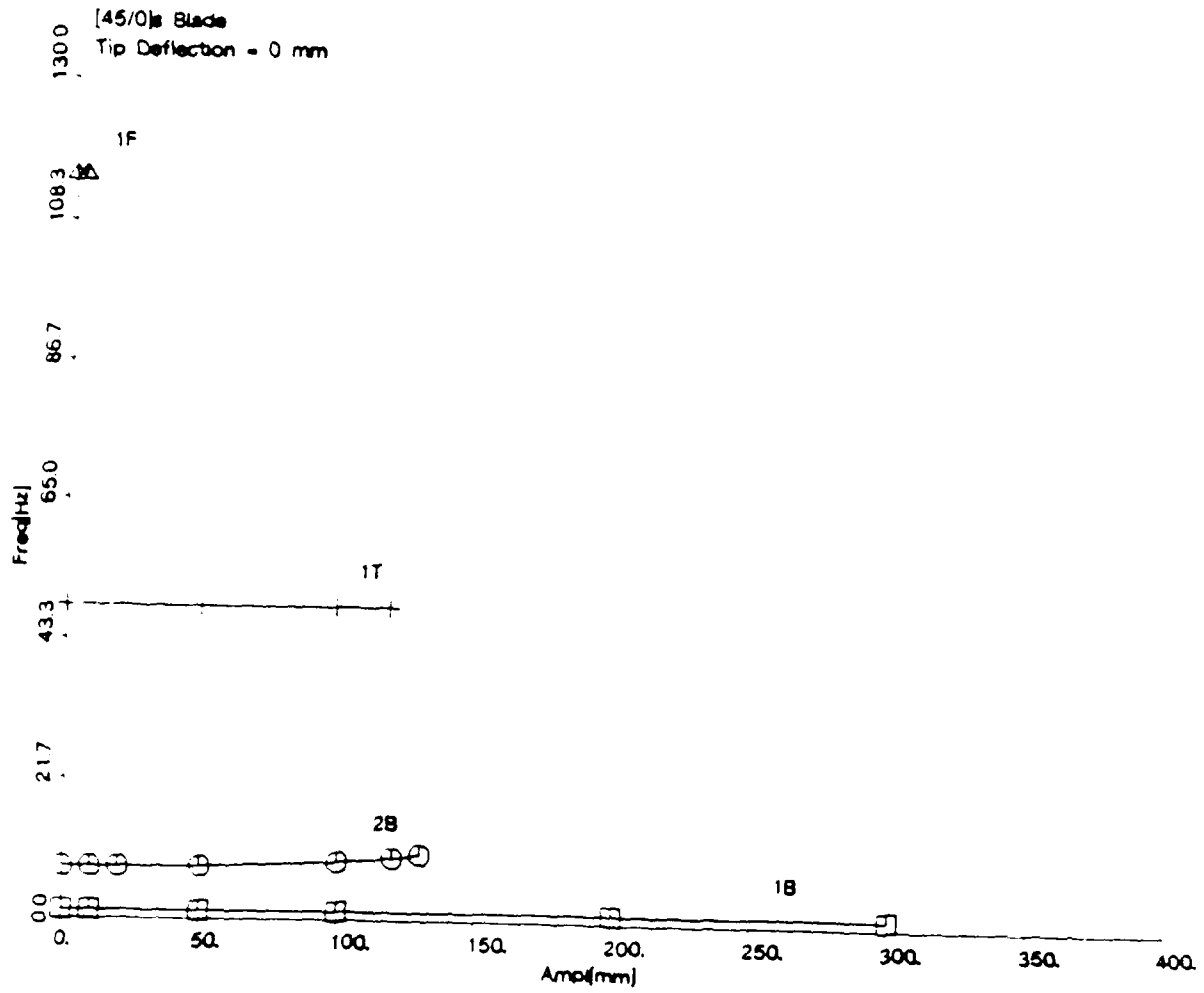


Figure 58: Frequency vs. Amplitude; [45/0]s, 0 mm tip deflection

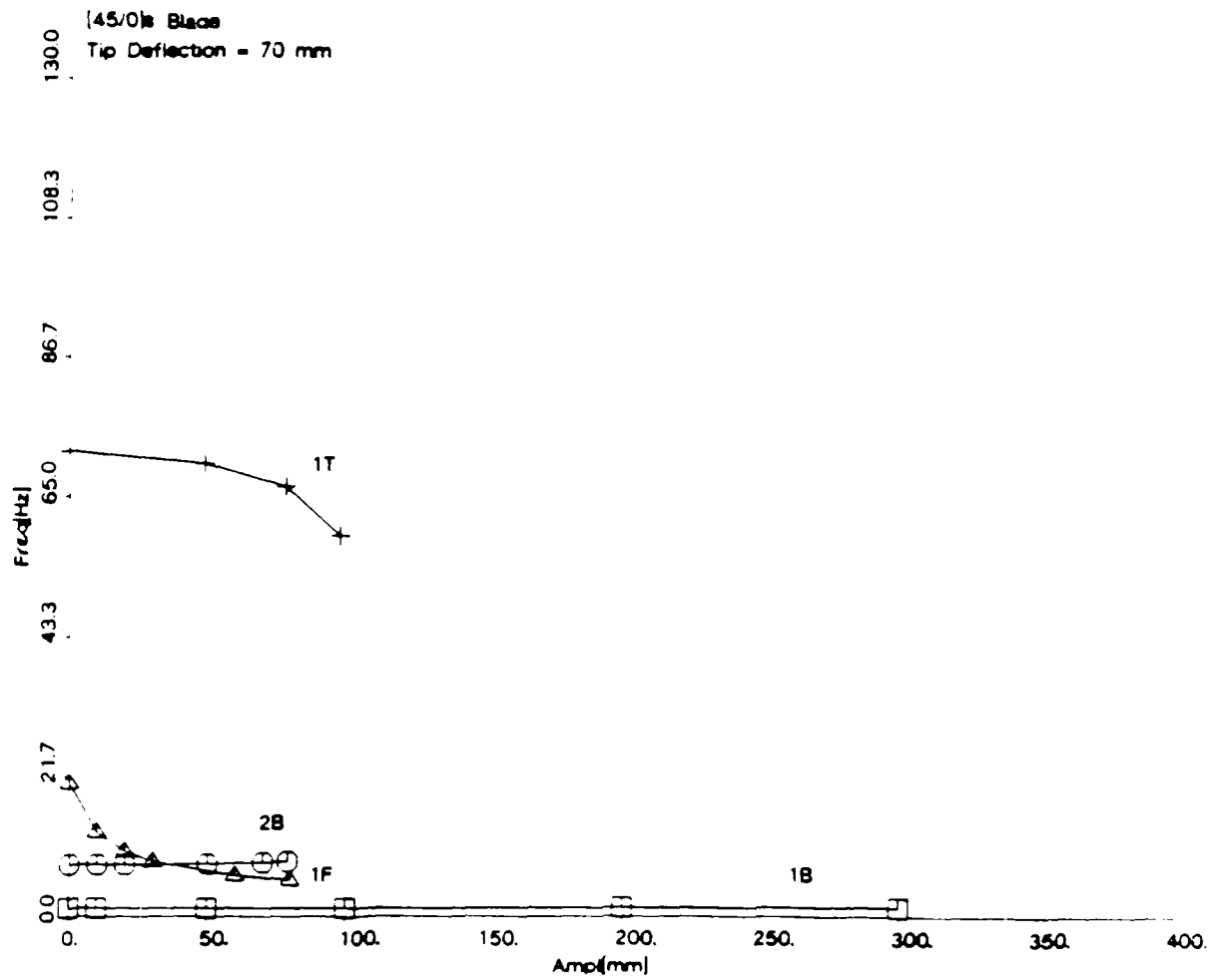


Figure 59: Frequency vs. Amplitude; [45/0]s, 70 mm tip deflection

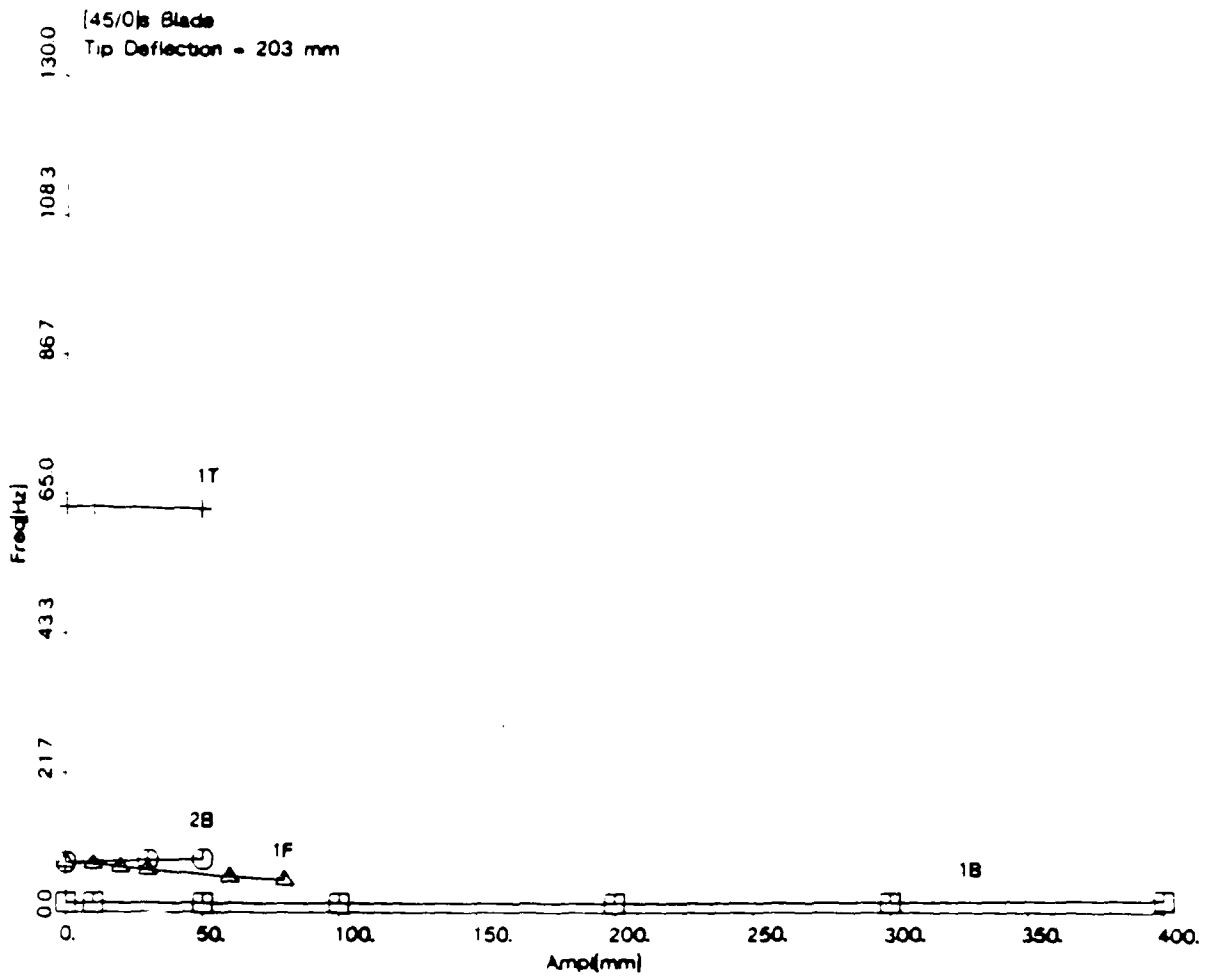


Figure 60: Frequency vs. Amplitude; [45/0]s, 203 mm tip deflection

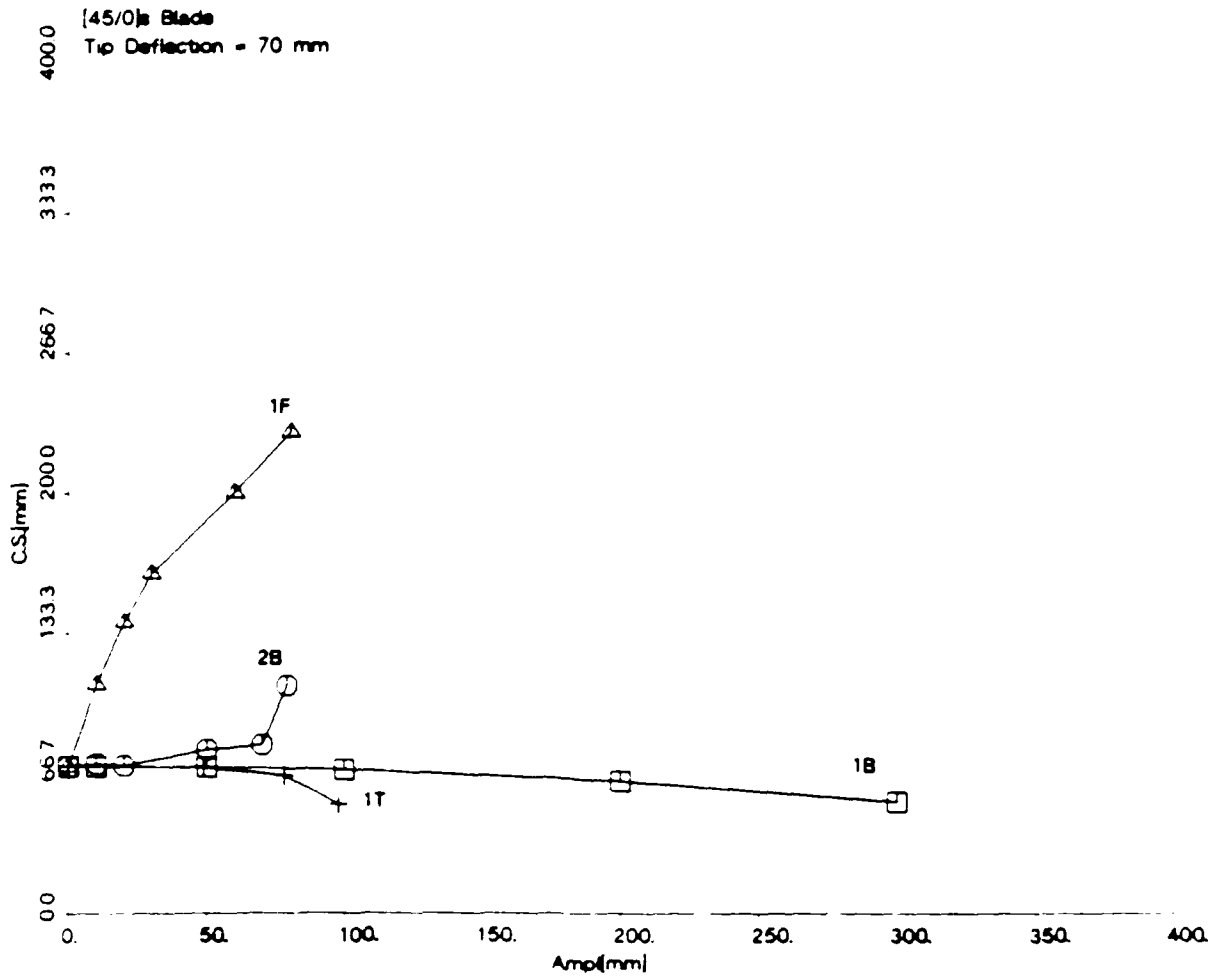


Figure 61: Centershift vs. Amplitude: [45/0]s, 70 mm tip deflection

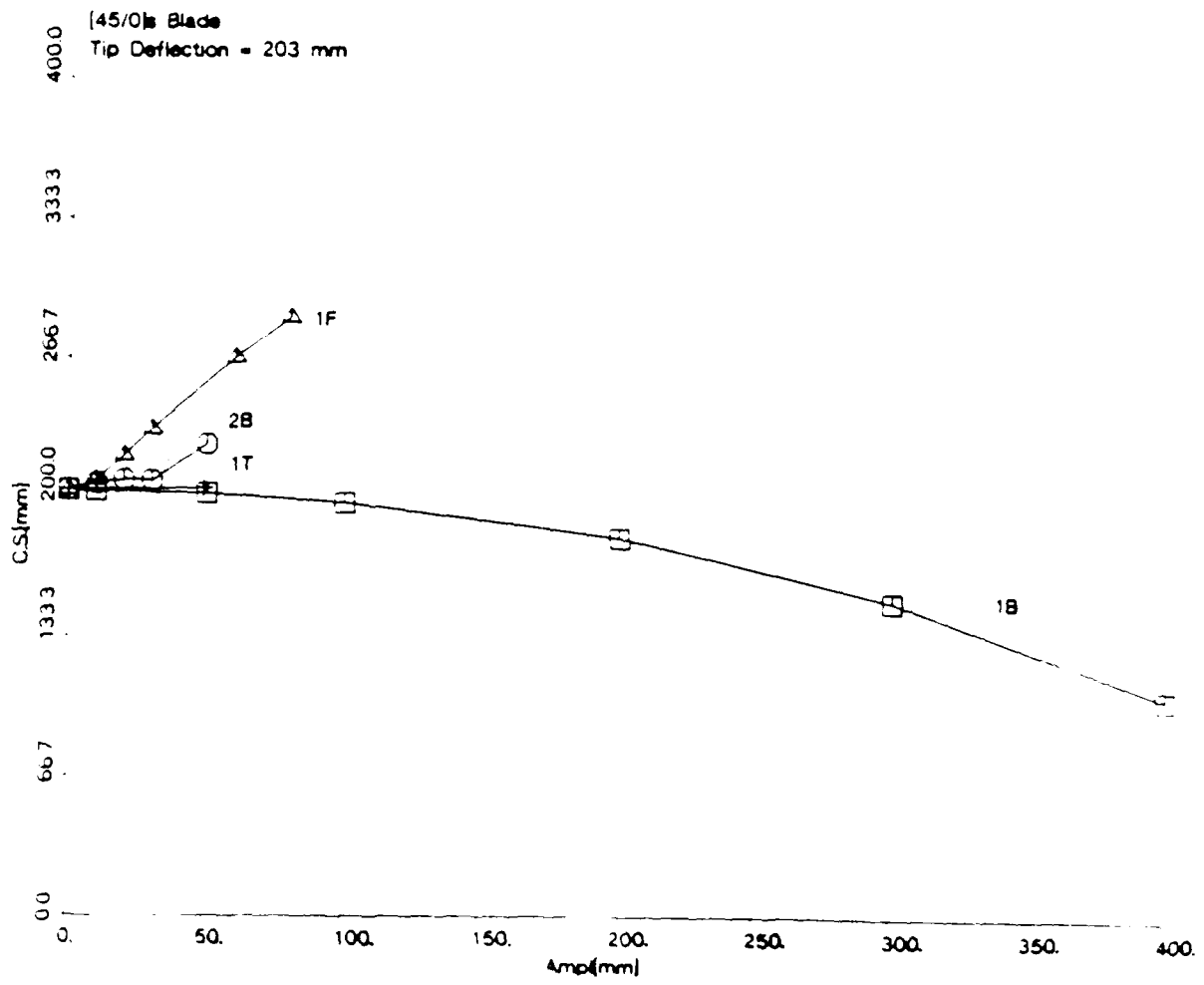


Figure 62: Centershift vs. Amplitude: [45/0]s, 203 mm tip deflection

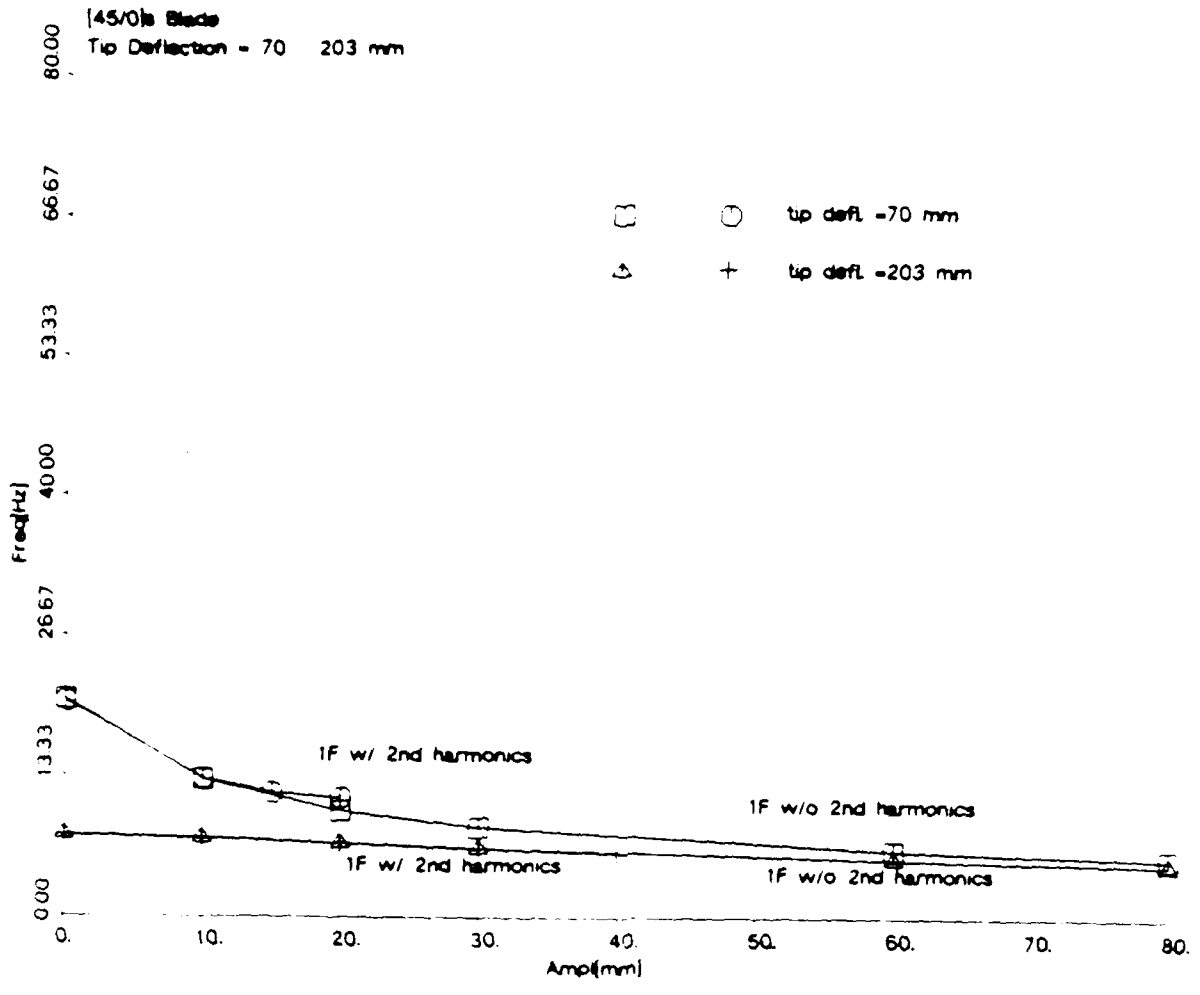


Figure 63: Frequency vs. Amplitude w o and w, 2nd harmonics; 145 01a, 70 mm and 203 mm tip deflection

[45/0]s Beam

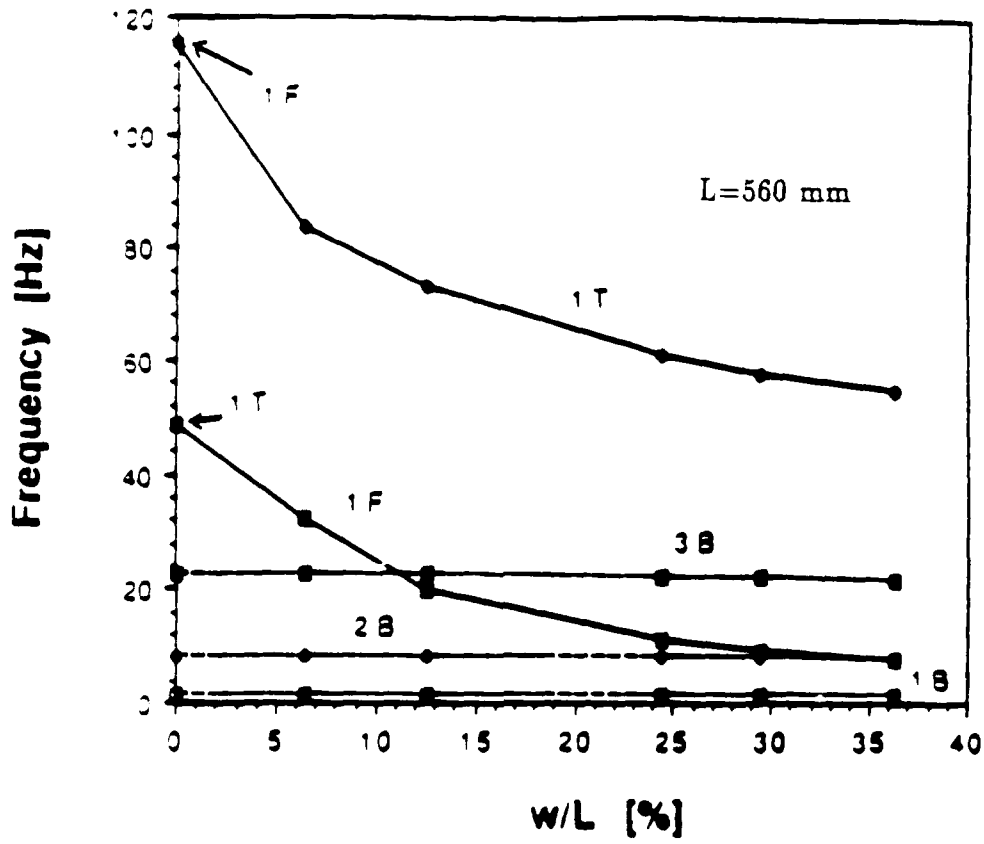


Figure 64: Natural Frequencies of [45/0]_s Beam as a Function of Tip Deflection (from Ref. 1)